Characterization of cellular heterogeneity in the SHH subgroup of medulloblastoma

Christopher Aiken

A thesis submitted to the Faculty of Graduate Studies of
The University of Manitoba
in partial fulfillment of the requirement of the degree of:

Master of Science

Department of Physiology and Pathophysiology
University of Manitoba
Winnipeg, Manitoba

Abstract

Medulloblastoma (MB) is the most common form of primary malignant pediatric brain cancer. MB is divided into 5 molecular subgroups; Wnt, Sonic Hedgehog (SHH) p53 mutant, SHH p53 wildtype, Group 3 and Group 4. Major research efforts have focused on the isolation and characterization of MB brain tumor stem cells, also known as brain tumor propagating cells (BTPC). Elucidating cell surface marker profiles that can be used to selectively isolate this cellular population is an imperative first step in the development of targeted therapies.

Given the variable results obtained for currently utilized markers, as well as the cellular heterogeneity within and between MB sub-groups, it is likely there are additional surface marker profiles capable of selecting for sub-type specific MB BTPCs. We set out to identify novel surface marker combinations capable of selecting for BTPCs in SHH MB.

We employed the BD Bioscience Lyoplate screening platform to compare the levels of 242 human cell surface markers in high and low self-renewing SHH MB sub-clones. The top 25 markers showing the greatest differences were refined by evaluating expression levels in SHH vs Group 3, Group 4 and Wnt variants in transcriptome datasets representing 548 patient samples. Four markers, CD271, CD106/VCAM1, EGFR and CD171/NCAM-L1 showed consistent differential expression in the SHH subtype relative to the other variants. Flow cytometry validation in additional cell lines as well as IHC in patient samples confirmed these findings.

Our laboratory focused on the functional validation of CD271 and CD106 and the role they play in MB tumorigenesis. Functional validation of CD271 in SHH MB *in vitro* and *in vivo* was performed. Using sorted cell populations and gain/loss of function studies, we showed that CD271 is a subtype specific marker that selects for a cellular population in the progenitor/stem cell state in SHH MB. Initial functional characterization of CD106 showed no effect of this cell surface marker on invasion, self-renewal or proliferation *in vitro*.

Additional studies evaluated the generally accepted principle that cell populations with higher self-renewal capacity *in vitro* generate larger tumors and exhibit increased tumor penetrance as well as decreased survival *in vivo*. We demonstrated that a SHH MB subclone derived from the Daoy cell line with a lower self-renewal capacity *in vitro*, when injected into the frontal cortex of NOD SCID mice, result in a shorter survival and increased tumor grade, when compared to a subclone derived from the same Daoy cell line displaying a higher self-renewal capacity. These results challenge the prevailing notion that results *in vitro* vs. *in vivo* are positively correlated.

This thesis was able to show that SHH medulloblastoma is a heterogeneous subgroup that has subgroup specific cancer stem cell markers. We were able to show that CD271 is a SHH MB specific marker that plays a significant role in tumorigenic potential. Future research studying the eradication of this population holds a great deal of promise in treating medulloblastoma clinically.

Acknowledgements

I would like to begin by saying thank you to everyone who has supported me, guided me, leant his or her expertise or has played any role in the seven years I have been part of the Werbowetski-Ogilvie laboratory. I would first like to thank Dr. Tamra Werbowetski-Ogilvie. I was her first student to work in the lab, and she has mentored, guided and pushed me throughout this experience. Thank you for the time you have taken towards my education and for being an excellent supervisor. I would not have accomplished what I did without her and for that I am eternally grateful.

I would like to thank Ludivine Morrison, our laboratory tech, without her the laboratory would not run the way it does and I would have been completely lost the majority of the time. Thank you for the help, the teaching and guidance. For that I am grateful, thank you.

I would like to thank Lisa Liang, we worked together tirelessly throughout our time in the laboratory as fellow PhD students. As a co-author, a portion of the work presented in this thesis was done by her and for that I am grateful. Thank you for your continued support throughout the years and best of luck in the future.

I would like to thank the people on my advisory board, Dr. Mark Nachtigal, Dr. Soheila Karimi and Dr. Brent Fedirchuk. Without their support, patience and understanding throughout the past 4 years, I would have never completed this thesis and graduated. The time and effort you put into working with me will forever be appreciated.

Thank you to Dr. Marc Del Bigio for taking the time to read, assess and grade the endless number of mouse brain samples we sent him over the years.

Thank you to Rhonda, Shawn and the rest of the team at the Animal Facility in the Basic medical science building, without you no surgeries would have ever happened.

I would also like to thank my family and friends who supported me and always believed in me.

I would lastly like to thank the following people for the time and expertise they leant to my work: Monroe Chan, Dr. Peter Cattini, Dr. Afshin Raouf, Ravinder Kaur, Richard Buist, Nazanin Tatari and Margaret Stromecki.

Table of Contents

Chapter 3: Results

Chapter 3.1: Functional characterization of novel biomarkers in selecting for subtype specific medulloblastoma phenotypes

List of Figures

List of Tables

List of Abbreviations

7AAD	7-Aminoactinomycin D
AML	acute lymphoblastic leukemia
APC	adenomatous polyposis coli
B-ALL	B cell acute lymphoblastic leukemia
Blbp	brain lipid binding protein
BMI	B cell-specific Moloney murine leukemia virus integration site
BSA	bovine serum albumin
BTPC	brain tumor propagating cell
CD	cluster of differentiation
CDH1	*Cadherin-1*
CK1α	casein kinase 1α
CNS	central nervous system
CSC	cancer stem cell
CSF	cerebral spinal fluid
CTNNB1	catenin beta-1 / β-catenin
CV-MSCs	chorionic villi derived mesenchymal stem cells
DDX3X	DEAD Box Helicase 3
DMEM	DMEM–Dulbecco's Modified Eagle Medium
DPBS	Dulbecco's phosphate-buffered saline
ECM	extracellular matrix
EGF	epidermal growth factor
EGFR	epidermal growth factor receptor
EGL	external granular layer
EMEM	Eagle's minimum essential media
EMT	epithelial-mesenchymal transition
EN1	homeobox 1
FACS	fluorescence activated cell sorting
FBS	fetal bovine serum
FGF	fibroblast growth factor
Fzd	Frizzled
Gbx2	gastrulation brain homeobox 2
GEM	genetically engineered mouse
GFAP	glial fibrillary acidic protein
GFD	growth factor dependent
GFI	growth factor independent
GFP	green Fluorescent Protein
GLI	glioma-associated oncogene
GNPC	granule neuron precursor cell
GSK3β	glycogen synthase kinase 3β
H&E	hematoxylin and eosin
hCNS-SC	human central nervous system stem cell

HLA	human leukocyte antigen
Hoxa2	Homeobox A2
IGL	internal granular layer
IHC	Immunohistochemistry
KD	Knockdown
LEF	lymphoid enhancer-binding factor
LRP	lipoprotein receptor-related protein
Math1	*mouse atonal homolog 1*
MB	Medulloblastoma
Meis1	*myeloid ecotropic viral integration site 1*
miRNA	microRNA
NCAM	neural cell adhesion molecule
ncRNA	non-coding RNA
NGFR	nerve growth factor receptor
NOD SCID	non obese diabetic severe combined immunodeficient
NSC	neural stem cell
OE	Overexpression
OTX2	Orthodenticle Homeobox 2
p75NTR	*p75 neurotrophin receptor*
Pax2/5/6/8	Paired Box 2/5/6/8
PCA	principal component analysis
pdgf	platelet-derived growth factor
Ptch	Patched
qPCR	quantitative polymerase chain reaction
RC2	radial glial cell marker-2
RFP	red Fluorescent Protein
RL	rhombic lip
RT	radiation therapy
RT-PCR	real time polymerase chain reaction
sas	subarachnoid space
SCID	severe combined immunodeficient
SDS-PAGE	sodium dodecyl sulfate polyacrylamide gel electrophoresis
SHH	sonic hedgehog
shRNA	short hairpin RNA
SL-IC	SCID leukemia initiating cell
Smo	Smoothened
Sox2	sex determining region Ptch-box 2
SR	self renewal
SSEA	stage specific embryonic antigen
SUFU	suppressor of fused
TBS	tris buffered saline
TCF	T-cell specific factor
TIC	tumor initiating cell

TPC	tumor propagating cell
TrkC	tropomyosin receptor kinase C
TrkC	tropomyosin receptor kinase C
VCAM	vascular cell adhesion molecule
VZ	ventricular zone
WHO	World Health Organization
Yap-1	yes-associated protein 1
ZIC	zinc finger of the cerebellum
Zic1 and *Zic3*	zinc finger protein 1 and 3

List of Copyright Material:

Morrison LC, McClelland R, Aiken C, Bridges M, Liang L, Wang X, et al. Deconstruction of medulloblastoma cellular heterogeneity reveals differences between the most highly invasive and self-renewing phenotypes. Neoplasia. 2013;15(4):384-98.

Liang L, Aiken C, McClelland R, Morrison LC, Tatari N, Remke M, et al. Characterization of novel biomarkers in selecting for subtype specific medulloblastoma phenotypes. Oncotarget. 2015;6(16):38881-900.

Aiken C, Werbowetski-Ogilvie T. Animal models of cancer stem cells: What are they really telling us? . Current Pathobiology Reports 2013;1(2):91-9.

Chapter 1: Introduction

1.0: Thesis aims:

The overall aims of this thesis are as follows:

1) To elucidate sub-type specific cell surface markers that are capable of selecting for cancer stem/progenitor cells in the primary malignant pediatric brain cancer medulloblastoma

2) To determine the functional role of newly identified cell surface markers and how they regulate stem cell properties such as self-renewal in medulloblastoma.

We hypothesize that since the medulloblastoma subtypes are highly heterogeneous, identified cell surface markers will select for cancer stem/progenitor cells in a subtype specific manner subtype specific.

NB. This thesis focuses on the medulloblastoma, a form of primary pediatric brain cancer. Medulloblastoma forms exclusively in the cerebellum and dorsal brainstem. This thesis will therefore only focus on the normal and abnormal development of the cerebellum and dorsal brainstem and will not discuss the normal and abnormal development of other brain structures.

1.1: Normal Cerebellar Development

1.1.1: Cerebellar structure and cell types

The cerebellum begins to form shortly after gastrulation in the developing embryo near the boundary between the midbrain and the hindbrain (1). This boundary and location of the primordial cerebellum is delineated by the expression of the homeobox genes orthodenticle homeobox 2 (*Otx2)* (rostral) and Homeobox A2 (*Hoxa2)* and gastrulation brain homeobox 2 (*Gbx2*) (caudal) (2, 3). These transcription factors (*Otx2 and Gbx2*) and the genes that are essential in the development of the cerebellar territory including Engrailed homeobox 1 (*EN1*) and Paired Box 2/5/8 (*Pax2/5/8*) are controlled by Secreted Wingless (WNT) and fibroblast growth factors (FGF) (4).

The cerebellum, similar to the cerebrum, is composed of an outer cortex that encases several cerebellar nuclei that function as output centers of the cerebellum (1). The anatomical and cellular organization of the cerebellum was established in the early 1900's (5, 6). There are eight types of neurons that make up the cerebellum, six classically described (7); Purkinje cells, lugaro cells, granule cells, golgi cells, stellate cells, basket cells, and two more recently described; the unipolar brush cell (8) and the candelabrum cell (9). These cells form a three-dimensional repeating matrix that gives rise to three discernable layers in the cerebellar cortex (Figure 1.1). The most superficial layer, the molecular layer, has a low cellular density but high synaptic density. The middle layer is a thin layer known as the Purkinje layer, where the cell bodies of the Purkinje cells lie. The deepest layer is the

granule layer, with the highest cellular density and contains the cell bodies of the granule cells, the most abundant neuron found in the human brain.

Input to the cerebellum consists of peripheral sensation and cortical inputs that arrive from the five main precerebellar nuclei located in the brainstem (10). Four of these nuclei project mossy fibres to the cerebellar granule neurons while the fifth precerebellar nucleus, the inferior olivary nucleus, projects climbing fibres directly to the Purkinje neurons (10). Despite the cerebellum having a large variety of cells and a complex structure, Purkinje cells are the only cells that project outside the cerebellar cortex (1, 11). With few exceptions, the Purkinje cells of the cerebellar cortex project to the deep cerebellar nuclei (dentate, two interposed and fastigial), which then in turn project to upper motor neurons in the cerebral cortex via the thalamus and spinal cord (1, 11). All seven other cell types act as regulatory interneurons forming complex circuits within the cerebellum processing synaptic input and regulating synaptic output of the cerebellar cortex (1, 11). The complex but highly repetitive temporal organization of the cerebellar cortex is a direct result of an intricate neural proliferation and migration pattern combined with neuronal differentiation and axonal growth that is highly regulated in the developing brain (11).

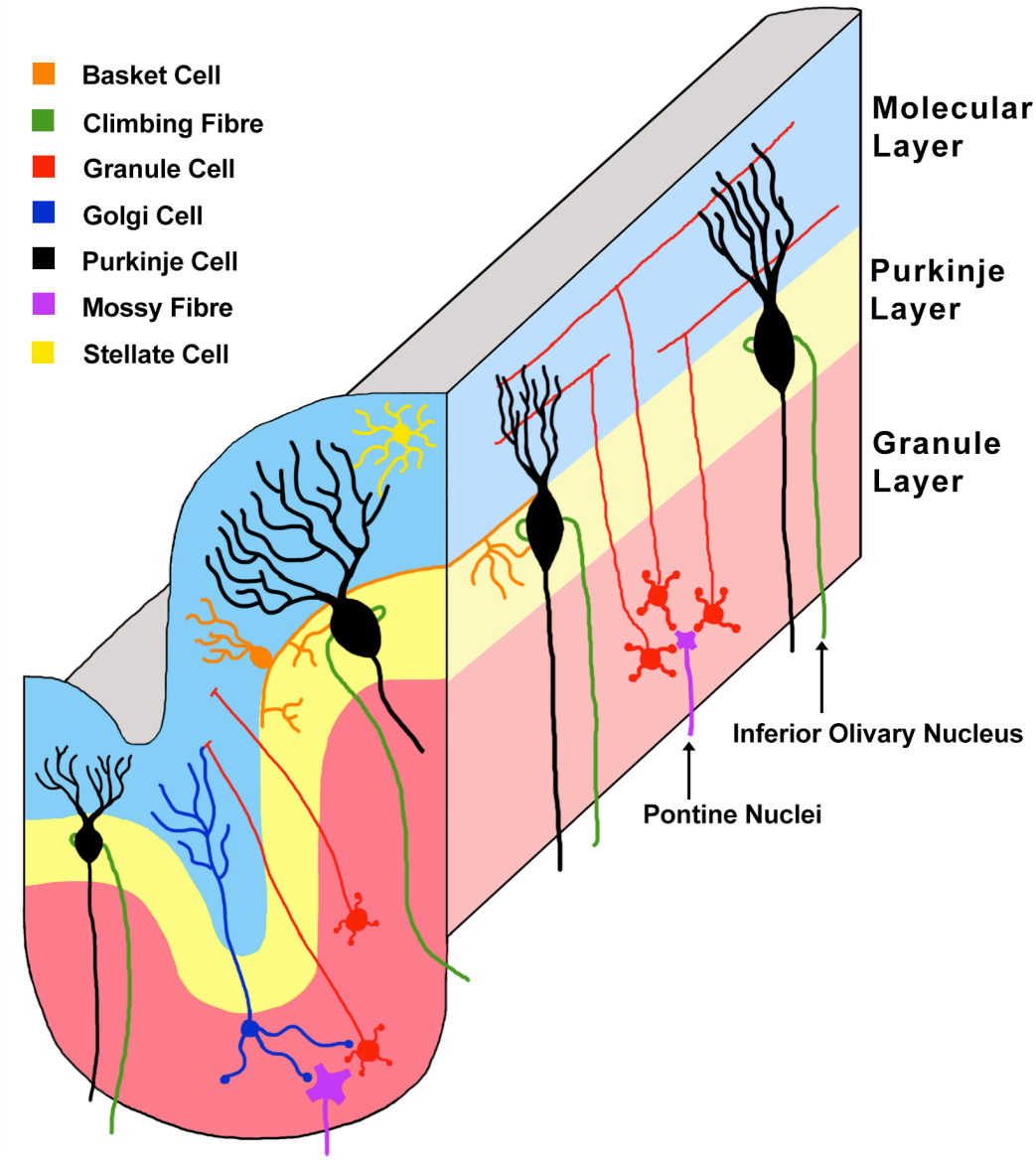

Figure 1.1: The cerebellar cortex is made up of three distinct layers. The most superficial layer is the molecular layer. This layer has low cellular but high synaptic density. This layer contains the synapses of the parallel fibres of the granule cells with the dendrites of the Purkinje cells. The middle layer is the Purkinje layer where the cell bodies of the Purkinje neurons lay. The deepest layer is the granule layer, named due to the presence of granule neuron cell bodies. The granule neuron is the most abundant neuron found in the human nervous system and therefore this layer has the highest cellular density of the all the cerebellar cortex layers. Input to the cerebellar layers is received from the pre-cerebellar nuclei. Input to the granule neurons arrives through mossy fibres, whereas climbing fibres send information directly to the Purkinje cells bypassing the granule neurons. Information in processed in the cerebellum and sent to the deep cerebellar nuclei exclusively through the Purkinje neurons where it is relayed to upper motor neurons in the cerebellar cortex.

The cerebellum develops from several progenitor regions including the rhombic lip (RL) and ventricular zone (VZ) surrounding the fourth ventricle (10-12). The progenitors of the VZ surrounding the fourth ventricle give rise to several cerebellar type neurons including the Purkinje neuron, the main output neuron of the cerebellar cortex, as well as several interneurons such as golgi, basket and stellate cells (1, 13). Proliferation of the VZ is nearly complete in utero while the rhombic lip derived progenitors continue to proliferate postnatally.

The RL, the second germinal zone of the hindbrain, is composed of a rostral (upper) and caudal (lower) segment. The caudal segment is responsible for giving rise to precerebellar regions in the brainstem that provide afferent input to the cerebellar cortex including the olivary nucleus and pontine nucleus (14). The rostral segment of the rhombic lip is of particular interest as it is this region that ultimately gives rise to the granule neurons of the cerebellar cortex (11, 13, 15).

Granule neurons play an important role as relay interneurons that transmit excitatory signals between the mossy fibres and the main output Purkinje neurons. Granule neurons are generated from progenitor cells called granule neural precursor cells (GNPCs) after expansion in a layer known as the external granule layer (EGL) during development. GNPCs in the EGL are marked by mouse atonal homolog 1 (*Math1/Atoh1*) (16), zinc finger protein 1 and 3 (*Zic1* and *Zic3*) (17), paired box protein 6 (*Pax6*) (18), myeloid ecotropic viral integration site 1 (*Meis1*) (19) and p75 neurotrophin receptor (p75NTR/CD271). Meanwhile, neural stem cells of the rRL are marked by intermediate filament associated proteins RC2 and nestin and glial fibrillary acidic protein (GFAP)(12) during early development.

Rostral rhombic lip progenitors begin to proliferate in mice at E10. Proliferation followed by migration of GNPCs from the rostral rRL in a lateromedial and posteromedial direction starting at E13 in mice form a layer of proliferating cells that covers the surface of the developing cerebellum forming the EGL by E15 (10). Around the time of birth, after clonal expansion in the superficial portion of the EGL, GNPCs give rise to post-mitotic granule cells in the deep layer of the EGL that migrate internally to form the internal granule layer where they then differentiate and stay for the remainder of their life. The migration and differentiation of GNPCs continues postnatally, with the process continuing until the EGL disappears around P15 in mice and 1 year in humans (20). The whole process is highly regulated and is controlled for the most part by the surrounding environment and associated cell-signaling pathways.

1.1.2: Normal Cerebellar development and cell signaling pathways

1.1.2.a: The WNT signaling pathway controls the proliferation of neural stem cells in the developing brain

The WNT signaling pathway plays a critical role in the development of the CNS and is essential for the formation of the midbrain/hindbrain boundary through the control of NSC proliferation. The *WNT* gene family consists of at least 19 members in vertebrates (21). β-catenin is the main signaling molecule in the canonical (β-catenin dependent) WNT signaling pathway (Figure 1.2) (21, 22).

When the WNT signaling pathway is inactive, β-catenin levels are kept low in the cytoplasm. This is accomplished by the phosphorylation-targeted destruction of β-catenin by a multi-protein destruction complex (22). This complex is composed of the proteins APC and Axin, which enable the phosphorylation of β-catenin by casein kinase 1α (CK1α) and glycogen synthase kinase 3β (GSK3β) (22). Phosphorylation of β-catenin leads to its eventual proteosomal destruction and subsequent gene target repression (21, 22). Low levels of β-catenin in the nucleus allow transcription factor T-cell specific factor/lymphoid enhancer-binding factor (TCF/LEF) to be associated with Groucho (a gene repression cofactor) leading to target gene repression (23, 24).

However, when a WNT family ligand binds a Frizzled (Fzd) receptor, and its co-receptor lipoprotein receptor-related protein 5/6 (LRP), the proteosomal degradation of β-catenin is blocked resulting in an accumulation of stable β-catenin in the cytoplasm (25, 26). Translocation of β-catenin into the nucleus causes cell-type specific gene activation by displacing Groucho and indirectly converting TCF/LEF from a transcriptional repressor to transcriptional activator (27, 28).

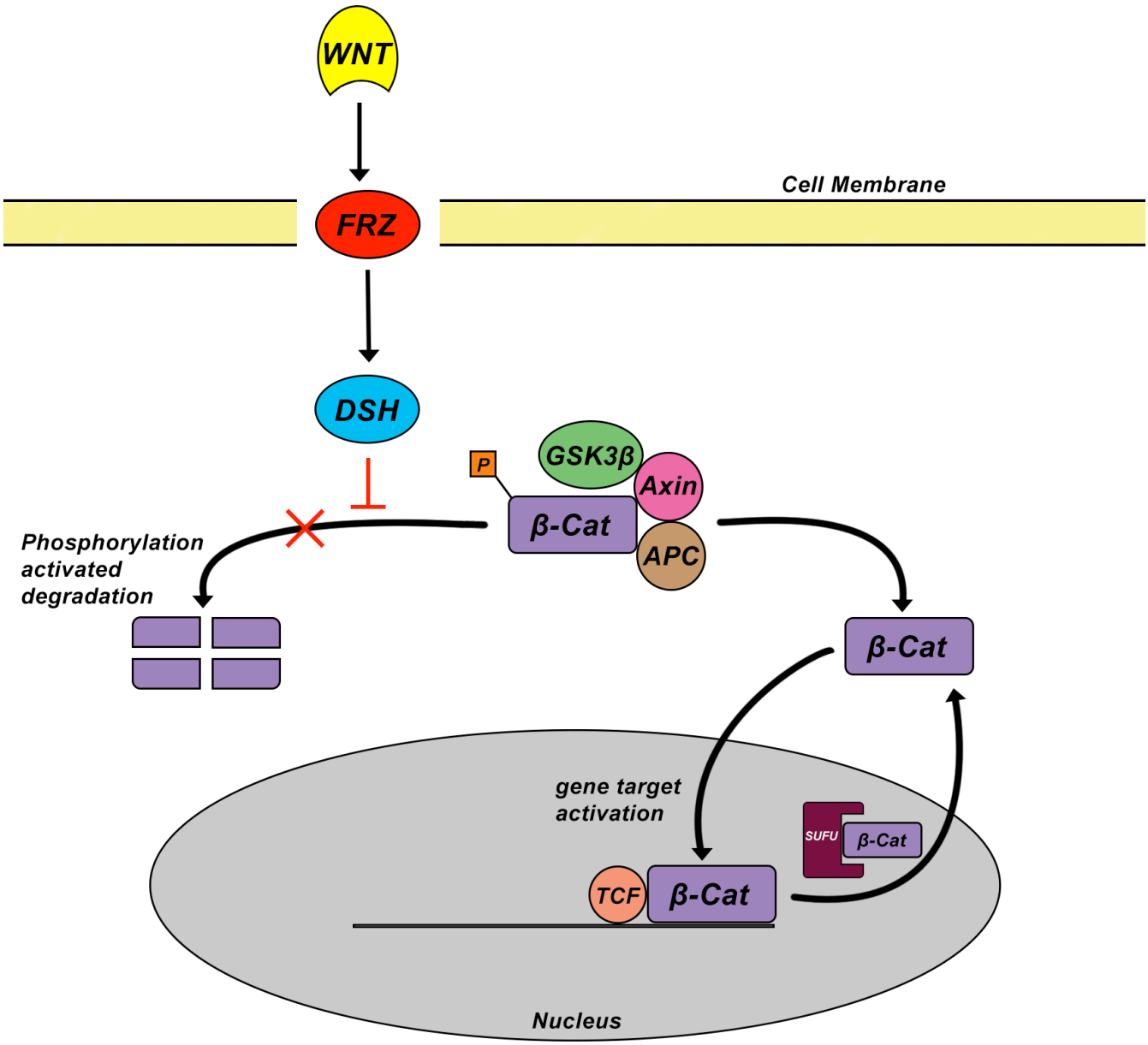

Figure 1.2: The Wingless (WNT) pathway plays a critical role in proliferation of neural stem cells in the developing brain. Canonical (β-catenin dependent) WNT signaling plays a key role in the formation of the midbrain/hindbrain boundary through the control of neural stem cell proliferation. When no WNT is present, β-catenin levels are kept low through phosphorylation-targeted destruction by the multi-protein destruction complex (Axin, APC and GSK3β). Low levels of β–catenin leads to gene target repression. Binding of WNT to the Frizzled (Fzd) receptor causes a rise in intracellular β-catenin through the inhibition of targeted destruction. Stable non-phosphorylated β-catenin is translocated into the nucleus causing targeted gene activation.

The WNT signaling pathway plays an essential role during development in the establishment of the embryonic axis and limb patterning (22). However, in the CNS, WNT signaling is not involved in primary pattering processes but instead is thought to play a general mitogenic role regulating proliferation of dorsal neural progenitor cells (29-31).

WNT-1 is exclusively expressed in the CNS during normal embryonic development (31). WNT-1, 3, 3a and 4 are highly expressed in overlapping regions of the developing CNS concentrated predominantly at the dorsal midline from spinal cord to forebrain (32). WNT-1 and 3A are the earliest WNT proteins to be expressed in mice coinciding with neural-crest differentiation in the dorsal neural tube (32).

Homozygous null *WNT1* mutant mice die at birth and show a complete lack of a developed midbrain and cerebellum (33, 34). This developmental defect is due to the role WNT1 plays in early embryonic development (before E9.5 in mice) of the midbrain and its effect on anterior-posterior pattern regulation in the CNS through the control of cell proliferation (35). When WNT-1 was ectopically expressed in the developing spinal cord, it caused a dramatic increase in precursor cells undergoing proliferation in the ventricular region and subsequent ventricular expansion (31). In mice with mutant forms of both WNT-1 and WNT-3A, there is a deficiency in neural crest derivatives and a reduction in dorsolateral neural precursor cells in the neural tube further demonstrating the mitogenic role the WNT family plays in CNS development (30). Wnt-3a mutant mice show an absence or underdeveloped hippocampus due to a reduction in neural progenitor cell proliferation in this region (29). This demonstrates the importance of WNT-3a in the normal development of

the hippocampus and the extended role the WNT family plays in normal CNS development (29).

More recently, research has shown that WNT induced proliferation is cell type dependent. Pei et al. showed that activation of canonical WNT signaling *in vivo* and *in vitro* in the form of β-catenin overexpression increases proliferation in NSCs of the developing cerebellar VZ (36) while contrary effects were seen in GNPCs overexpressing β-catenin with this population showing impaired proliferation (36). Although increased proliferation was seen in NSCs, the self-renewal and differentiation ability of these cells was also impaired *in vitro* presumably leading to the marked defect in neuronal and glial production that was observed in the developing mouse cerebellum (36). Loss of β-catenin production also led to a reduction in self-renewal capacity in NSCs, while also increasing neuronal differentiation *in vitro* (36).

Overall WNT signaling plays a strictly mitogenic role in the development of the CNS. Although mutations in the WNT ligands result in underdevelopment of the midbrain/hindbrain boundary alluding to a role of this pathway in the development of CNS polarity, it has been shown that this is in fact a result of decreased proliferation of NSCs. WNT signaling is present very early in development of the CNS and is crucial for the proper formation of the cerebellum and survival of the developing embryo.

1.1.2.b: SHH signaling pathway controls the proliferation of granule neuron precursor cells in the developing cerebellum

Control of GNPC proliferation in the EGL as well as glial differentiation in the cerebellar cortex has been shown to be regulated by the SHH pathway (37-39). SHH is a secreted signaling protein and its subsequent signaling pathway play an essential role in the proper development of several body systems including the limbs and central nervous system (40). The mechanism of the SHH pathway is complex and not fully understood (Figure 1.3). The SHH protein binds the membrane bound receptor Patched (*PTCH*) (40). Unbound *PTCH* plays an inhibitory role that when inactivated, represses SHH signaling. Binding of SHH to *PTCH* releases the inhibitory effect *PTCH* has on Smoothened (SMO), a member of the G protein-coupled receptor family (41). De-inhibition of SMO results in the activation of the zinc-finger proteins of the GLI transcription factor family including GLI1, GLI2 and GLI3 (40).

GLI proteins can function as either transcription activators or repressors. In the absence of SHH, GLI2 and GLI3 are phosphorylated leading to their proteolytic cleavage to generate their repressor forms (40). With the activation of SMO, GLI proteolytic processing is blocked, meanwhile transcriptionally active forms of GLI are formed in combination with inhibition of suppressor of fused (SUFU), a protein responsible for sequestering GLI in the cytoplasm (40, 42). Inhibition of SUFU allows the activating forms of GLI to translocate to the nucleus where they replace the repressor forms of GLI on target genes leading to transcriptional activation (42).

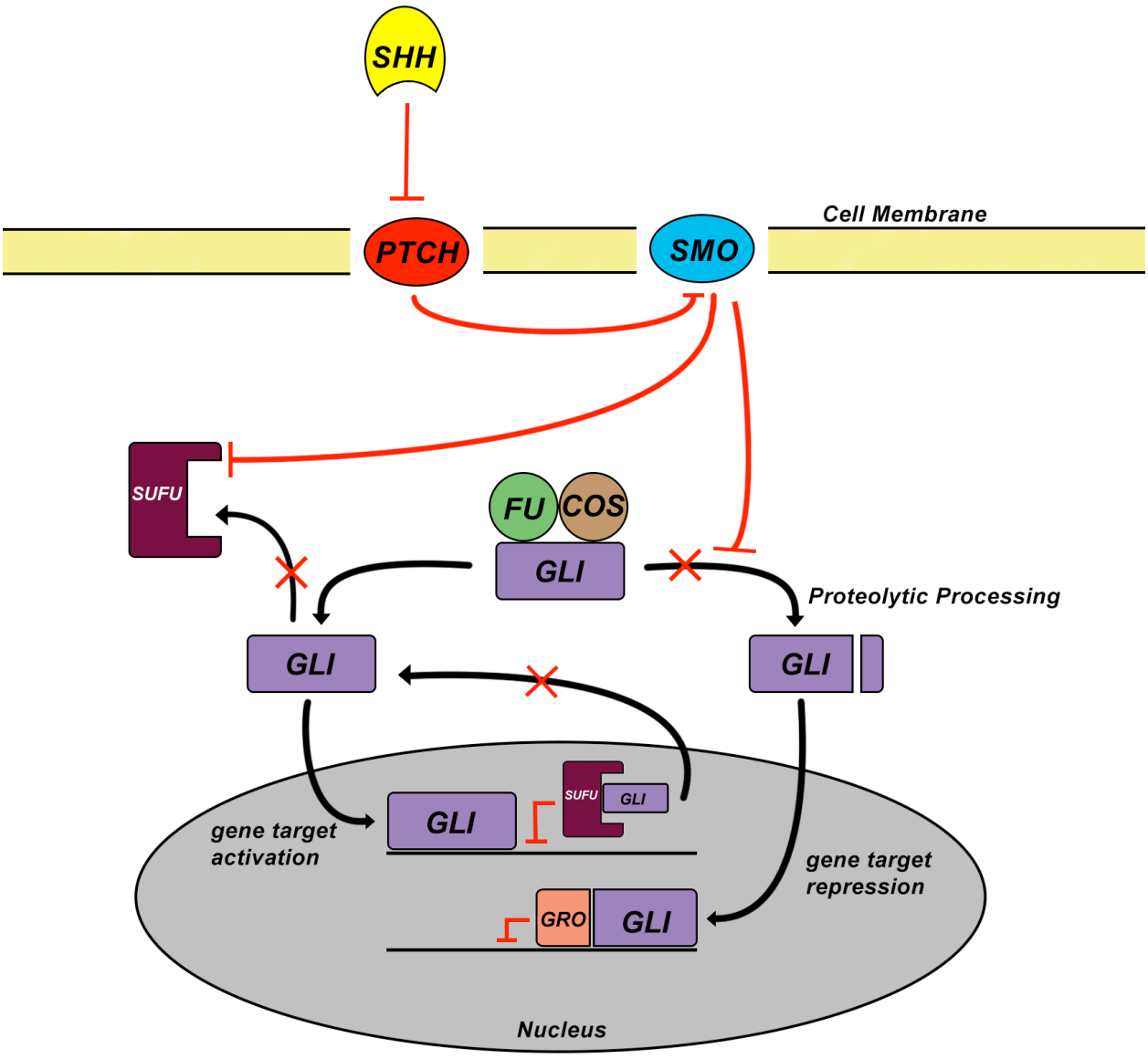

Figure 1.3: Sonic Hedgehog (SHH) signaling controls the proliferation of granule neuron precursors in the developing cerebellum. Proliferation of granule neuron precursor cells in the external granule layer of the cerebellum is strictly controlled through SHH signaling. When SHH is not present, the Patched (*PTCH*) receptor plays an inhibitory role repressing SHH signaling. Binding of SHH to *PTCH* releases the inhibitory effect *PTCH* has on Smoothened (SMO). De-inhibition of SMO results in activation of GLI transcription factors. Suppressor of fused (SUFU) is found in the cytoplasm and nucleus, and plays a role in sequestering GLI proteins when SHH is not bound to *PTCH*. Binding of SHH to *PTCH* leads to inhibition of SUFU resulting in translocation of GLI to the nucleus. SHH binding ultimately results in targeted gene activation through a complex signaling pathway.

Purkinje cells of the developing cerebellum are responsible for regulating proliferation of GNPCs in the EGL through secretion of SHH (Figure 1.4). Blocking Shh signaling in the developing brain of mice results in the development of a hypoplastic cerebellum, abnormal Purkinje neuron positioning and reduction or absence of granule neurons while treatment with Shh prevents GNPCs from exiting the cell cycle to differentiate while prolonging proliferation (37-39). However, *Gli1* knockout mice show no deficiencies in GNPC division in the EGL (43), leading to hypotheses that other proteins such as Nmyc, which is expressed by GNPCs and upregulated by Shh are required for GNPC proliferation (44).

The extracellular matrix (ECM) has been shown to play an important role in the timing of cell cycle exit in GNPCs (45). Laminin, an ECM protein and its integrin receptor subunit α6 are expressed in the superficial layer of the EGL where GNPCs are actively proliferating (45). Vitronectin, an ECM protein and its integrin receptor unit αv are expressed in the inner layer of the EGL where postmitotic undifferentiated GNPCs are abundant (45). Pons et al. showed that laminin increases SHH-induced proliferation of GNPCs whereas vitronectin reduces the effect SHH had on GNPCs allowing them to stop proliferating, exit the cell cycle and begin differentiation (45). It was therefore hypothesized that while moving through the EGL, GNPCs that are proliferating in the superficial layer encounter vitronectin as they progress to the deeper layer of the EGL. Interaction with vitronectin in turn reduces the sensitivity to SHH, causing the cells to exit the cell cycle and leave the proliferation program to enter a differentiation program leading to the formation of mature granule cells.

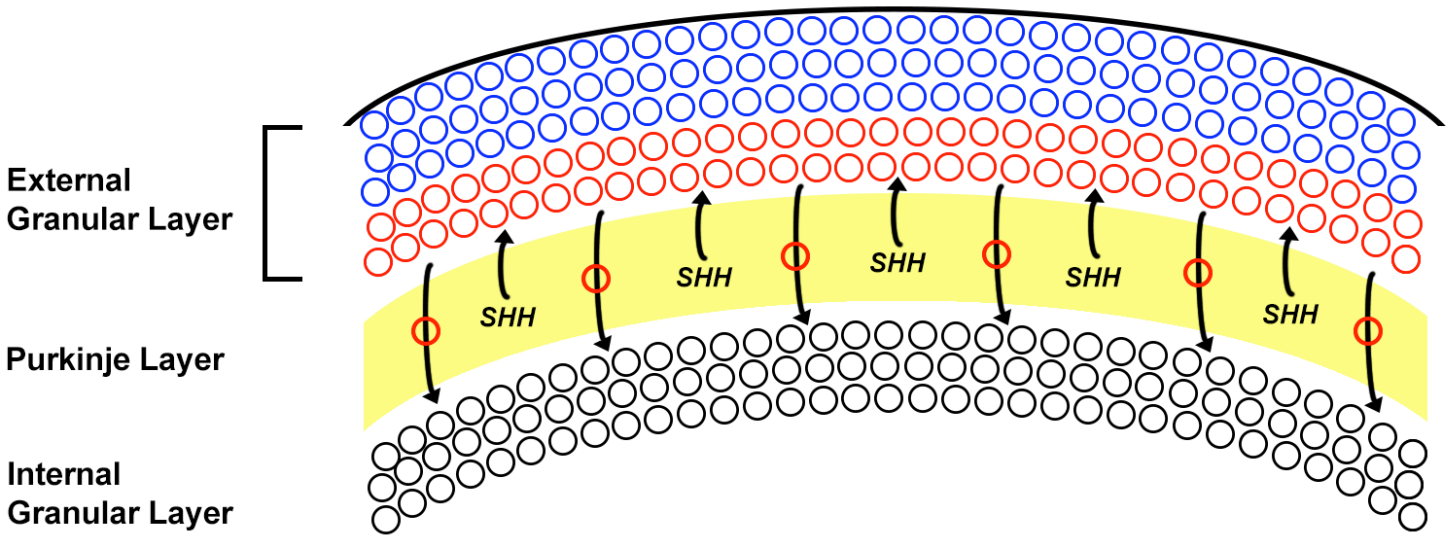

Figure 1.4: SHH is released by Purkinje cells in the developing cerebellum resulting in GNPC proliferation in the EGL. Proliferation of GNPCs in the external granule layer is controlled by SHH. SHH is released by Purkinje cells of the Purkinje layer during development. As these cells proliferate they begin to migrate through the Purkinje layer deep where they form the internal granule layer. Once they have reached the internal granule layer, they exit the cell cycle and terminally differentiate due to a reduced sensitivity to SHH signaling. In humans, this process is not complete until approximately one year of age.

1.1.3: Conclusion

Taken together, the canonical WNT and SHH signaling pathways play important roles in the developing cerebellum. These roles are predominantly mitogenic and are associated with neural stem cell and progenitor proliferation and differentiation in the germinal VZ and external granule layer. Proliferation in NSCs and GNPCs are predominantly regulated by two different cellular signaling pathways, canonical WNT and SHH respectively. This becomes important in the next section when we begin to talk about aberrant signaling in the cerebellum and the role these pathways play in the formation of medulloblastoma, a disease of abnormal neural development.

1.2: Aberrant development of the hindbrain results in Medulloblastoma, a pediatric neuronal malignancy

Medulloblastoma (MB) is the most common form of primary pediatric malignant brain cancer in North America (46). MB is classified as a grade 4 tumor (mitotically active, necrosis-prone neoplasms, generally associated with a rapid pre and postoperative evolution of the disease) by the World Health Organization (46), and, for unknown reasons, is more common in males than in females, affecting approximately 1.5 males for every female (46). Typical presentation of this disease incudes headaches, nausea/vomiting, seizures and gait disturbances.

1.2.1: Treatment

All patients diagnosed with MB undergo a total or near total resection based on tumor position. Patients who undergo a total or subtotal resection of a non-metastatic tumor have a higher survival rate than patients who undergo radiation alone (47). Current prognosis and treatment are determined by; risk of recurrence which is based on presence of metastasis and extent of resection at diagnosis, and age, with patients under the age of three at a much higher risk of neurological damage due to radiation treatment (48). Based on these criteria, patients are classified into three treatment groups (48). **1. Children greater than three years of age with average risk disease**, defined as total or near-total resection at time of surgery and no evidence of dissemination by imaging or cerebrospinal fluid (CSF) analysis (48). **2. Children greater than three years of age with high risk disease**,

defined as the presence of greater than 1.5 cm^2 of residual tumor after surgery and/or dissemination or metastasis (48). These patients are at an increased risk for recurrence and death when compared to patients in the average risk group. **3. Children younger than three years of age.** Although radiation can improve disease control, the use of multi-agent chemotherapy is recommended to delay or remove the need for RT, and allow the nervous system an opportunity to further develop (48).

1.2.2: Pathology

MB has been traditionally classified based on its histological properties. MB appears as a small round blue cell tumor, a characteristic of tumors seen on hematoxylin and eosin (H&E) staining due to a large nucleus and scant cytoplasm typically indicating undifferentiated cells. (49). Histologically, MB can be broken up into three main variants: **classic, desmoplastic, and large cell/anaplastic** (50). Most MB tumors (70%) belong to the classic histology variant, followed by desmoplastic at 16% and large cell/anaplastic at 10%, however these proportions shift slightly between infants, children and adults (51).

Several markers of prognosis have been elucidated for patients with MB. Metastatic disease at diagnosis is the only clinical feature that has been shown to be negatively correlated with prognosis (52). Immunopositivity of mutant p53, ErbB2 are negative prognostic markers while immunopositivity of *TrkC* and nuclear β-catenin are positive prognostic tumor markers (52-55). β–catenin accumulation in the nucleus is associated with activation of the WNT pathway (53). Genetic

prognostic events include *CTNNB1* mutation in combination with monosomy 6, 6q deletion, gain of 6q and 17q and genomic amplification of *MYC* or *MYCN* (55-58).

Despite the existence of histopathological subtyping and recognized immunohistological and genetic markers of prognosis, risk stratification conducted at the time of diagnosis based on metastatic state and age are currently the only considerations used to design treatment regimens for all patients with MB. It was therefore necessary to develop a new risk stratification system that could reliably classify MB tumors while better predicting prognosis and driving treatment options, something that the previously mentioned histology-based classification system could not do effectively.

1.2.3: Molecular classification of Medulloblastoma subtypes

The need for a better system that could more accurately predict clinical outcome and guide treatment decisions, combined with the advancement of genomic sequencing and microarray technology have recently resulted in the creation of a new MB classification system that, since its introduction, has undergone further subclassification of subgroups. Initial subgroup classification schemes categorized MB into 4 distinct subgroups based on dominant genomic alterations and gene expression profiling; **WNT, SHH, Group 3 and Group 4** (49, 59). This novel molecular classification system could reliably predict patient prognosis and in time has the potential to drive subtype specific treatment regimens (49, 59). Since this initial classification system was published, more recent publications have demonstrated more extensive intratumoral heterogeneity and

further divided the 4 subgroups into additional subtypes (60, 61). Schwalbe et al further classified MB into 7 subtypes based on comprehensive molecular profiling, including DNA methylation profiling (61). The WNT subgroup was unchanged, while SHH was subdivided into age dependent subtypes greater or less than 4.3 years of age. Group 3 and Group 4 were both further split into low-risk and high-risk subtypes. Cavalli et al. (60) further split the 4 subgroups into 12 subtypes based on genome-wide DNA methylation and gene expression data, which enabled enhanced rigor and more definitive subtyping. Although these classification systems have not gained wide spread use clinically due to a lack of reliable subtype-specific immunohistological markers, the 4 subgroup classification system, with further subtyping of SHH into P53 wildtype and P53 mutant, has been adopted by the World Health Organization (62).

The subtypes differ in their demographics, transcriptomes, somatic genetic events and clinical outcomes (49). Of the four, only SHH and WNT variants have well established genetic pathways driving tumorigenesis, while drivers of Group 3 and 4 tumorigenesis are relatively unknown. Genetically engineered mouse (GEM) models are used extensively to study characteristics of MB. With the exception of Group 4, GEM models have been generated for all the MB subgroups that can recapitulate clinically relevant features observed in MB patient tumors.

Both the WNT and SHH pathways, as discussed in the normal development section, play critical roles in the regulation of NSC and GNPC proliferation in the developing hindbrain. Thus, aberrant expression of these pathways and their downstream effectors will result in the uninhibited proliferation of said cellular

populations as cancers are capable of originating from both normal stem cells and more restricted progenitors. Both pathways examined above are specific to the cell type they affect. SHH-controlled proliferation in the cerebellum is restricted to the GNPC population while WNT signaling-controlled proliferation is specific to the NSC population. Thus, it is not surprising that the WNT and SHH variants develop from distinct cell types in the developing hindbrain.

Prior to the reclassification of MB into molecular subgroups, and the development of mutant mouse models for the SHH and WNT variants, it was assumed that all MB tumors had the same cell of origin. Several studies from the late 1990's and early 2000's tried to deduce the cell of origin for MB with differing and conflicting results (63). Previously, it was assumed that MB tumors originated from GNPCs based on the location of the tumors on the surface of the cerebellum and expression of markers commonly associated with GNPs such as CD271/p75NTR, TrkC (tropomyosin receptor kinase C), Zic1 and Math1 in fully formed tumors (64-68). However other researchers have found that MBs express markers associated with normal stem cells such as CD133, *Sox2,* musashi-1, *bmi-1*, maternal embryonic leucine zipper kinase, and phosphoserine phosphatase (69, 70).

Inferring the cell of origin through marker expression in the bulk tumor has limitations. In particular, the early stages of human tumorigenesis are not accessible; therefore researchers typically relied on the analysis of well-developed, often malignant tumors and murine models to make predictions about tumor initiation. Additionally, because tumorigenesis is such a dynamic process, the markers expressed in malignant tumors may not be representative of those

expressed during tumor initiation and early development. However, with a better understanding of the subtype specific driver mutations, a better insight into the molecular characteristics of tumors, and the development of mutant mouse models, we have a significantly better understanding of what initiates these tumors, what drives their development and most importantly how to treat them.

Each MB subgroup has unique demographics, response to treatment, tumor drivers, cells of origin and GEM models used to study them. Below, I will describe each MB subgroup and discuss in detail the following characteristics:

- **Demographics**
- **Driver Mutations**
- **Cell of origin**
- **Mouse models used to study the variant**

1.2.3.a: WNT Subtype

Demographics

The WNT subgroup has the best 5 year survival of all MB subgroups, at close to 90% (49). The 10% that do not survive long term often succumb to complications from therapy or secondary neoplasms caused by radiotherapy rather than WNT MB recurrence (49). WNT tumors represent the smallest group of tumors at just 11% of diagnoses (51). The male to female ratio in WNT tumors is nearly equal. Nearly all tumors in this subgroup (97%) fall in the classic MB category histologically. WNT tumors are not typically seen in infants, with a peak incidence at 10-12 years of age.

WNTα is comprised mainly of children while older patients fall into the WNTβ subgroup (60).

Driver Mutations

The first indication that mutations in the WNT pathway caused a form of MB came from the study of patients with Turcot syndrome, a rare disease that predisposes people to high rates of benign adenomatous polyp growths in the gastrointestinal tract and a 92-fold increased risk of developing MB (71, 72). In addition, somatic mutations of *CTNNB1* encoding β–catenin, *AXIN1* and *APC*, all downstream targets in WNT signaling were found in sporadic MB (73-77). Together this led to the hypothesis that aberrant WNT signaling was the dominant molecular driver of this MB subgroup.

WNTα subgroup has near ubiquitous monosomy 6 while WNTβ are frequently diploid for chromosome 6 (60). The majority of WNT subgroup tumors show stabilizing mutations in the WNT signaling pathway gene *CTNNB1* (catenin beta-1/β-catenin) (70-90%) and monosomy 6 (90%) (49, 51, 78-80). However a small number of WNT subgroup MB tumors lack mutations in *CTNNB1* and *APC*, implying that other mechanisms lead to aberrant WNT signaling and tumorigenesis in these cancers (78, 79, 81). WNT subgroup specific tumors lacking *CTNNB1* mutations have been reported to exhibit mutations in the Cadherin-1 (*CDH1)* gene (78). This protein is responsible for sequestering β-catenin at the cellular membrane, and alterations in this process may also result in aberrant activation of the WNT signaling pathway in this molecular subgroup (82).

In addition to WNT signaling aberrations, approximately 50% of WNT subgroup tumors show mutations in the DEAD Box Helicase 3 (*DDX3X*) gene (78, 80). DDX3X is a RNA helicase that has been implicated in mRNA splicing and processing, translational control, chromosome segregation, cell cycle regulation and cancer progression (83, 84). This is somewhat WNT subgroup specific as only 10% of SHH and no Group 3 or 4 tumors exhibit mutations in the *DDX3X* gene (78, 80). Other mutations such as *SMARCA4*, *CREBBP*, *TRRAP* and *MED13*, all regulators of gene expression through chromatin remodeling, have also been discovered in WNT tumors (28, 78, 85-87). Together, these show that canonical WNT signaling has a strong role in the pathogenesis of this tumor subgroup. However, in addition to stabilization of CTNNB1, formation of WNT subtype MB may require disruption of chromatin remodelling at WNT-responsive genes.

Cell of Origin / GEM models

Tumors of the WNT subtype have been shown to originate in cells outside the cerebellum in progenitor cells of the dorsal brainstem (88). Based on anatomical differences between WNT tumors which are found in the 4th ventricle and infiltrate the dorsal brainstem and SHH tumors which predominately form in the cerebellar hemispheres, it was hypothesized that WNT tumors have a distinct cell of origin (88). Regional expression of a WNT MB 24 gene signature was charted using software that generates 3-dimensional gene expression maps across the developing mouse brain (88). It was found that WNT MB signature genes were predominately

expressed in the lower rhombic lip at embryonic day (E) 11.5 and in the dorsal brainstem at E15.5 (88) (88).

Based on these data, mice were generated that carry concurrent WNT pathway effector *Ctnnb1* (catenin beta-1/β-catenin) mutations in the progenitor populations of the hindbrain. This was done by selectively expressing the mutant *Cttnb1* gene in cells that exclusively express the *Blbp* gene, which includes ventricular zone progenitors, GNPCs of the EGL and Olig3+ progenitor cells of the LRL (88, 89). Additional mice were formed that carried both the *Ctnnb1* mutation and a mutation in the tumor suppressor gene *Tp53*. A third population of mice were generated that selectively expressed mutant Ctnnb1 in only GNPCs using the enhancer of the *Atoh1/Math1* gene.

No persistent cellular masses or tumors were found in the cerebellum or dorsal brainstem of mice harboring the Ctnnb1 tumors in GNPCs (*Athoh1* driven *Ctnnb1* mutations) (88). In contrast, all mice with *Blbp*-driven *Ctnnb1* mutations formed aberrant cell collections in the dorsal brainstem. Upon aging, only mice that harbored a mutation in the *Tp53* gene formed classic medulloblastoma that were confined to the dorsal brainstem and displayed expression profiles similar to WNT-subgroup MB.

In a study by Rogers et al., WNT pathway over activation was induced in a *Myc* immortalized cerebellar progenitor cell line through the overexpression of WNT1 (90). When transplanted into a mouse recipient, cells overexpressing WNT1 formed tumors that resembled classic MB, while control cells did not form a tumor (90). *In vitro*, activation of the WNT pathway inhibited neuronal differentiation

reinforcing previous studies demonstrating that WNT signaling activation keeps this cell population in a more undifferentiated or "stem like" proliferative state (90).

Together, these studies show that *CTNNB1* mutations have little effect on the proliferation and differentiation of GNPCs in the developing cerebellum. More importantly, the WNT MB subgroup has a distinctive cell of origin than SHH MB. WNT MB is caused by aberrant WNT signaling in progenitors of the dorsal brainstem that originate in the LRL of the developing CNS. Pathogenesis of WNT pathway activation in these cells is most likely attributable to the inability of these cells to differentiate and migrate. Remaining in a stem-like proliferative state leads to persistent cellular masses, which in combination with additional cellular abnormities become tumorigenic and malignant. However, the exact cellular lineage of the dorsal brainstem progenitor that initiates tumorigenesis has not been delineated at this time.

1.2.3.b: SHH Subtype

Demographics

SHH tumors occur in a 1:1 ratio in males:females, with this tumor type found predominantly in infants and adults and rarely in children aged 3-16 (49, 59). When they do occur in ages 3-16, these tumors are predominately SHHα (60). SHH tumors make up approximately 28% of all MBs diagnosed, and have an intermediate prognosis similar to Group 4 (see below) (49). The prognosis of SHH tumors differs significantly between age groups. There is a 77% 5 and 10 year overall survival (OS) rate in infants, however that drops to 68% and 51% 5 and 10 year OS in children

and 75% and 34% OS in adults (49). This difference in survival has partly been explained by the most recent MB reclassification system (60). SHHα, which is predominately found in ages 3-16 has the worst prognosis of all SHH subtypes. Infant SHH tumors are mainly distributed across SHHβ and γ. SHHβ has the second worst survival outcome of the SHH subtypes, most likely attributable to its high rate of metastasis (33%) (60). SHHδ has the best prognosis of all SHH subtypes and is primarily found in adults. This difference in survival between age groups has been attributed to the high percent of SHH tumors in infants exhibiting desmoplastic /extensive nodularity which has been shown to be a positive prognostic factor in these young patients (91). Nearly all desmoplastic/nodular variants are of the SHH subtype, however 50% of all SHH tumors are not desmoplastic (49). Cavalli et al showed that SHHγ is enriched for MB with extensive nodularity (MBEN), in that almost all SHH tumors of the MBEN type were SHHγ, however only a minority of SHHγ tumors are MBEN. They also showed that there is no survival difference in SHHγ patients with MBEN and non-MBEN tumors. This reinforces the concept that histopathology is no longer an effective classification system, and that molecular subtyping is necessary to fully understand clinical implications. This also underscores the importance of finding alternatives to histological cellular features for diagnosis and the need for widespread clinical acceptance of the molecular subtype classification system.

Driver Mutations

The SHH signaling pathway is believed to drive tumor initiation in all of the tumors found in this subgroup (49). The link between MB and the SHH pathway was made through studies of individuals with Gorlins syndrome. Hereditary mutations in the SHH receptor *PTCH* result in Gorlin syndrome (also known as devoid basal cell carcinoma syndrome), a disease characterized by macrocephaly, skeletal abnormalities and in some patients a high rate of cancers, including MB (49, 92). Germline mutations of the SHH inhibitor *SUFU* also predispose individuals to MB. Somatic mutations of *PTCH, SMO*, and *SUFU* as well as amplification of *GLI1* and *GLI2* have been found in sporadic MB. All pointing towards the SHH signaling pathway as the primary driver of tumorigenesis in this MB subtype.

Deletion of chromosome 9q, the location of the *PTCH* gene, is limited to SHH MB and is the most common chromosomal abnormality found in the subgroup (21-47%) (51, 59, 93). SHHα is enriched for *MYCN* amplifications, *GLI2* amplifications and for 9q loss, 10q loss, 17p loss and *YAP1* amplification (60). Other genomic abnormalities include gain of chromosome 3q and 9p, and loss of 20p and 21p (93, 94). *TP53* mutation status has also been shown to be an important prognostic factor in the SHH variant MB (95). In a large cohort study, 21% of patients with SHH variant MB harbored a *TP53* mutation. These mutations in SHH tumors are almost exclusively found in patients between the age of 5 and 18, a rare age for SHH tumors. Of these patients aged 5 years and older, 72% of those that died had a *TP53* mutation (95). Patients with a *TP53* mutation exhibited a 5 year OS of 41% + 9% whereas patients with no *TP53* mutation had a 81% + 5% survival. *TP53* mutation status was shown to be the most important independent risk factor in SHH variant

MB when compared to age, sex, histology and presence of metastasis at diagnosis (95). More recent research has shown that TP53 mutations are highly enriched in the SHHα subtype (60). Further analysis showed that TP53 mutations are only prognostic in SHHα tumors and not in non-SHHα tumors. This had been previously shown in the WNT subtype where *TP53* mutations have very little, if any relationship to prognosis (95). Furthermore, *TP53* mutations are not seen in any Group 3 and Group 4 tumors.

Cell of Origin

As previously discussed, during normal development of the cerebellum, SHH signaling plays a crucial role in the proliferation of GNPCs in the EGL. As SHH signaling diminishes, these cells begin to differentiate and migrate inward to the internal granule layer. It has been therefore hypothesized that aberrant SHH signaling will cause prolonged proliferation of GNPCs in the EGL, the anatomical region where SHH tumors originate. Several studies have shown in mutant mouse models of SHH MB that GNPCs are in fact the cell of origin for SHH subtype MB.

Schüller *et al.* demonstrated that acquisition of GNPC identity is essential for SHH MB tumorigenesis in early multipotent progenitors (GFAP+ and Olig2+) and late unipotent (Atho1+/Math1+) progenitor cells of the cerebellum overexpressing SMO (12). Additionally Yang *et al* (96) showed that over activation of the SHH pathway through deletion of *Ptch* can lead to MB in both neural stem cells (GFAP+) and granule neuron progenitors (Atoh1+/Math1+), but only after commitment to, and expansion of, the neuronal lineage. Both these studies show that SHH MB can

form from neuronal stem cells or GNPC progenitor cells of the cerebellum, however, commitment to the GNPC lineage is a necessary step in SHH MB tumorigenesis, confirming that GNPCs are the SHH MB cell of origin.

1.2.3.c: Group 3/Group 4

These two "non-SHH/WNT" subtypes share some similar clinical presentations and molecular characteristics and will therefore be discussed together. Of the four groups, the least is known about Group 3 and 4.

Demographics

Group 3 tumors are found 2:1 in males as compared to females and are observed primarily in infants and children, but rarely in adults (49). Group 3 makes up approximately 27% of MB diagnoses (51). Group 3 patients have the worst prognosis of the four subgroups, with infants having a 5 year OS of 45% and 10 year OS of 39%, while children have a 5 and 10 year OS of 58% and 50% respectively (51). Group 3 tumors have a very high rate of metastasis that is a major contributor to their poor prognosis. Group 3 has recently been subdivided into 3 distinct subtypes, each with distinct copy-number and clinical outcomes (60). Nearly 60% of MB patients under the age of 3 fall into the Group 3α subtype. Clinically, group 3α and 3β have a more favorable prognosis than 3γ, which has the worst prognosis. Group 3β has a low rate of metastasis while group 3α and 3γ have similar rates of metastasis at diagnosis (60).

Group 4 makes up the most common subtype of MB (>40%) (51, 60). Despite this, the Group 4 subgroup is the least understood. (49). Similar to Group 3, the majority of cases exhibit a classic histology, with some desmoplastic and large cell/anaplastic cases (49). Gender distribution is approximately 2:1 males to females, with this subgroup arising across all age groups, peaking in children (59). Prognosis of Group 4 tumors is intermediate, similar to the SHH subgroup (49). Group 4α, 4β and 4γ all show similar survival and metastatic dissemination at diagnosis (60).

Driver Mutations

As opposed to the WNT and SHH subgroups, less is known about the molecular drivers of Group 3 and Group 4 variants. Evaluation of genetic abnormalities and gene expression has revealed that Group 3 is the only variant that has a large amplification and overexpression of *MYC* and not *MYCN* (49, 80). Group 3γ frequently harbors increased MYC copy numbers and have a poor prognosis independent of MYC amplification (60). Previous work by Cho *et al.* in 2011 had proposed subtypes within Group 3 based on the presence/absence of *MYC* amplification. They broke Group 3 into 3α and 3β based on their MYC gene status. Group 3α, those patients with amplification of the *MYC* gene (15%), were at a much higher risk of recurrence and death when compared to those patients with no *MYC* amplification in the subset Group 3β, who have a prognosis similar to patients in Group 4 (97). With the more recent findings by Cavalli et al., the high-risk Group 3 patient population has been expanded to include not only patients with MYC

amplifications as shown by Cho et al. but all Group 3γ tumors regardless of their MYC status (60).

WNT is the only other subgroup that has a high *MYC* amplification; however, it also shows *MYCN* amplification (59, 80). To date, no definitive genetic event or transcriptional pathways have been shown to drive tumorigenesis in Group 4. Group 4 tumors have little to no expression of MYC or MYCN except for a few tumors that show *MYCN* amplification (59, 80). Group 4α is enriched for MYCN amplifications (17%) while no tumors in Group 4β or 4γ showed MYCN amplifications (60). In addition, the oncogenes *OTX2 and FOXG1B* are also amplified and overexpressed in Group 3, as well as Group 4 (59).

Isochromosome 17q is the most common cytogenetic change observed in 66% of all Group 4 tumors and 26% in Group 3 (59, 80, 98). 17p deletion is also seen in these tumors (49). Group 3 tumors are more likely than Group 4 tumors to show gain of chromosome 1q, and/or loss of chromosome 5q and 10q (49).

More recent studies have found that various disruptions of chromatin genes that are associated with histone methylation may be critical events driving Group 3 as well as Group 4 tumor development (78, 80). Mutations in genes including *EZH2, KDM6A, CHD7* and *ZMYM3* appear to disrupt chromatin marking of genes including *OTX2*, *MYC* and *MYCN* (78, 80, 99, 100). Epigenetic disruptions were also found in WNT MB (28, 78, 85-87) and indicate that these mutations are likely subgroup specific and are necessary components of tumorigenesis in the MB subtypes.

Three recurrently mutated genes including *ZMYM3*, *KDM6A* and *DDX3X* are found on the X chromosome (78). *ZMYM3* and *KDM6A* mutations are found almost

exclusively in tumors from males, giving a possible explanation as to why Group 3 and 4 show a bias towards male patients (78, 101). The third gene mutation, *DDX3X* is commonly found in WNT tumors (78). Three out of four female MB tumors show a mutation in this gene that escapes X inactivation, meaning although this mutation is found on the inactivated X chromosome, it is still expressed (78, 102). Interestingly, 80% of all females with Group 4 tumors show a loss of the X chromosome within the tumor (49, 97) thus an additional explanation as to why Group 3 and 4 show an increased bias towards males vs. females while SHH and WNT do not.

Cell of Origin / GEM models

Less is known about the cell of origin for Group 3 and 4 tumors. Two independent groups developed a mouse model that recapitulated Myc-subgroup (Group 3) tumors (103, 104). Overexpression of Myc combined with a mutant p53 gene resulted in highly aggressive tumors that histologically and molecularly resemble Group 3 tumors, albeit using different cells of origin. Kawauchi et al. (103) overexpressed Myc in a GNPC whereas Pei et al. (104) used a cerebellar stem cell (Prominin1/CD133+, Lineage-), both resulting in similar tumor types. Both groups found that expression profiles of their *Myc* driven tumors showed significant similarities with neural stem cells, induced pluripotent stem cells and embryonic stem cells expression profiles suggesting that Group 3 MB may arise from a neural stem cell or a de-differentiated GNP cell that takes on a stem cell like phenotype (103-105).

The Group 4 cell of origin is currently unknown. Studies conducted by Swartling et al. (106, 107) have shown that *N-myc* driven tumors arising from embryonic versus postnatal cerebellar NSCs demonstrate Sonic Hedgehog (SHH) dependence and SHH independence, respectively. However, there is currently no reliable mouse model of Group 4 MB, making it difficult to pinpoint the cell of origin. Clearly, MB subtypes are ontogenetically diverse adding to the complexity of the disease.

1.2.4: Conclusion

The re-classification of MB into 4 molecularly distinct subgroups and up to 12 distinct subtypes has the potential to transform how we treat these tumors and improve the outcome of patients with this disease. Not only does it give researchers a better understanding of what drives these tumors, but based on the literature I have summarized thus far, it is easy to see how treatment regimes can be tailored to each subtype. Despite the advances we have made in understanding the molecular and genetic characteristics of MB and the consequences this has on treatment success, this system is not in wide spread clinical use. The technology currently used to dissect the molecular and genetic profiles of a tumor is expensive and not readily available. We must therefore define new ways to subtype these tumors that are reliable, cheap and accessible in medical laboratories around the world. Additionally, to fully appreciate the power of the new classification system and the data that have been amassed for each subtype, we must now begin to translate our

molecular and genetic knowledge into a better functional understanding of these tumors to truly take this area of research from the bench to bedside.

1.3: Tumor heterogeneity and the evolution of the cancer stem cell hypothesis

More than ever, cancer is now considered to be a highly heterogeneous disease. We now know that tumor heterogeneity plays an important role in treatment failure and recurrence in a wide spectrum of cancers. Tumors are not a homogenous mass of cancer cells but a mixture of malignant cells that display distinct and varying genetic, molecular and cellular characteristics. This includes differences in morphology, gene expression profiles, genetic abnormalities, cellular differentiation, proliferation, response to therapy and metastatic potential (108-111).

Phenotypic and functional tumor heterogeneity can arise in three distinct ways; **genetic and epigenetic changes, tumor microenvironment, and the cancer stem cell hierarchy**. Through these mechanisms, tumor heterogeneity goes on to play an important role in tumor progression, treatment resistance, recurrence and response to therapy.

1.3.1: Genetic/Epigenetic Mechanisms of Heterogeneity

The most well recognized mechanisms leading to heterogeneity are the stochastic genetic or epigenetic changes to tumor cells (112, 113). Extensive heterogeneity exists not only between tumors (intertumoral heterogeneity) but within tumors (intratumoral heterogeneity). A seminal paper in 1976 by Nowell laid out the concept that cancer was an evolutionary process driven by sequential

acquisition of somatic genetic mutations leading to sub-clone selection and expansion (112). Confirmation of this theory has been possible with advancements in next generation sequencing technology. For example, phylogenetic studies have shown that tumor cells from single patients are composed of a heterogeneous mixture of distinct subclones that arise through evolutionary branching (114, 115). The unique mutations in each subclone have varying affects on the cells, leading to distinct cellular characteristics that contribute to heterogeneity. Subclones evolve through mutations that are advantageous, neutral passenger mutations, and mutations deleterious to the cell. Although mutation rates are high, phenotypes that result from these mutations are not as common and the effect these phenotypes have on cellular characteristics is determined by what genes are mutated. This intrinsic type of selection is also known as clonal evolution and typically leads to a more aggressive cancer as cells that gain favorable changes will thrive while cells within the tumor that do not gain or lose favorable characteristics may undergo senescence or cell death (112).

Genetic inter- and intratumoral heterogeneity have real consequences when trying to effectively study and treat cancers. A study using renal cell carcinoma looking at mutations across spatially distinct regions of the tumors found that 63% to 69% of all somatic mutations were not detectable across all tumor regions (116). Furthermore, gene expression profiles associated with good and bad prognosis were found within the same tumor in differing regions (116). A similar study looking at 11 glioblastoma tumors displayed multiple unique transcriptome subtypes within each tumor when several distinct tumor fragments were analyzed

(117). Genetic expression profiles linked to positive and negative prognosis are directly related to differences in response to therapy between sub-clones. Chemotherapy agents destroy fast dividing cells while sparing the more dormant cellular types. Therefore, therapy can result in further clonal evolution by selecting for the most resistant types of cells allowing them to proliferate, self-renew and/or migrate/invade while cells lacking selective mutations are abrogated (118-120). Several studies in leukemia have shown that patients that relapse frequently harbor a clonally different tumor type than the clone that formed the primary tumor (121, 122). In approximately 50% of cases, the sub-clone that caused relapse shared limited genetic identity with the dominant primary sub-clone.

Clonal diversity between primary and metastatic tumors has also been shown in cancers such as pancreatic cancer (123, 124), breast cancer (125) and medulloblastoma (MB) (126). Wu *et al.* showed that genetic mutations found in the MB metastasis could only be found in a limited subclone within the primary tumor indicating that only unique and rare subclones in the primary tumor have the ability to metastasize (126). Similar results were recently shown by Morrissey et al. (127). After tumor resection and image-guided radio therapy was performed on a genetic mouse model of recurrent Shh MB, it was found that there was "substantial genetic divergence" between the primary tumor and the dominant clone responsible for recurrence post therapy (127). In both mice and human cases, the dominant clone that caused recurrence after therapy was a rare clone found in the primary tumor (127). Further complicating the situation, targeted therapy against the primary tumor will most likely be ineffective against recurrent disease resulting in failed

clinical trials and no significant benefit to the patient. These results show that complex branching evolution gives rise to distinct subclones that differ in their aggressiveness and response to current and next generation targeted treatment strategies.

In addition to genetic mutations, researchers are beginning to understand the importance of non-genetic factors such (i.e. epigenetics) play in tumoral heterogeneity. Epigenetics is defined as heritable changes in genetics without a change in DNA, such as DNA methylation, histone modifications, microRNA (miRNA) and other non-coding RNA (ncRNA), all factors that can control gene expression (113, 128, 129). As briefly mentioned in the "driver mutation" sections of WNT and Group 3/4, mutations in epigenetic controllers such as DDX3X, *ZMYM3*, *KDM6A, SMARCA4*, *CREBBP*, *TRRAP* and *MED13* have all been linked with MB tumorigenesis (28, 78, 80, 85-87). Epigenetic factors have also been associated with a variety of cancers and correlated with tumor propagation, self-renewal, tumor progression and response to therapy (130-134).

Although genetic sequencing and epigenetic studies have enabled a better understanding of the heterogeneity in subclones that make up the tumor, challenges still exist as to how to prioritize and fully utilize this information. For example, what cells drive these tumors and are they clonally distinct from one another? What clones are capable of metastasizing, and what further evolution will occur during tumor progression? To better answer these questions, one must complement these sequencing studies with functional assessments.

1.3.2: Tumor microenvironments contribute to intratumoral heterogeneity

In addition to stochastic events, extrinsic factors such as the tumor microenvironment can result in phenotypic and functional changes. Tissue microenvironments are complex with a multitude of factors such as extracellular matrix components, hypoxia as well as a variety of cellular components including endothelial, epithelial, stromal and immune cells that can influence nearby malignant cells. Research has shown that conditions within a tumor can provide selective pressure for tumor evolution and progression to invasion (135). Tumor environments continuously select for cells that exhibit the greatest survival and proliferative capacity. Hostile tumor micro environmental factors such as anoxia and a diverse extracellular matrix have been mathematically theorized to exert a greater pressure on the tumor cells within that environment than cells that are found in less hostile microenvironments (136). This results in a selective pressure of the more aggressive tumor subclones leading to clonal evolution and in some cases invasion and metastasis. It is well recognized that tumorigenesis is highly influenced by the microenvironment (135, 137, 138). Links to tumor microenvironment and its potential for initiating stem cell programs in cancer have been recently recognized. However the exact mechanism by which the microenvironment exerts these effects is still not well understood and a better understanding will be crucial to fully elucidate the mechanisms associated with tumor heterogeneity.

1.3.3: Cancer stem cells and their contribution to tumor heterogeneity

The differentiation of stem-like cells in a tumor provides a mechanism for the generation of phenotypic and functional heterogeneity that cannot be fully attributed to clonal evolution and environmental pressures. Over the past 20 years, researchers have developed the cancer stem cell (CSC) hypothesis. This hypothesis proposes that there is a population of cells within a tumor that display stem cell like properties; the ability to self-renew (maintain themselves in a primitive stem cell state), and the ability to undergo multi-lineage differentiation (139) (Figure 1.5). That is, tumorigenic cancer stem cells differentiate into non-tumorigenic cancer cells (cells that are no longer able to propagate the tumor) while concurrently forming successive cancer stem cells that propagate the tumor indefinitely.

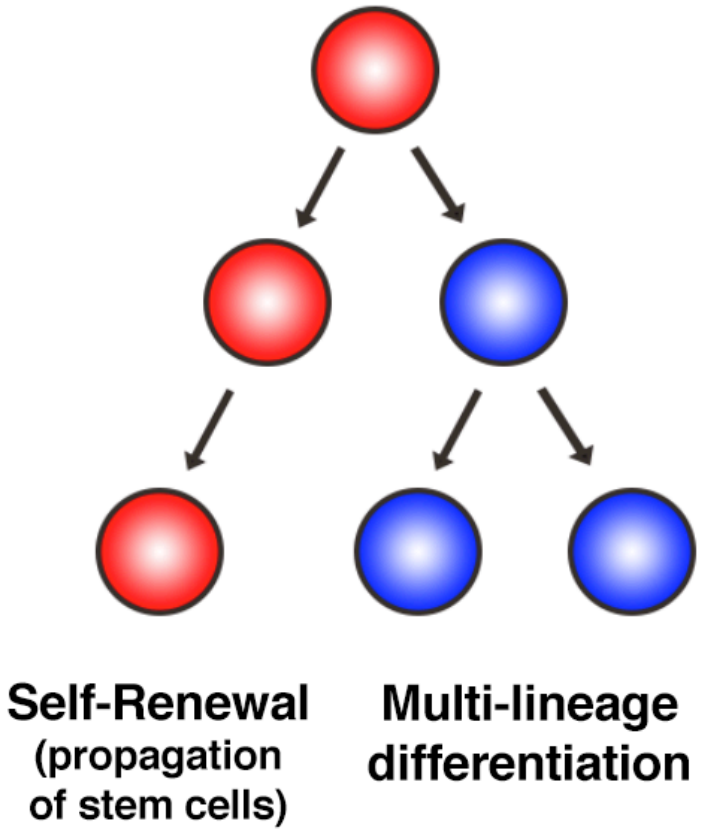

Figure 1.5: Stem cells and cancer stem cells must possess two characteristics, self-renewal and multi lineage differentiation. Self-renewal is the ability to propagate oneself indefinitely. This is a characteristic only stem cells possess. Progenitors cells also have the ability to self-renew, however they will eventually exhaust that ability and terminally differentiate. Self-renewal can occur as asymmetrical division, as shown above whereby one stem cell gives rise to one stem cell and one further differentiated cell. In asymmetrical stem cell division, the stem cell population is never expanded staying at a constant number. Alternatively, stem cells can undergo symmetrical division, whereby one stem cell gives rise to two stem cells (not shown). This allows the stem cells to expand increasing the number of stem cells. NB. Red denotes a stem cell, blue denotes a further differentiated cell such as progenitor or terminally differentiated cell

The modern concept that cancers maintain an element of normal developmental programs goes back to seminal studies performed on teratocarcinoma, lung cancer and breast cancer in the 1960's, 70's and 80's (140-144). These studies proposed that tumors were made up of a mixture of differentiated cells that originated from stem-cell-like cells within the tumor. Similar observations were made using cytokinetic labeling in leukemia. It was shown that lineage restricted "blasts" were replenished by a rare highly proliferative cell population, which were theorized at the time to be produced from a slowly cycling leukemic "stem cell" (145-147). All of these studies would lay the foundation for the hypothesis that several forms of cancer are propagated by a stem-cell-like population that was capable of forming a hierarchal organization within the tumor, "similar" to the hierarchical development seen in normal development.

While the idea of cancer stem cells dates back several decades (148), it was the development of fluorescence activated cell sorting (FACS) (149) and improvements in xenografting techniques into immunodeficient mice that allowed the seminal work in 1994 by Lapidot et al. and Bonnet and Dick in 1997 to be performed (150, 151). These two studies would form what is now known as the modern cancer stem cell hypothesis. Lapidot et *al.* were able to show in severe combined immunodeficient (SCID) mice that AML is initiated by a relatively rare cellular population that could be selectively isolated by sorting on the surface marker combination of CD34+CD38- using FACS (151). These cells, termed the SCID leukemia initiating cells (SL-IC) were capable of homing to the bone marrow, proliferating and recapitulating the leukemic cell morphology found in the

originating patient (151). Although they suspected that these cells were stem cells and not progenitors, researchers at the time were unable to show conclusively that the leukemia-initiating cell was in fact an AML stem cell due to limitations in the mouse models available.

With the development of the non-obese diabetic severe combined immunodeficient (NOD SCID) mouse (152), Bonnet and Dick were able to prove this rare CD34+ CD38- cell population was in fact a stem cell and not a more mature progenitor (150). This was made possible using secondary transplants in NOD SCID mice, something that researchers were unable to accomplish using the SCID mouse due to significantly lower engraftment rates requiring much higher human cell numbers. Most progenitors in AML, also knows as blasts, have limited proliferative capacity and must be constantly replenished by primitive cells capable of self-renewal. Therefore, the capability of this cellular population to be serially transplanted from mouse to mouse and recapitulate the original tumor was proof that the SL-IC was in fact a leukemic stem cell capable of self-renewal *in vivo* and not a more mature progenitor cell providing the first proof of the modern day cancer stem cell hypothesis (150).

Since this pioneering work, researchers around the world have demonstrated the existence of cancer stem cells (more correctly referred to as tumor initiating cells (TIC) or tumor propagating cells (TPC)) in a variety of solid tumors including breast (153), brain (70, 154), colon (155, 156), pancreatic (157) and ovarian (158-161) to name a few. Breast cancer was the first solid tumor to be shown to follow the cancer stem cell model. Al-Hajj *et al*. demonstrated that breast

cancer TICs, the population solely responsible for capitulating the tumor, could be isolated using the cell surface markers $CD44^{+}CD24^{-}$ (153). This population was capable of serial transplantation in immunodeficient mice with resulting tumors recapitulating the parent tumor. Each of these seminal studies in solid tumors showed that tumor propagation was restricted to a phenotypically defined population of cells responsible for hierarchal organization.

The existence of brain tumor CSCs, also known as brain tumor propagating cells (BTPC) was first demonstrated by Singh *et al*., using the cell surface marker CD133 to select for a cell population showing increased self-renewal *in vitro* and *in vivo* (70, 162). Although highly conserved throughout the animal kingdom, little is known about the biological function of CD133. Also known as Prominin 1, CD133 was first used as an alternative to CD34 to isolate human hematopoietic stem cells and early progenitors (163). Several years later, Uchida et al. revealed that CD133 could be used to isolate normal human neural stem cells (NSC), referred to as central nervous system stem cells (hCNS-SC) (164). Single cells sorted on CD133 were capable of neurosphere initiation, self-renewal, expansion and multi-lineage differentiation into neurons and glial cells, all characteristics of neural stem cells (164).

While CD133 is the most commonly utilized BTPC marker, more recent studies have shown that CD133- cells exhibit self-renewal capacity and can generate highly aggressive tumors *in vivo* (70, 162, 165). This is complicated by the fact that CD133 is not exclusive to the TPC populations and is also expressed in normal stem cells and a variety of differentiated epithelial cells (165). In addition, stage specific

embryonic antigen (CD15/SSEA1) has also been shown to select for cells that have tumorigenic capacity in a *Ptch* mutant mouse model of Shh MB (166, 167). Read et al. (166) demonstrated that tumors are not propagated by a stem-like $CD133^+$ population but by cells marked by the neuronal progenitor markers Math1 and CD15. Ward et al. also demonstrated the tumorigenic capacity of $CD15^+$ cells from $Ptch^{+/-}$ mice; however, these authors suggested that the $CD15^+$ population represents a stem-like rather than a progenitor cell phenotype (166, 167). Our laboratory has recently shown that CD271, also known as p75 neurotrophin receptor (p75NTR), a nerve growth factor receptor (NGFR) selects for a neural precursor or stem/progenitor cell in a SHH variant human medulloblastoma (168). This is the subject of the results section presented in Chapter 3.1.

More recently, the stem cell marker Sox2 has been shown to play a role in SHH MB tumor propagation (118, 169). Vanner et al (118) showed that the $Sox2^+$ cell population was enriched following treatment with chemotherapy and SHH pathway antagonists, resulting in tumor growth and relapse. This $Sox2^+$ population was shown to have a higher colony forming capacity *in vitro* when compared to the $Sox2^-$ population, as well as a higher tumor initiating capacity when allografted into immunodeficient NOD SCID gamma (NSG) (118). In the bulk tumor, 40% of *Ptch* tumor cells were CD15/SSEA-1^+, with more than 80% of $Sox2^+$ cells concomitantly displaying CD15/ SSEA-1, however less than 10% of CD15/ SSEA-1^+ cells were $Sox2^+$. Ward *et al.* and Read *et al.* demonstrated that CD15 can be used to isolate TPCs in *Ptch* driven mouse models of SHH medulloblastoma, however further work

by Vanner *et al.* has shown that in order to reliably isolate the TPC population, CD15 must be used in combination with Sox2 (118, 166, 167).

It is important when studying TICs to understand that not all TICs are the same within a cancer and TICs are not static but rather a continually fluctuating cell type. In light of recent research in the field, it is becoming commonly accepted that TICs and the non-tumorigenic cells exhibit extensive cellular plasticity (170). Research conducted within our laboratory has shown that the cell surface marker CD271 marks a progenitor or lower self-renewing stem cell in a subtype specific manner in SHH variant MB but not WNT, Group 3 and Group 4 variants (171). TICs are also not static and do not always follow the strict hierarchy normal stem cells do. *In vitro* studies in cell lines have shown that not only can enriched sorted populations of TICs give rise to non-TICs but sorted populations of **non-TICs can give rise to TICs** (130, 134, 172). This can happen spontaneously based on the context in which the cell is found, or can be done deliberately as Chaffer *et al*. showed using epithelial-mesenchymal transition (EMT) factors (173). This shows that cells can turn on and off the ability to self-renew and re-enter the stem cell state depending on the context they are found.

More recently, three histologically identical but molecularly distinct tumor subtypes were described in the SHH MB Patched (*Ptch*)+/- mouse model (174). These subtypes were cell of origin dependent, with cell state dictating the resulting subtype of the tumor. These three tumor subtypes were classified based on their ability to form tumorspheres in serum free neural stem cell (NSC) media containing the growth factors epidermal growth factor (EGF) and fibroblast growth factor

(FGF): (Growth factor dependent [GFD]), serum free NSC media void of growth factors (Growth factor independent [GFI]) or the inability to form spheres in either media (NG) (174). It was found that tumor cells formed by SHH activation in early NSCs formed exclusively GFD subtype tumor initiating cells (TIC) whereas tumor cells formed by activation of SHH in committed EGL progenitors (GNPCs) formed exclusively NG subtype tumor cells that were not capable of forming tumorspheres *in vitro*. Activation of the SHH pathway in NSCs resulted in tumors in young mice whereas activation in GNPCs lead to tumors forming in adult mice, leading the authors to question if childhood and adult SHH MB may have different cells of origin (174). Interestingly, GFD TICs when exposed to cyclopamine, a potent SHH pathway inhibitor, did not rely on the SHH pathway for proliferation, self-renewal or survival. This further demonstrates that heterogeneity of a tumor plays an important role in targeted therapy resistance when using pathway inhibitors against drivers of the bulk tumor.

However, not all cancers contain cancer stem cells and heterogeneity alone does not indicate the existence of a cancer stem cell hierarchy. For example, B cell lymphoblastic leukemia has an unusually high frequency of tumorigenic cells that do not show hierarchal organization in a mouse model of the disease and appear homogeneous in patient samples (175). These characteristics indicate that B cell lymphoblastic leukemia does not follow the cancer stem cell hypothesis (175). Kelly *et al*. demonstrated that as little as 10 cells (10% of the tumor cell population) from transgenic mouse models of B cell lymphoma, thymic lymphoma and AML could be used to initiate tumors when transplanted into recipient mice (176). In addition,

Quintana et al showed that formation of melanoma by injection with a single tumor cell was possible in 1 out of 4 mice (25% of tumor cell population) when using NSG mice that are more highly immunocompromised as compared with non-obese diabetic severe combined immunodeficient variety (177). However hierarchal organization of the resulting tumors was not investigated and it is important to note that frequency is not a defining characteristic of a cancer stem cell. This cellular population needs not be rare to adhere to the cancer stem cell hypothesis (139). In addition, the cancer stem cell model does not infer that the cell of origin is a normal stem cell. Hierarchal organization can result from normal stem cells acquiring mutations that result in over-activation of the self-renewal program (96, 178). However a tumor with hierarchal organization can also arise from a progenitor or differentiated cell that has undergone mutation and subsequently turned its self renewal program back on leading to a more shallow cellular hierarchy (179-181).

In the end, functional and phenotypic heterogeneity within a large portion of cancers are most likely driven by all three forms of influence; clonal evolution, microenvironment pressures and the cancer stem cell hierarchy. Tumor heterogeneity has real consequences on treatment success in both the primary tumor and recurrent disease. All three mechanisms play important roles in contributing to therapy resistance and recurrence and must be fully understood when developing new therapy strategies. As discussed in Morrissy *et al.,* clonal heterogeneity between primary and recurrent tumors is most likely responsible for clinical trial failure in a large portion of cutting edge targeted drug trials (127). Strong evidence that therapy resistance and stemness are linked has been shown in

a variety of solid cancers including MB, glioblastoma, colon cancer, breast cancer, and several others (118-120, 182-184). In addition, studies in leukemia have shown that subclonal genetic diversity exists between functionally defined tumor initiating cell populations (185-187). One could therefore envision a model in which the dominant clone that makes up the majority of the primary tumor is ablated by standard therapy. Meanwhile, due to subclonal genetic diversity within the tumor initiating cell population, a rare non-dominant clone survives and is capable of causing recurrence in the same location or metastasizing to a distant site (Figure 1.6). Not until we fully understand each individual factor and how it contributes to heterogeneity will we be able to effectively treat both the bulk tumor and the cells responsible for tumor propagation and recurrence.

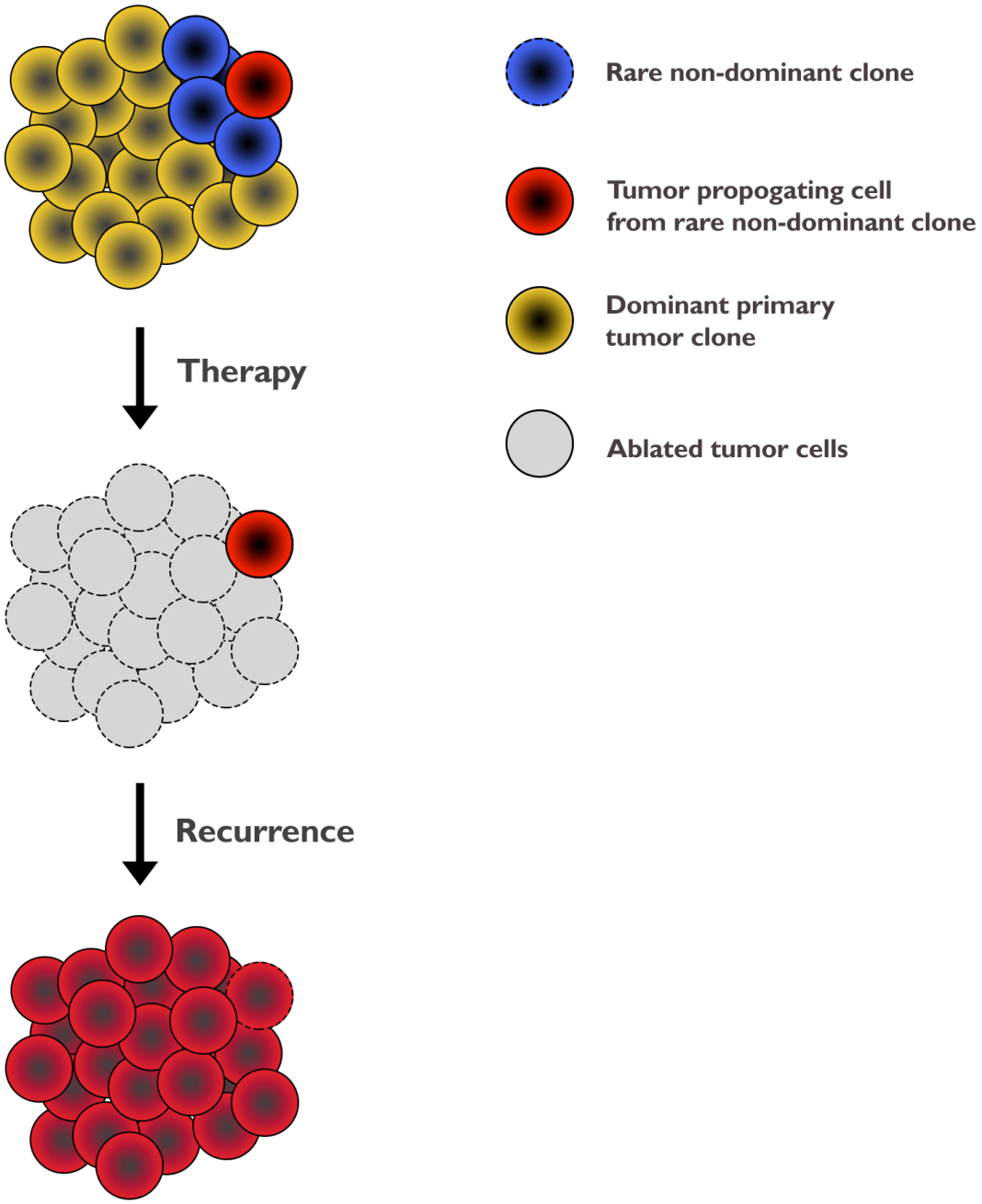

Figure 1.6: Subclonal genetic diversity and the tumor propagating cell population play an important role in therapy resistance and recurrence. Bulk tumors are typically made up of several genetically distinct subclones. One or several subclones are dominant and make up a large portion of the tumor. Additionally, genetically distinct tumor propagating cell subclones are also present within the tumor. Following treatment, a rare non-dominant subclone frequently causes local or distant recurrence thereby reducing the effectiveness of any targeted therapy strategies used to treat the primary tumor.

1.4: Modeling of cancer stem cells

A large portion of this section comes directly from Aiken and Werbowetski-Ogilvie, 2014 (188) with permission from the publisher.

1.4.1: *in vitro* modeling of cancer stem cells

Stem cells and cancer stem cells must display two characteristics to be considered a "stem cell", self-renewal and multi lineage differentiation (139). In order to study the function, regulation and role in disease, we must use *in vitro* and *in vivo* models. These models must be able to distinguish stem/progenitor cells from more differentiated cells by their ability to self-renew and differentiate. Although a multitude of surface markers have been found to mark normal and/or cancerous stem cells, reliability is an issue and therefore stem cells have historically been studied using assays that can measure their functional characteristics (189).

While functional *in vivo* modeling of stem cells is the gold standard, *in vitro* assays have numerous advantages such as simplicity, short experiment times and strict control of experimental variables. Normal stem cells and cancer stem cells that possess the ability to self-renew are typically grown in low adherent conditions as sphere in serum free medium supplemented with fibroblast growth factor (FGF) and epidermal growth factor (EGF) (189). Reynolds and Weiss performed the first *in vitro* culture of stem cells in 1992, in which they grew neural stem cells from the subventricular zone of an adult human brain as floating spheres in serum free media in the presence of EGF (190). To demonstrate self-renewal, spheres were dissociated into a single cell suspension and passed into secondary culture, where a

population of cells again gave rise to neurospheres. Further, when plated onto an adherent dish and EGF withdrawn, cells from dissociated spheres formed neurons and glial cells, proving that these cells were neural stem cells (190).

Further research determined that neural stem cells could be cultured from all ventricular areas of the nervous system, however EGF and FGF were needed to grow stem cells that originated outside the SVZ (191, 192). It was discovered that the neurosphere assay needed to be performed at clonal density. Clonal density is defined by the density of cells (cells per µl of media) that allows spheres to form from a single cell, which corresponds to 0.2 - 20 cells per µl (189, 193). Theoretically, each sphere that forms in a neurosphere assay is derived from a single clonal stem cell. Additionally, the spheres were determined to be composed of cells in all states of differentiation, from stem cells, progenitors and further differentiated cell types. Thus, the neurosphere assay was developed to quantitatively measure the number of *in vivo* stem cells in tissue and enrich for cell populations that had the capability to self-renew and differentiate. Not only can this assay be used to measure self-renewal in normal stem cell populations, it has been utilized by the cancer stem cell research community to enrich for and measure self-renewal in cultured populations of tumor cells demonstrating stem cell properties.

When used to measure the self-renewal of a cancer cell population, this assay is termed tumorsphere assay. Despite the *in vitro* tumorsphere assay being an excellent measure of self-renewal, the gold standard technique to measure self-renewal of cancer cell populations is still *in vivo*. Limiting dilutions combined with serial passaging into immunodeficient mice allows the quantitative measurement of

self-renewing population. Dissociated human tumor cells can be isolated from normal mouse nervous system cells using fluorescent activated cell sorting and re-xenografted into a new mouse producing the *in vivo* equivalent of the tumorsphere assay. Self-renewal is then measured by the ability of the cellular population to maintain tumor initiation capacity through subsequent passages. The remainder of this chapter will focus on the animal modeling of cancer stem cells and the controversy and limitations of this technique. Comparative results in xenograft and GEM (transgenic and knockout) animal models will be discussed. Each model will be evaluated in terms of putative CSC frequency, cell surface phenotyping and correlation with in vitro stem cell assays, as well as hierarchical arrangement of cell populations within tumors. Emerging alternative systems such xenograft zebrafish models are also examined.

1.4.2: Xenotransplantation assays, GEM models and the frequency issue

Xenotransplantation into immunodeficient mice has become the gold standard for evaluation of CSC properties from human tumors *in vivo*. Researchers have used this assay to determine the tumor initiating capacity of both unsorted and sorted fractions of human cells based on specific combinations of cell surface markers in a variety of cancers. Dissociation of primary tumors and transplantation into secondary mouse recipients enables one to evaluate self-renewal in vivo. Combined with data from limiting dilution analysis, the results for primary and secondary tumors are used to calculate a tumor-initiating cell frequency using a maximum-

likelihood estimation method (194, 195). This will determine whether a small or large subset of cells from different cancers can initiate tumor growth.

While utilization of this assay to define CSCs has led to seminal findings in cancer research, it should be emphasized that human cells in a mouse microenvironment differ from those cancer cells that grow and thrive in patients. Mouse and human tissues exhibit differences between their normal tissue stroma (196). It is well known that the normal cell microenvironment, consisting of stromal fibroblasts, vascular networks, extracellular matrix and autologous immune cells, plays an important role in regulating tumorigenesis (197). This includes both positive and negative effects on tumor growth and maintenance (197). There are obviously vast differences in the immune cell function between autologous and xenogeneic systems. Case in point, transplantation of human cells into even more immunodeficient mouse models has yielded very different results from those studies utilizing NOD/SCID mice. Quintana et al. (177) demonstrated that transplantation of melanoma cells into the highly immunocompromised NOD/SCID IL2Rγ^{null} mice led to an increase in the detection of tumorigenic cells by several orders of magnitude. NOD/SCID IL2Rγ^{null} mice lack natural-killer cell activity relative to NOD/SCID mice and therefore provide an even more permissive environment for successful engraftment of human cells. In fact, compared to the tumor-initiating capacity of 1 in 1 090 000 in NOD/SCID mice (198), xenotransplantation assays in NOD/SCID IL2Rγ^{null} mice resulted in an average of 1 in 9 melanoma cells forming tumors (177). These results indicate that modified *in vivo* assay conditions can dramatically change the CSC output, and that in some cases,

tumors that appeared to have a rare subpopulation of tumor initiating cells or CSCs were actually maintained by a large number of cells with tumorigenic capacity.

While rarity is not a prerequisite for tumor-initiating capacity in melanoma, for other cancers such as AML, transplantation of human cells in multiple mouse models still supports the CSC hierarchical model and the maintenance by a relatively less frequent subpopulation of tumor cells (199). For example, detection of long-term engrafting and self-renewing leukemic stem cells was demonstrated with transplantation of as few as 10^3 highly purified CD34+/CD38-human AML cells into NOD/SCID IL2Rγ^{null} mice (119). Even with this improved, more permissive xenograft assay, CSC populations in AML still appear to be relatively rare. Kennedy et al. (199) reported similar findings using a model of human B cell acute lymphoblastic leukemia (B-ALL). The frequency of leukemic stem cells in these tumors was approximately 1% (199), and increased by orders of magnitude above previously reported results (177). Most recently, Eppert et al. (200) used stem cell gene expression signatures from functionally validated sorted primary human AML fractions to predict poor patient prognosis. These studies underscore the clinical relevance of CSC populations and suggest that these cellular phenotypes are not merely an artifact of xenotransplantation (200).

As the use of more immunodeficient NOD/SCID IL2Rγ^{null} mice gained momentum, researchers began to conduct side-by-side experiments with other mouse models. Most recently, Ishizawa et al. (201) directly compared the growth of human pancreatic, head and neck carcinomas and lung cancers in NOD/SCID and NOD/SCID IL2Rγ^{null} mice. Despite an up to 10-fold increase in the detection of

tumorigenic cells in NOD/SCID IL2Rγ^{null} mice and extensive variability within tumors, the frequency remained relatively low at less than 1:2500 cells for all tumors investigated (201). However, there were notable differences between the malignancies studied. For example, the frequency of CSCs in pancreatic and head and neck cancer did not significantly differ between NOD/SCID and NOD/SCID IL2Rγ^{null} mice (201). In contrast, there was a statistical increase in the readout for all cases of squamous cell lung carcinoma when tumor cells were injected into NOD/SCID IL2Rγ^{null} mice (201). Similar results were obtained for comparative studies in high-grade serous ovarian cancer where the frequency of CSCs was significantly higher in 4 of 10 cases when injected into NOD/SCID IL2Rγ^{null} mice (160). As the more permissive NOD/SCID IL2Rγ^{null} microenvironment did not alter the functional characteristics of pancreatic and head and neck CSCs, perhaps these malignancies more closely adhere to the CSC model.

As putative human CSCs must be transplanted into immunocompromised mice to effectively assay tumor initiation *in vivo*, this has led to questions regarding the relevance of certain models in recapitulating human disease. Perhaps one of the most contentious issues among scientists studying CSCs is the frequency of this subpopulation within a tumor. Researchers have reported a wide variation in the percentage of cells that can initiate tumorigenesis using xenograft models (139). For cancers such as melanoma, animal models like NOD SCID mice vastly underestimate the frequency of tumorigenic cells (177). However, it should be noted that rarity is not an obligatory feature of CSC populations. A higher cell frequency does not exclude a subpopulation from following a CSC hierarchical model. It has been

suggested that these common tumorigenic cells may be part of a more "shallow" or limited hierarchy (139). However, cancers such as malignant peripheral nerve sheath tumors, exhibiting a higher frequency of tumorigenic cells, have yet to be hierarchically evaluated (202). Interestingly, melanoma has also been one of the few cancers to be reprogrammed by nuclear transfer (203) as well as by ectopic expression of Oct4, Klf4 and c-myc to the induced pluripotent stem (iPS) cell state (204). Perhaps the incredible plasticity and adaptability of melanoma cells in various microenvironments suggests that these tumor cells may be the exception and not the rule in CSC biology.

While serial xenotransplantation assays and limiting dilution analysis are traditionally the gold standard for in vivo assessment of putative human CSC populations, these models have been plagued by a series of technical issues. Murine microenvironments and inappropriate immune responses combined with variations seen with transplantation site, recipient mouse sex and strain have prompted scientists to move towards studying CSC properties in immunocompetent, genetically engineered mouse (GEM) models.

Kelly et al. (176) were the first to challenge the notion that CSCs are a rare subpopulation by reporting that tumorigenic cells were more common in certain mouse models of lymphoma (both B cell and T cell) as well as a PU.1 deficient model of AML. Transplantation with as few as 10 cells resulted in tumor development (176). Similar trends were also observed using a mouse model of B-ALL (175).

For solid tumors, higher frequencies of CSCs or tumorigenic cells have been reported in mouse models of melanoma (205), peripheral nerve sheath tumors

(202), breast (206) and brain (207, 208). Buchstaller et al. (202) reported a range of tumorigenic cell frequencies using multiple mouse models of peripheral nerve sheath tumors. Frequency was dependent on both the genotype of the mouse model utilized and the specific assay conditions used to report tumor-initiating capacity (202). Similarly, Tamase et al. (207) demonstrated that the tumorigenic cell population varied from about 16-50% in individual brain tumors derived from a Ras induced p16Ink4a/p19Arf-deficient mouse model of glioblastoma combined with a GFP reporting system. However, in this model system, the authors did not distinguish between stem cells and progenitors suggesting that either or both cell types could contribute to the tumor-initiating capacity (207). Collectively, these studies using GEM models have underscored the notion that tumors do not have to be driven by a rare CSC phenotype. In many instances, the tumorigenic cell frequency is upwards of 50% or more. As rarity is not a prerequisite defining feature of CSCs, it is becoming increasingly acceptable for a more common cell population to be considered a CSC, tumor initiating or propagating cell.

1.4.3: In search of new and improved *in vivo* models

As CSC research moves forward, we will continuously look for ways to improve existing models and optimize methods for putative CSC detection. Researchers are now working with more "humanized" xenograft models by co-injecting human cancer cells or sorted cancer cell populations with normal carrier cells (172) or extracellular matrix proteins such as Matrigel (160, 177, 209). To date, these methods have been successful in not only enhancing the readout or

frequency of cells with known tumorigenic capacity, but also the number of different phenotypes capable of transplanting disease. *In vivo* models that combine tumor cell populations and accessory proteins or support cells represent a step towards a more realistic view of the true complexities of the heterogeneous tumor microenvironment.

Recent studies have proposed other systems for the study of CSC populations. For example, Barbieri et al. (210) have isolated CSC-like cells from feline mammary carcinoma. Upon injection into NOD SCID mice, these cells generate heterogeneous tumors that recapitulate the original phenotype (210). Cocola et al. (211) have conducted similar experiments with canine mammary carcinoma. Eguiara et al. (212) have proposed using zebrafish xenograft models as an alternative to the highly expensive mouse experiments that require more maintenance and can last upwards of several months. In particular, zebrafish embryos were utilized as a functional assay for breast cancer stem-like cell identification (212). Zebrafish are increasingly employed as useful pre-clinical models for therapeutic testing and high-throughput screening, as they can be bred in large numbers, are easy and inexpensive to maintain, are immunodeficient for up until 11 days post-fertilization and are therefore permissive to human cancer cells (213-215). Using this model system, Eguiara et al. (212) found that breast cancer cell lines grown as tumorspheres formed masses and migrated to the tail at a higher frequency then cells grown as monolayers. While definitely not mainstream, the zebrafish model may provide a viable alternative for future large-scale studies that attempt to identify new therapeutic strategies specifically aimed at eradicating the

CSC population.

1.4.4: Conclusion

The last 20 years have been an exciting time in cancer research. With the identification of CSC populations in a variety of cancers including leukemia (151, 216), breast (153), brain (162, 217), colon (155, 218), pancreatic (157) and ovarian cancers (159-161, 219), researchers are now focusing their efforts on finding new therapies that will specifically target and eradicate this cell population. Despite these intensive efforts, CSC theory has been riddled with controversy. The *in vivo* models used to define these populations have several caveats including differences in frequency or readout of CSCs, discrepancies in the cell surface markers that select for CSCs, and variation in the number and phenotype of cell populations that display tumorigenic capacity. Furthermore, the relationship between CSCs and highly invasive or metastatic cells is still underdeveloped with few studies to date directly comparing these properties (220-225). In our laboratory, we have shown that medulloblastoma tumorspheres from cell lines exhibit downregulation of a cell motility transcription program *in vitro (168)*. It will be interesting to see whether highly malignant pediatric brain tumor cells in a "stem cell state" also display this same suppression of cell motility genes *in vivo*. An inverse correlation would suggest that drugs targeting cells in the migratory or invasive state will not abrogate the putative CSCs in a state of enhanced self-renewal. Furthermore, recent studies demonstrating interconversion between stem cell and more differentiated states raise more questions: Will one cell phenotype compensate for another following

treatment, thereby negating the long-term benefit of cell-directed therapies? If CSCs are a "moving target", then how can we expect to tackle the daunting task of completely eradicating them? Our long-term goal is to identify novel therapeutic targets that will eliminate not only the cells responsible for tumor initiation and propagation but also the highly infiltrative cells that are the basis for recurrence.

Whether most or only a few cancers follow a CSC model remains an unanswered question. *In vivo* transplantation assays combined with more cell specific marking and fate mapping and advanced imaging technologies will be imperative for the future. Whether your system of choice is a "humanized" xenograft, a GEM or a zebrafish, we will continue to question whether these models can ever truly recapitulate the human tumor microenvironment? However, any cell population that displays the ability to initiate tumorigenesis, to maintain it, or to invade and/or metastasize in any model system should be carefully studied and dissected. As optimization of animal models continues, and our understanding of cancer stem cell theory evolves, our view of CSCs within a heterogeneous tumor environment will likely become even more complex.

Chapter 2: Materials and Methods

2.1: Culture of cell lines and primary MB cells

Daoy human MB cells (originally derived from a desmoplastic cerebellar MB(226)), D341, and D283 were purchased from the American Type Culture Collection (ATCC, Rockville, MD, USA). D341 (227) was utilized as a representative of Group 3 MB. D283 cells (228) have been classified as Group 4 (229); however, other studies suggest that this cell line is Group 3 given the high c-myc levels (230). Daoy cells were cultured in Eagle's minimum essential media (EMEM) (ATCC) containing 10% FBS (Fisher Scientific, Ottawa, Ontario). Upon reaching confluency, cells were dissociated in Accutase (Invitrogen, Burlington, ON, Canada) and passed 1:10. Daoy MB subclones were derived by single cell deposits into 96-well plates using flow cytometry as described (168). MED311-FH cells were obtained from Dr. James Olson (Fred Hutchinson Cancer Research Center) and have been subtyped using nanoString as SHH (231). MED311-FH cells were cultured in NeuroCult proliferation medium (Stem Cell Technologies, Vancouver, BC, Canada) on laminin-coated plates (BD Biosciences, San Jose, CA, USA). Upon reaching confluency, cells were dissociated in Accutase and passed 1:4. D283 were cultured as adherent cultures in EMEM containing 10% FBS. D341 were cultured in ultra low attachment plates, with DMEM/F12 containing 15 B27, 1% N2, 20 ng/ml EGF, and 20 ng/ml bFGF (neural precursor medium).

UI226 cultures were established under an IRB approved protocol by the Central Nervous System Tissue Bank, Department of Neurosurgery, University of Iowa, and obtained through a material transfer arrangement by Translational

Genomics, Inc. UI226 cells are SHH MB as analyzed by NanoString (231) and were originally passaged (<10 times) in nude mice as flank injections. UI226 cells were then adapted to cell culture in StemPro® Neural Stem Cell Serum Free Medium (Life Technologies, Burlington, ON, Canada) on laminin-coated plates (BD Biosciences). UI226 cells cultured as tumorspheres in ultra low attachment plates were also grown in StemPro® medium.

2.2: Tumorsphere Assay

Cells were dissociated and aliquots of 2500 or 5000 cells from Daoy CD271 OE cells, Daoy CD271 KD and their respective controls were plated in 24-well ultra-low attachment plates in neural precursor media. 2500 cells/well were used for tumorsphere size counts; whereas, 5000 cells/well were used for tumorsphere number and total cell counts. MED311 CD271 KD cells were also dissociated and $1x10^4$ cells per well were plated in the same conditions as mentioned above. For UI226 KD cells, dissociated cultures were re-plated in ultra-low attachment plates at 5000 cells/well. Cells were incubated for 5 days, after which tumorspheres were counted and measured. Tumorspheres from each population were then dissociated and re-plated in aliquots of the respective cell number for secondary and subsequent tertiary tumorsphere assays. Secondary and/or tertiary tumorspheres were counted at day 5.

2.3: High throughput flow cytometry screening

Flow cytometry was performed using BD Lyoplate Human Screening Panels (BD

Biosciences) consisting of 242 cell surface markers and 9 isotype controls. Tumorspheres from higher and lower self-renewing Daoy subclones were dissociated and resuspended in Dulbecco's phosphate-buffered saline (DPBS) (Fisher Scientific, Ottawa, ON, Canada) containing 0.5% FBS. 2 x 10^4 cells were plated in 96 well plates in a total volume of 100 µl. Ten microliters of diluted antibody was added to each well and incubated for 20 minutes on ice. Cells were washed twice using 0.5% FBS/PBS. Fifty microliters of secondary goat anti mouse or goat anti rat antibody was added to cells and incubated on ice for 20 minutes. Cells were then washed twice more using FBS/PBS and 0.5 ul of 7AAD was then added to the cell suspensions as an indicator of cell viability. Cells were then analyzed using the Guava easyCyte flow cytometer (EMD Millipore, Etobicoke, ON, Canada). Results were analyzed and compiled using FlowJo software and exported to a Microsoft Excel 2007 template for generation of heat maps. This enables side-by-side comparative analysis of multiple screens from different cell types.

CD271, CD106, CD171 and EGFR levels were validated in Daoy subclones, as well as MED311, UI226, D283, and D341 cells cultured as tumorspheres in ultralow attachment plates with neural precursor medium. On day 4, tumorspheres were fed by removal and replacement of 1 ml of medium. On day 7, tumorspheres were dissociated, washed, and resuspended in DPBS containing 0.5% FBS. Cells were then stained with one of the following antibodies: CD271, CD106, CD171, and EGFR. All antibodies were obtained from BD Biosciences. Flow cytometry was performed on the Gallios Flow Cytometer (Beckman Coulter, Mississauga, ON, Canada) and analyzed using Kaluza software (Beckman Coulter).

2.4: Cell surface marker profiling in MB transcriptome datasets

CD271 (p75/NTR), CD171 (L1CAM), EGFR, and CD106 (VCAM1) expression levels were examined in 3 independent previously described transcriptome datasets comprising 548 patient samples (Boston (N=199 samples using Affymetrix_HT- HG-U133A chips (97)), Heidelberg (N=64 samples using Agilent Whole Human Genome Oligo Microarrays (232)), and Toronto (N=285 samples using Affymetrix Gene 1.1 ST Arrays (233))). Expression of the 4 markers across all samples was presented in boxplot format as $\log_2$-transformed signal intensity. All subgroups were compared using a Kruskal-Wallis test for significance.

2.5: Medulloblastoma patient sample subgrouping

Samples were obtained in accordance with the local research ethics board at the University of Manitoba. Additional samples were obtained from the Brain Tumour Tissue Bank (Brain Tumour Foundation of Canada, London Health Sciences Centre, London, Ontario, Canada). Total RNA was extracted from 3-5 paraffin scrolls using the Qiagen RNeasy FFPE kit and 200ng of total RNA was analyzed by NanoString as previously described (231). Subgroup determination was performed in the R statistical environment (v3.1.2) as previously described by PAM prediction using the pamr package (v1.55). A total of 10 samples were subtyped and utilized for immunohistochemistry: 1 WNT, 6 SHH, 1 Group 3 and 2 Group 4.

2.6: Immunohistochemistry

Paraffin embedded tissue from patient samples as well as 23-week human fetal cerebellum was deparaffinized in xylene and processed through a graded series of alcohol concentrations. Antigen retrieval was performed at 95-100°C for 20 minutes in Citrate Buffer pH 6.0. Samples were blocked with 3% lamb serum in 1XPBS (for CD271) or 5% Goat serum / 1% BSA (for CD171 and CD106) in TBS and subsequently treated with primary antibody diluted in 1% lamb serum in 1XPBS (for CD271) or 1% goat serum / 1% BSA in TBS (for CD171 and CD106) overnight at 4^{o}C: CD271: (1:400) (Millipore, Etobicoke, Ontario, Canada), CD171 (1:150) (Biolegend, San Diego, CA, USA), CD106/VCAM-1 (1:500) (Abcam, Cambridge, MA, USA). Slides were washed in (CD271): 1XPBS, (CD171/CD106): 1XTBS and treated with secondary antibody: for CD271 (1:500), for CD106 (1:200) (Biotin-SP-Affinipure Goat Anti-Rabbit IgG (Jackson Immunoresearch, West Grove, PA, USA) and for CD171 (1:200) (Biotin-SP-AffiniPure Sheep Anti-Mouse IgG (H+L) (Jackson Immunoresearch) diluted in (CD271): 1% lamb serum in 1XPBS, (CD171/CD106): 1% goat serum / 1% BSA diluted in TBS for 2 hours at room temperature. Slides were treated with 1:400 dilution of Streptavidin/HRP (Jackson Immunoresearch) in (CD271): 1XPBS (CD171/CD106): 1XTBS for 30 min and subsequently developed using DAB. Slides were counterstained with hematoxylin. Coverslips were mounted with Permount (Fisher Scientific).

2.7: Lentiviral Infection

CD271 was overexpressed in Daoy by transducing the cells with the

pReceiver-Lv105 lentiviral construct (GeneCopoeia, Rockville, MD, USA) containing a puromycin resistance gene (Figure 2.1). Lentifect™ Lentiviral Particles were used as a negative control. Puromycin was used for selection and was replenished every 3 days. CD271 OE was assessed by Western blot and flow cytometry.

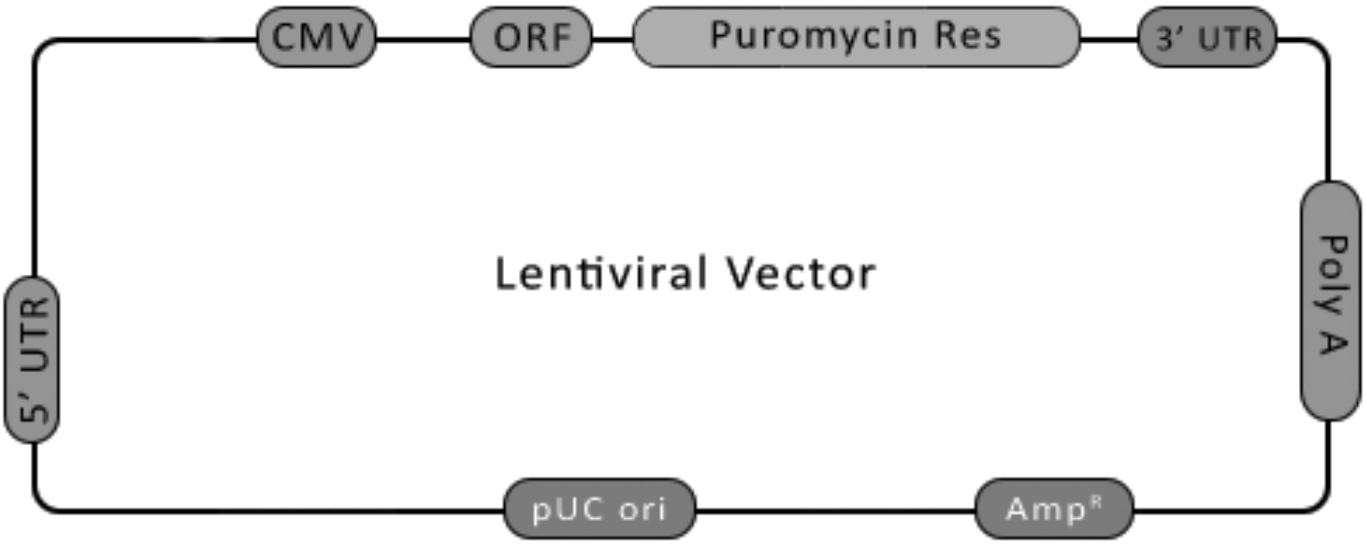

Figure 2.1: Lentiviral constructs and validation for stable overexpression of CD271 A. pReceiver-Lv105 lentiviral construct used for stable overexpression of CD271 in Daoy cells.

Stable overexpressing CD106 cells were generated by infecting Daoy parental cells with a precision LentiORF lentiviral construct (Fisher Scientific, Ottawa, ON, Canada) containing a blasticidin resistance and turboGFP reporter gene (Figure 2.2). Lentifect™ Lentiviral (RFP) particles were used as a negative control. Stably transduced cells were first selected using FACS sorting based on GFP^{+high}, and further enriched using blasticidin selection. CD106 overexpression was confirmed using flow cytometry using anti-VCAM1 conjugated antibodies (BD Bioscience, San Jose, CA, USA).

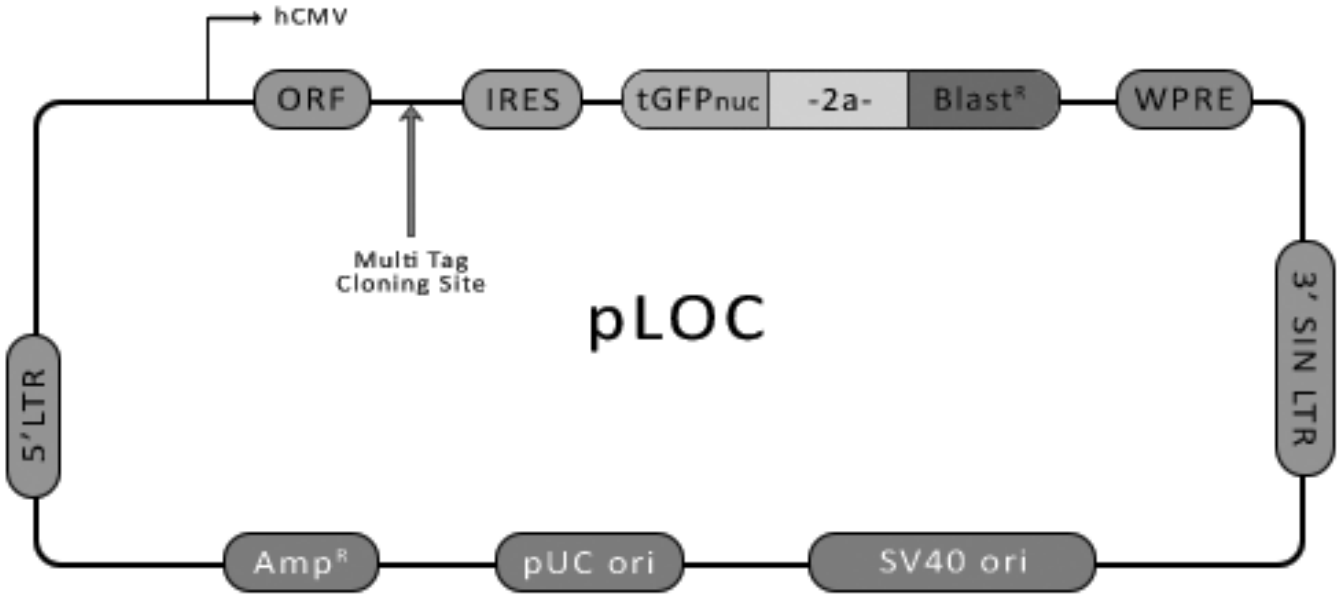

Figure 2.2: CD106 overexpression in the Daoy MB cell line A. Viral vector used in lentiviral infection. Backbone shows turboGFP reporter gene (tGFPnuc) and Blasticidin resistance gene (BlastR) (Thermo scientific precision LentiORF collection technical manual).

CD271 was stably knocked down in Daoy OE, UI226, and MED311 cells using 2 shRNAmir constructs (GeneCopoeia) consisting of a dual expression system with TurboGFP as a transduction marker. A non-silencing (scrambled) shRNA sequence was used as a negative control. CD271 knockdown (KD) was assessed by Western blot following stable selection, Daoy OE KD, UI226 KD, MED311 KD, and their respective controls were subjected to tumorsphere assays.

2.8: Core/Migrating Dissection Assay

Daoy MB cells were prepared as hanging drops as previously described (234, 235). Cells were incubated for 3 days and resultant spheroids were transferred into an adherent plate containing EMEM with 10% FBS. Spheroids were incubated for 2 days, at which time the "core" was mechanically dissected from the migrating cells under a dissecting microscope at 4x magnification (Figure 2.3). The dissected cores as well as the remaining migrating cells were dissociated separately, resuspended in DPBS with 0.5% FBS, and stained with antibodies for CD57, CD106, D108, CD171, CD271, CD273, EGFR, SSEA4 and GD2 for analysis by flow cytometry.

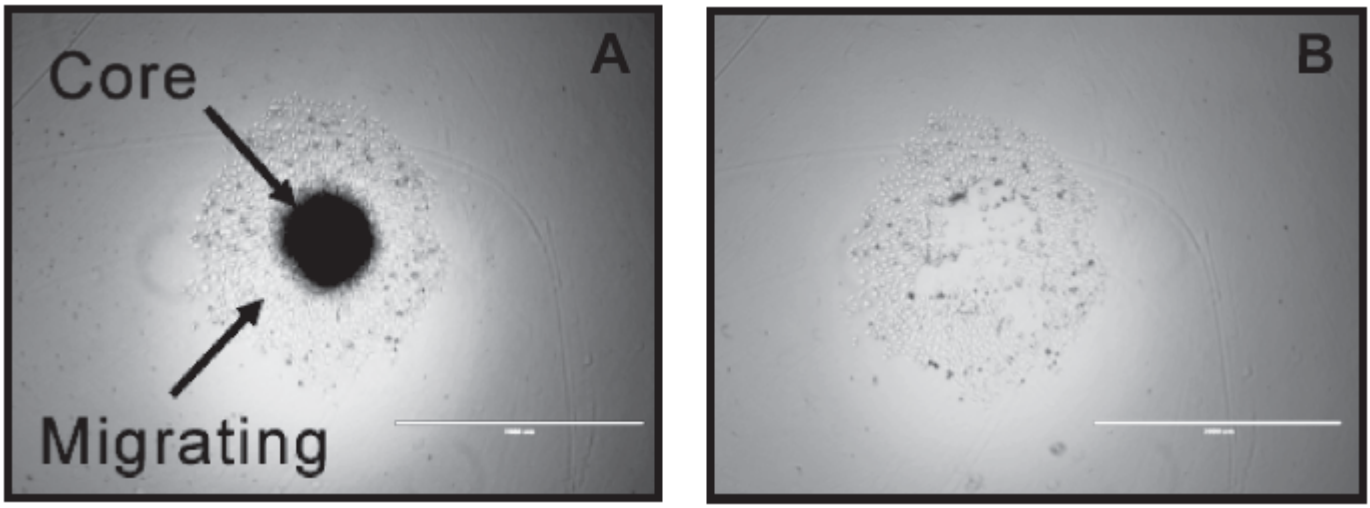

Figure 2.3: Core and dissecting assay. A-B. Spheroids composed of Daoy cells were allowed to adhere and migrate on adherent 24 well plates in EMEM with 10% FBS for 2 days. Following incubation, the core was dissected from the migrating cells using a pipette tip under a dissecting microscope. Dissected cores and migrating cells were dissociated separately and stained in preparation for flow cytometry analysis. Scale Bars = 2000 μm

2.9: Invasion Assay

Cells were dissociated and aliquots of 2.5×10^4 cells were prepared as hanging drops in 20 µl as described (234). Hanging drops were incubated for 3 days to form aggregates and then transferred to collagen type I gels (VWR, Mississauga, ON, Canada) prepared as previously described (234). Following collagen gelation at 37°C, embedded aggregates were then overlain with EMEM containing 10% FBS. Aggregate measurements were taken at day 0 and invasion was measured at 72 hours (day 3) using a Zeiss Primo Vert microscope (Carl Zeiss Canada Ltd., Toronto ON, Canada) with micrometer.

2.10: Western Blot

Protein was isolated from all cells and their respective controls using the All-In-One Purification Kit (Norgen Biotek, Thorold, ON, CA) according to manufacturer's instructions. Twenty micrograms of protein from Daoy CD271 OE, CD271 OE/KD cells and their controls were separated by SDS PAGE using 10% acrylamide gels. Forty micrograms of protein from MED311 KD, UI226 KD along with control cells were also separated by SDS PAGE. Protein was transferred using a semi-dry transfer method to nitrocellulose membrane (BioRad). Membranes were blocked in 5% non-fat milk in Tris Buffered Saline with Tween 20 (TBST) and then incubated at 4°C overnight with antibodies to CD271 (Millipore, 1:1000) and CD271-ICD (Promega, 1:500). Membranes were washed several times with TBST before application of goat anti-rabbit horseradish peroxidase secondary antibody (BioRad Laboratories Ltd,

Mississauga, ON, Canada,1:3000). Membranes were developed using SuperSignal West Pico (Fisher Scientific).

2.11: Intracerebral Transplantations and Histology

2.11.a: CD271+/- and CD271OE

The University of Manitoba Animal Care Committee approved all procedures and protocols. Daoy FACS sorted CD271+ and CD271- cells grown in tumorsphere conditions and CD271 control and CD271 OE cells grown in tumorsphere conditions were intracerebrally injected into non-obese diabetic severe combined immunodeficient (NOD/SCID) mice as previously described (70, 168, 236). In total; 5 x 10^4 $CD271^+$ cells (N = 3), 5 x 10^4 $CD271^-$ cells (N = 6), 1 x 10^3 $CD271^+$ cells (N = 5), 1 x 10^3 $CD271^-$ cells (N = 4), 5 x 10^4 CD271 control (N = 4) and 5 x 10^4 CD271 OE (N = 6) cells were injected. Mice were anesthetized with isoflurane and a burr hole drilled 2 mm lateral to midline on the right and 1 mm anterior to bregma. Ten microlitres of dissociated cell suspension containing pre-determined cell numbers re-suspended in Dulbecco's phosphate-buffered saline (DPBS) (Fisher Scientific, Ottawa, ON, Canada) containing 0.5% FBS was loaded into a 10 µl Hamilton syringe and inserted 3.5 mm past the surface of the skull using a Kopf stereotactic frame. The syringe contents were injected manually by hand over a period of one minute into the right caudate/putamen nucleus, left in place for 3 minutes, then slowly withdrawn.

End points for experiments were set at 20 weeks (FACS sorted

CD271^{+}/CD271^{-}) and 12 weeks (CD271 control/CD271 OE), or 25% weight loss from maximum weight due to illness, whichever came first. End points were as follows: 14 weeks for 5 x 10^4 CD271^{+}/CD271^{-}, 18 weeks for 1 x 10^3 CD271^{+} and 16 weeks for 1 x 10^3 CD271^{-}. At end point, cardiac perfusions were performed and the brains were extracted, placed in formalin for 2 to 7 days, embedded in paraffin, and then sectioned (5 μm thickness). Sections were de-waxed in xylene and rehydrated through a graded series of alcohol concentrations. Samples were stained with hematoxylin and eosin. Slides were mounted and imaged using an EVOS xl core micro- scope (AMG, Seattle, WA, USA).

Malignant cell growth was scored, from a scale of 0 to 4 in arbitrary units, where 0 = no malignant cells with certainty, 1 = indicates rare clusters of malignant cells confined to subarachnoid compartment, 2 = malignant cells in subarachnoid compartment and infiltrating perivascular spaces, and 3 = features in 2, in addition to tumor nodules growing in other areas of the brain or cerebellum. For each tumor sample, two slides containing six to seven brain sections were scored and averaged to obtain a grade. Slides were assessed by a neuropathologist who was blinded to cellular identity.

Stained slides were also scanned using an Aperio ScanScope CS slide scanner (Leica Microsystems Inc., Concord, ON, Canada) at 20x maximum magnification. Tumor area was measured using Aperio ImageScope software (Leica Microsystems Inc., Concord, ON.). Tumor was freehand selected and calculated using the area measure function (Figure 2.4). Total area was measured in 6 slices, each 2 mm in

distance apart, representing the anterior to posterior region of brain. Total tumor area for each sample was calculated by adding tumor area in all the slices

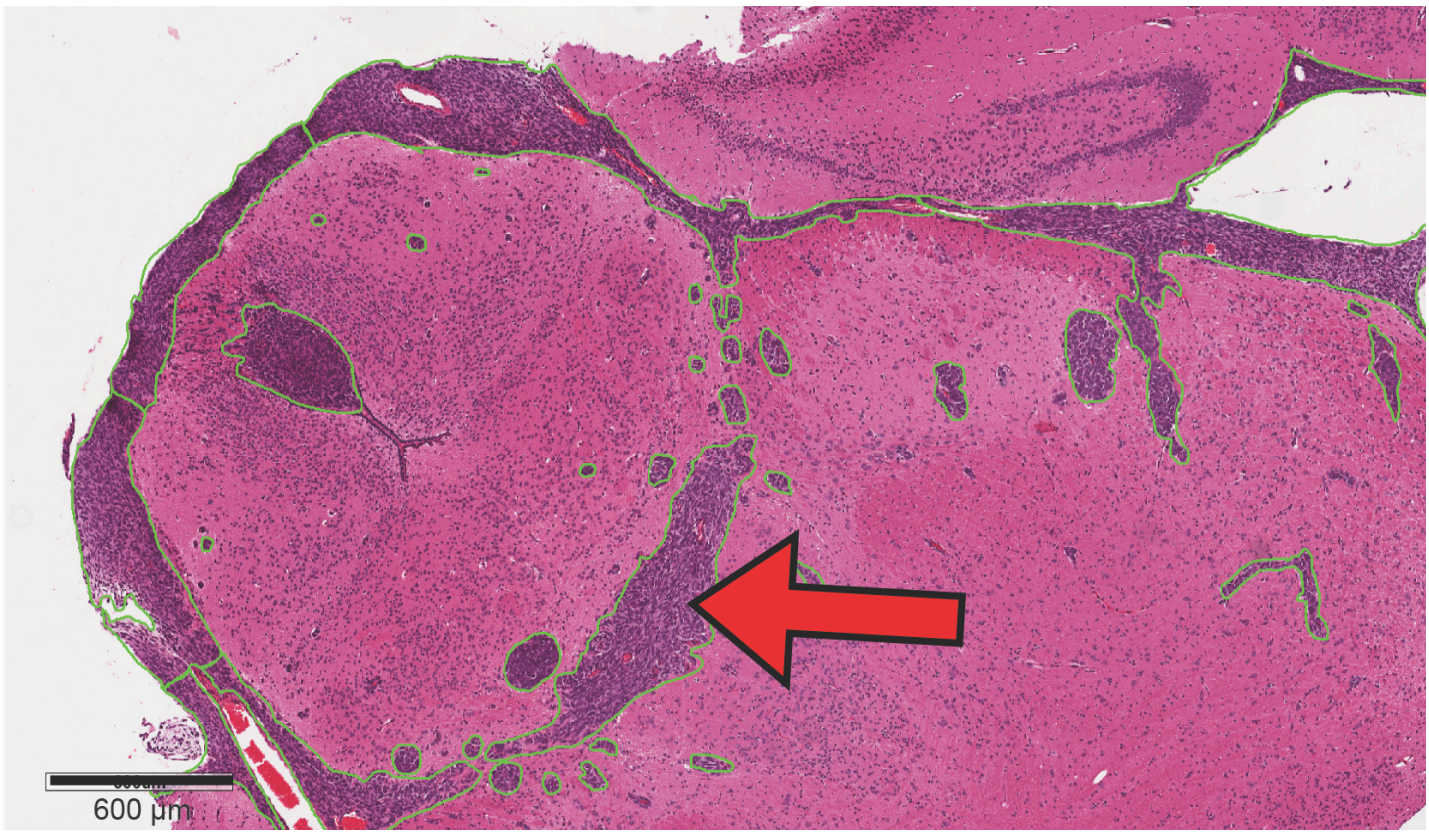

Figure 2.4: Representative image of tumor area measurement. Area was calculated from 6 slices, each 2 mm in distance apart, spanning the anterior to posterior region of brain. Tumor was freehand selected and calculated using area measure function. Total tumor area for each sample was calculated by adding tumor area in all slices. Arrows denote tracing path of tumor area.

2.11.b: Higher and non self-renewing subclones

The University of Manitoba Animal Care Committee approved all procedures and protocols. Higher and lower self-renewing Daoy clones were grown in tumorsphere conditions and injected into the cerebral cortex of NOD/SCID mice as previously described (70, 168, 236). In total; 5 x 10^4 low SR cells (N = 6), 5 x 10^4 high SR cells (N = 6), 1 x 10^3 low SR cells (N = 5), 1 x 10^3 high SR cells (N = 4), 1 x 10^2 low SR cells (N = 2) and 1 x 10^2 high SR cells (N = 3) were injected. Implantation was performed in the same manner as described above.

End points for experiments were set at 14 - 15 weeks or 25% weight loss from maximum weight due to illness. Perfusion, staining and analysis were then performed as described above.

2.12: Secondary Tumor Transplantations

2.12.a: CD271+/-

Daoy parental cells were sorted using FACS based on CD271+/CD271-. Ten thousand cells were injected into the right frontal cerebral cortex of NOD SCID mice as previously described above. Tumors were allowed to form over 12 – 14 weeks. The mice were euthanized using CO_2, brains removed and the right frontal lobe mechanically minced and placed in dissociation media containing; 259 U/ml collagenase (Invitrogen, Carlsbad, CA, USA), 86 U/ml hyaluronidase (Sigma-Aldrich, St. Louis, MS, USA), 86% DMEM F12, 9% accutase (Fisher Scientific, Ottawa, ON, Canada), 4% FBS and 1% Pen/Strep (100x). The brain material and dissociation

media were mechanically agitated for 12 hours at 37° C. After dissociation was complete, the cell suspension was rinsed several times with PBS and cell counts performed. Cells were stained using conjugated anti-HLA (BD Bioscience, San Jose, CA, USA), and anti-CD45 (Miltenyi, Bergisch Gladbach, Germany) antibodies. HLA allows isolation of human Daoy cells from normal mouse neural cells while CD45 allows us to discard hematopoietic cells. HLA^{+} $CD45^{-}$ cells were isolated using FACS and collected (Figure 2.5. These cells were then injected into NOD SCID mice at cell numbers of 2600-6500 cells/mouse, depending on the number of sorted cells obtained. Tumors were allowed to grow until the first mouse reached medical endpoint (25% weight loss) at 92 days, followed by the remainder of the mice sacrificed between 92 and 93 days. Brain specimens were then processed in the same manner as described above.

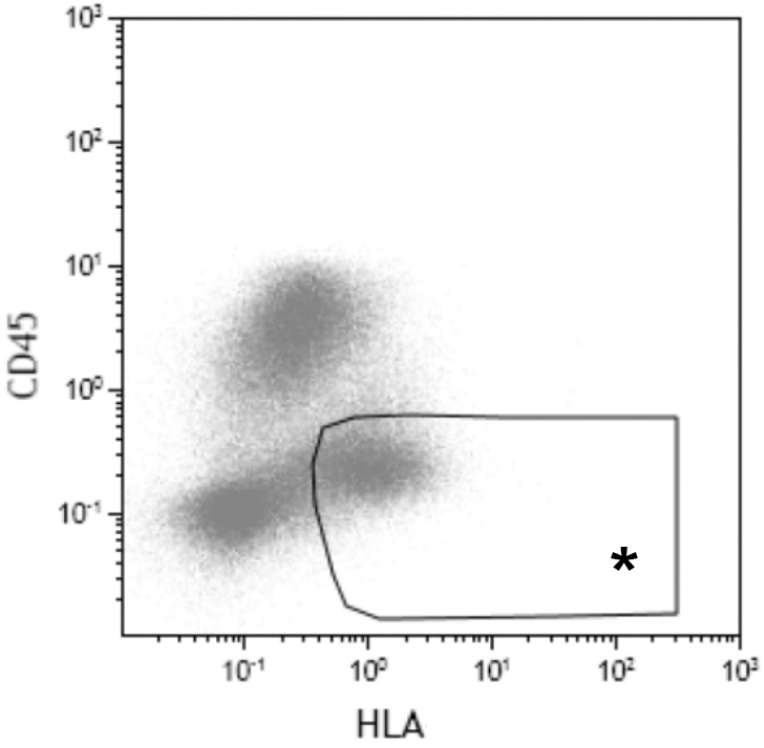

Figure 2.5: Isolation of tumors cells derived from CD271+ and CD271- primary tumors. A. Flow cytometry plot of FACS sorting used to distinguish human tumor cells from mouse neural cells after brain extraction. Cells were sorted based on HLA+ CD45-. Gates used for isolation marked with [*]. CD271 status was not used as a sort parameter for secondary injections.

2.12.b: Higher/Lower self-renewing subclones

RFP expressing higher and lower SR Daoy subclones cells were generated using Lentifect™ Lentiviral Particles to allow for simpler isolation of human tumor cells from normal mouse brains (Figure 2.6 A). Puromycin was used for selection and was replenished every 3 days. Fifty thousand RFP+ cells grown in tumorsphere conditions (Figure 2.6 B) were injected into the right frontal cerebral cortex of NOD SCID mice as previously described. After 12-14 weeks, the mice were euthanized using CO_2, brains extracted and RFP expressing tumor dissected using a dissecting microscope. Dissected tissue was mechanically minced and placed in dissociation media as described above. The brain material and dissociation media were mechanically agitated for 12 hours at 37° C. The cell suspension was then rinsed several times with PBS. RFP+ cells were sorted using FACS and collected (Figure 2.6 C-D). Five thousand cells were then injected into NOD SCID mice. After 10-11 weeks, brain specimens were then processed in the same manner as described above.

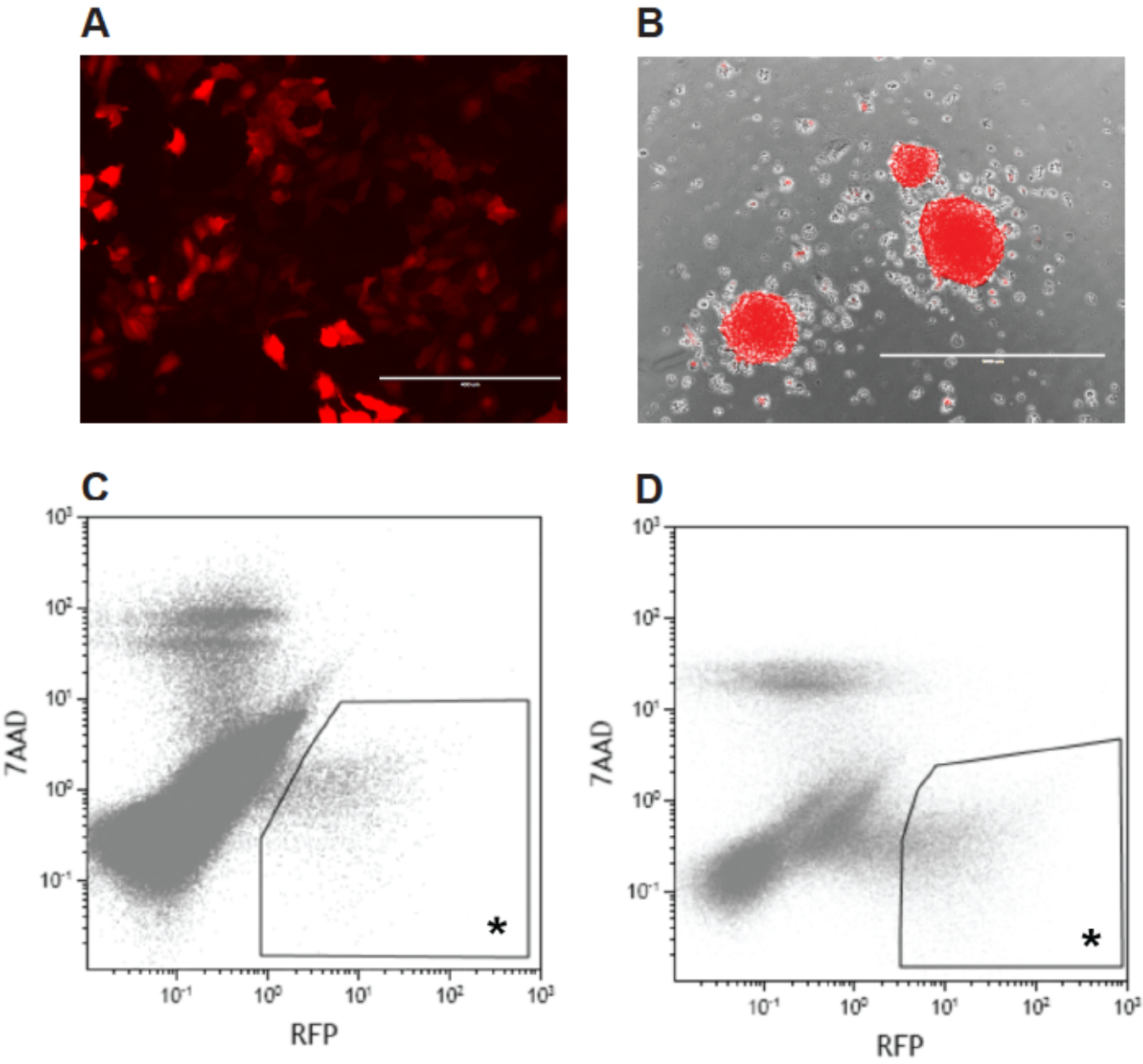

Figure 2.6: Isolation of RFP+ human Daoy cells from primary tumors removed from the cerebral cortex of NOD SCID mice. A. Adherent Higher SR Daoy subclones after transduction with RFP reporter construct. Scale bar = 400 µm **B.** RFP/white light superimposed image showing lower SR Daoy subclone expressing RFP reporter construct in tumorsphere conditions prior to injection into NOD SCID mice. Scale bar = 1000 µm **C-D.** Flow plots of FACS sorting gates utilized to separate higher SR subclone **(C)** tumor cells and lower SR subclone **(D)** tumor cells from mouse neural cells after removal of the brain and associated tumor tissue. Cells were sorted based on RFP+ and 7AAD- status. Cells located in gate denoted by * were collected.

2.13: Magnetic Resonance Imaging

Mice were anaesthetized using 5% isoflurane in O_2/N_2O and maintained at 2% isoflurane in O_2/N_2O with a nose cone. Respiration and external body temperature were monitored during imaging using an MR-compatible small animal monitoring and gating system (SA Instruments, Stony Brook, NY, USA). External body temperature was maintained at 37 °C with a heating circulator bath (Thermo Scientific Haake, Karlsruhe, Germany). Mouse heads were held in place with a tooth bar inside a custom-built 24 mm diameter, 300 MHz inductively coupled quadrature RF volume coil (NRC Institute for Biodiagnostics, Winnipeg, MB, Canada). The entire apparatus was placed inside a Bruker BGA12-S actively shielded gradient system with integrated shim coils (Bruker BioSpin, Milton, ON, Canada). All MR experiments were performed on a 7 T 21 cm Bruker Avance III NMR system with Paravision 5.0 (Bruker BioSpin). The mouse brain was imaged in prone position rostral to caudal using 12 slices with a slice thickness of 0.75mm and an interslice distance of 1.0mm.

2.14: Statistical Analysis

All tests were performed using Prism 5 software (GraphPad Software, La Jolla, CA, USA) or SPSS Statistics (IBM, Armonk, NY, USA). Descriptive statistics were used to determine significant differences including mean and SEM along with one-way analyses of variance (ANOVA), independent sample two-tailed t tests, Mann Whitney tests, and Tukey's test for multiple comparisons. P values less than .05 were considered significant.

Chapter 3: Results

Chapter 3.1: Functional characterization of novel biomarkers in selecting for subtype specific medulloblastoma phenotypes

NB. Chapter 3.1 is mainly derived from published work conducted by another graduate student in the lab, Lisa Liang, and myself. I have indicated what work was performed by myself, and what was done by others. Text has been duplicated from Liang *et al. (171)* with permission from the publisher.

3.1.1: Rationale

Currently, the majority of studies on the 5 MB variants focus on mutation analysis and differential gene expression (237-239). While this work has revolutionized our understanding of pediatric brain tumor heterogeneity, the specific functional role of mutated and differentially expressed genes is not always understood and will likely have to be considered in a subtype specific manner. Understanding how these genes contribute to cellular heterogeneity will also provide a more complete picture of disease complexity.

Although the SHH variant is associated with an intermediate prognosis and a 5-year survival rate of 60-80% (49), recent studies have demonstrated heterogeneity within the subtype (60, 61, 94, 95). In addition, the cell of origin for SHH MB is still under debate (118, 166, 167). Identification of additional cell surface markers that select for stem and/or progenitor cells will be necessary to further delineate the cellular complexity within these tumors. Given the heterogeneity observed between and even within the MB variants, these signatures may also be distinctly associated with a particular subtype.

Identification of surface markers capable of enriching for TPCs in a cancer is generally achieved using flow cytometry with a small number of single antibodies selective for surface markers already known to play a role in normal stem cell biology (70, 166-168). This practice has major bias towards the surface markers selected and does not cover a large majority of known human cell surface markers. A more efficient, less biased system capable of screening high numbers of surface markers is necessary. To this end, we employed a high throughput flow cytometry screening platform to identify additional cell surface markers associated with stem/progenitor cell phenotypes specifically in the SHH molecular variant. This platform has recently been introduced as a mechanism for identifying primary vs. metastatic colon cancer cell lines (240), for distinguishing cells at various stages of neural lineage specification (241), and most recently, for identification of adhesion receptors contributing to glioblastoma self-renewal and tumor growth (242).

Twenty five markers were found to be differentially expressed in higher vs low self-renewing phenotypes. Of these 25, 4 markers were found to be differentially expressed in SHH MB as compared to the other 3 subtypes; CD271, CD106/VCAM1, CD171/NCAM-L1 and EGFR. Initial functional characterization of CD106 and extensive functional characterization of CD271 and was performed as proof of principle to demonstrate the power this unique approach has in identifying novel markers associated with the SHH MB subtype.

3.1.2: High throughput flow cytometry screens and MB transcriptome datasets reveal 4 cell surface markers that are differentially expressed between self-renewing vs. non- self-renewing SHH MB tumorspheres and SHH vs. the other MB variants

Utilizing a BD Lyoplate™ 242 human cell surface marker panel (Figure 2.1), we screened for differential expression in self-renewing (continue to form tumorspheres over subsequent passage) vs. non-self-renewing (gradually lose tumorsphere forming capacity and become adherent) Daoy MB subclones. These sub-clones were previously developed and characterized by our laboratory (168). Subclones were derived from the long established DAOY SHH MB parental cell line originally derived from a 4 year old Caucasian male in 1985. The Daoy MB cell line is derived from a desmoplastic MB (226), has been shown to exhibit global activation of SHH-pathway genes (243-245) and is statistically classified as SHH subgroup based on hierarchical clustering and PCA analysis with patient samples (246). This cell line continues to be utilized as an alternative or supplement to working with fresh patient tissue or minimally cultured samples (243, 247, 248), as it has been very difficult to establish cultures from primary MB tumors and maintain them over subsequent passage. Single parental cells were plated using FACS in 96 well dishes and expanded. Self-renewal of each clone was measured using a tumorsphere assay. Two clones, one with high and one with low self-renewal capacity were then chosen to carry out comparative assays.

Using self-renewing and non-self-renewing Daoy tumorspheres, we

conducted 2 independent screens and the results were reproducible between trials (Figure 3.1.1). Twenty-five markers were found to be differentially expressed between the phenotypes, with more than a 2 fold difference in frequency and mean fluorescence intensity (Table 3.1.1).

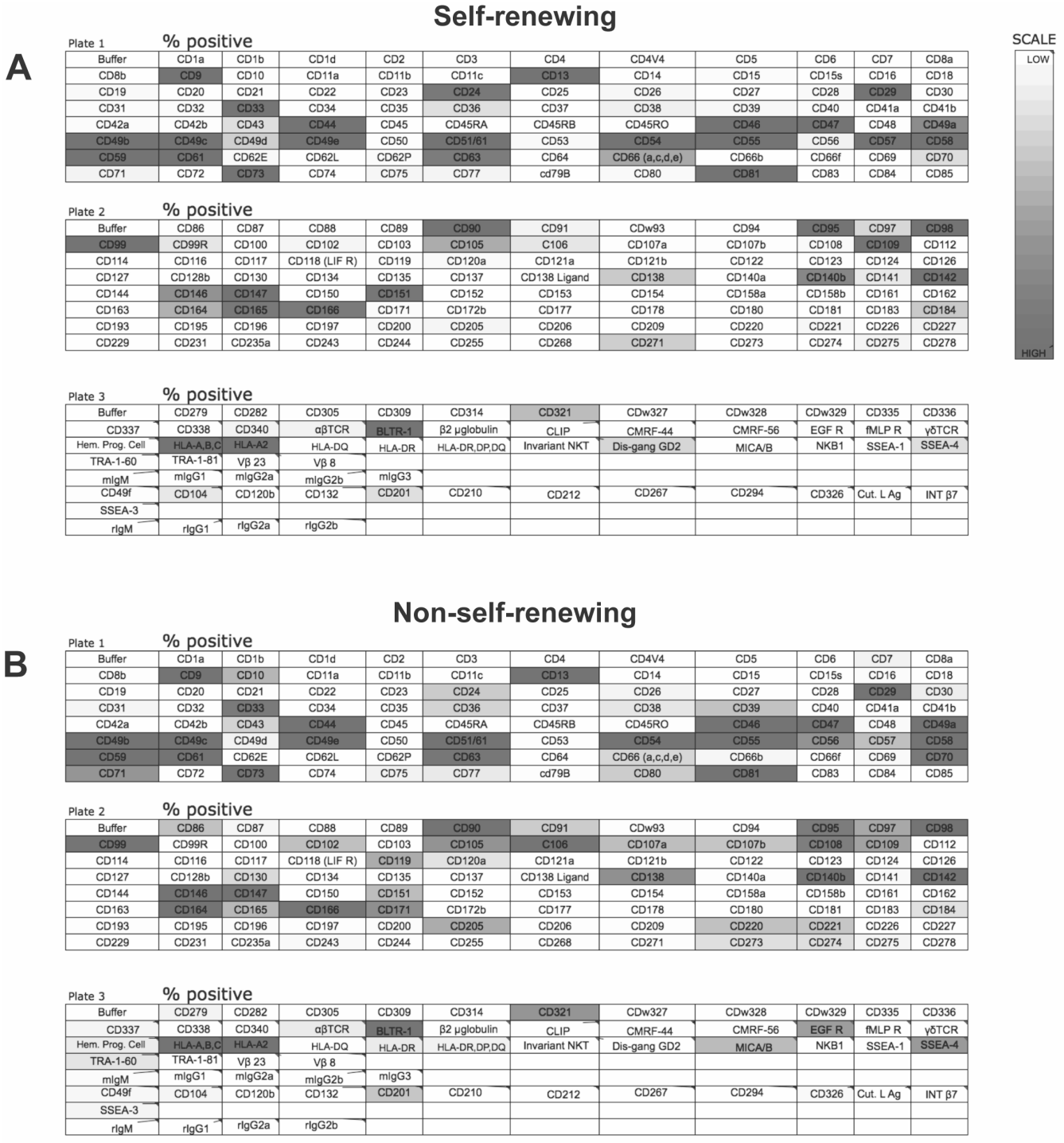

Figure 3.1.1: Heat maps showing frequencies of cell surface markers in self-renewing (SR) tumorspheres (A) and non-self-renewing (NSR) tumorspheres (B) from the Daoy cell line. Darker shading indicates high expression and white indicates negligible or absent expression.

Cell Surface Marker	Higher SR Tumorspheres		Lower SR Tumorspheres		Fold change of Higher vs Lower SR	
	% Positive	MFI	% Positive	MFI	% pos	MFI
Disialoganglioside GD2	21.25	5.63	0.25	0.99	85.91	5.70
CD227	16.80	2.28	1.94	1.11	8.66	2.05
CD271	23.45	2.75	3.13	1.19	7.49	2.32
CD57	90.05	19.99	28.50	2.27	3.16	8.80
CD97	16.55	2.23	43.00	4.93	-2.60	-2.21
SSEA-4	16.45	1.63	49.20	4.50	-2.99	-2.76
CD70	18.80	1.19	58.65	3.07	-3.12	-2.59
CD71	9.98	1.84	38.15	4.48	-3.82	-2.43
CD39	4.21	1.46	17.16	4.28	-4.08	-2.94
CD106	14.50	2.04	73.75	34.88	-5.09	-17.09
TRA-1-60	2.40	0.98	13.20	2.69	-5.50	-2.74
CD171	5.45	1.49	40.40	4.61	-7.42	-3.10
CD10	3.00	1.24	22.55	2.54	-7.52	-2.04
CD326	1.10	0.74	9.76	2.33	-8.91	-3.16
CD107b	2.32	1.05	22.00	3.84	-9.50	-3.67
CD86	2.52	1.23	25.20	2.84	-10.02	-2.32
EGF-r	2.67	1.39	38.40	4.83	-14.38	-3.47
CD108	4.50	1.45	67.65	10.33	-15.05	-7.15
Hem. Prog. Cell	1.07	1.18	17.54	2.43	-16.38	-2.06
MIC A/B	1.53	1.16	26.25	3.53	-17.14	-3.04
CD107a	1.71	1.14	29.90	5.38	-17.49	-4.71
CD274	1.84	1.34	35.00	3.72	-19.07	-2.77
CD119	2.10	1.49	40.65	3.05	-19.36	-2.05
CD130	0.84	1.21	24.60	2.42	-29.46	-2.01
CD273	0.57	0.97	27.45	2.81	-48.50	-2.90

MFI = Mean Fluorescent Intensity

Table 3.1.1: Twenty-five differentially expressed cell surface markers in self-renewing vs. non self-renewing Daoy tumorspheres using the BD Lyoplate ™ Human Cell Surface Marker Screening Panel. Candidates were assessed based on both frequency and mean fluorescence intensity. Only cell surface markers that exhibit at least a 2-fold difference in both properties were considered for additional validation studies.

We next determined whether any of the 25 candidates cell surface markers also exhibit differential expression in SHH patient samples relative to samples from the other MB subtypes. Three independent transcriptome datasets derived from gene expression profiling of MB samples across multiple centers, patient populations and technical platforms that together represent 548 patient samples were interrogated (97, 232, 249). Most candidates exhibited differential expression across subtypes in 1 or 2 datasets. However, 4 of the 25 cell surface markers displayed consistent and differential expression in SHH MB compared to WNT, Group 3, and Group 4 MB patient samples across all 3 datasets. CD271, CD106/VCAM1, and EGFR were upregulated; whereas, CD171/NCAM-L1 was downregulated in SHH MB relative to the other variants (Figure 3.1.2).

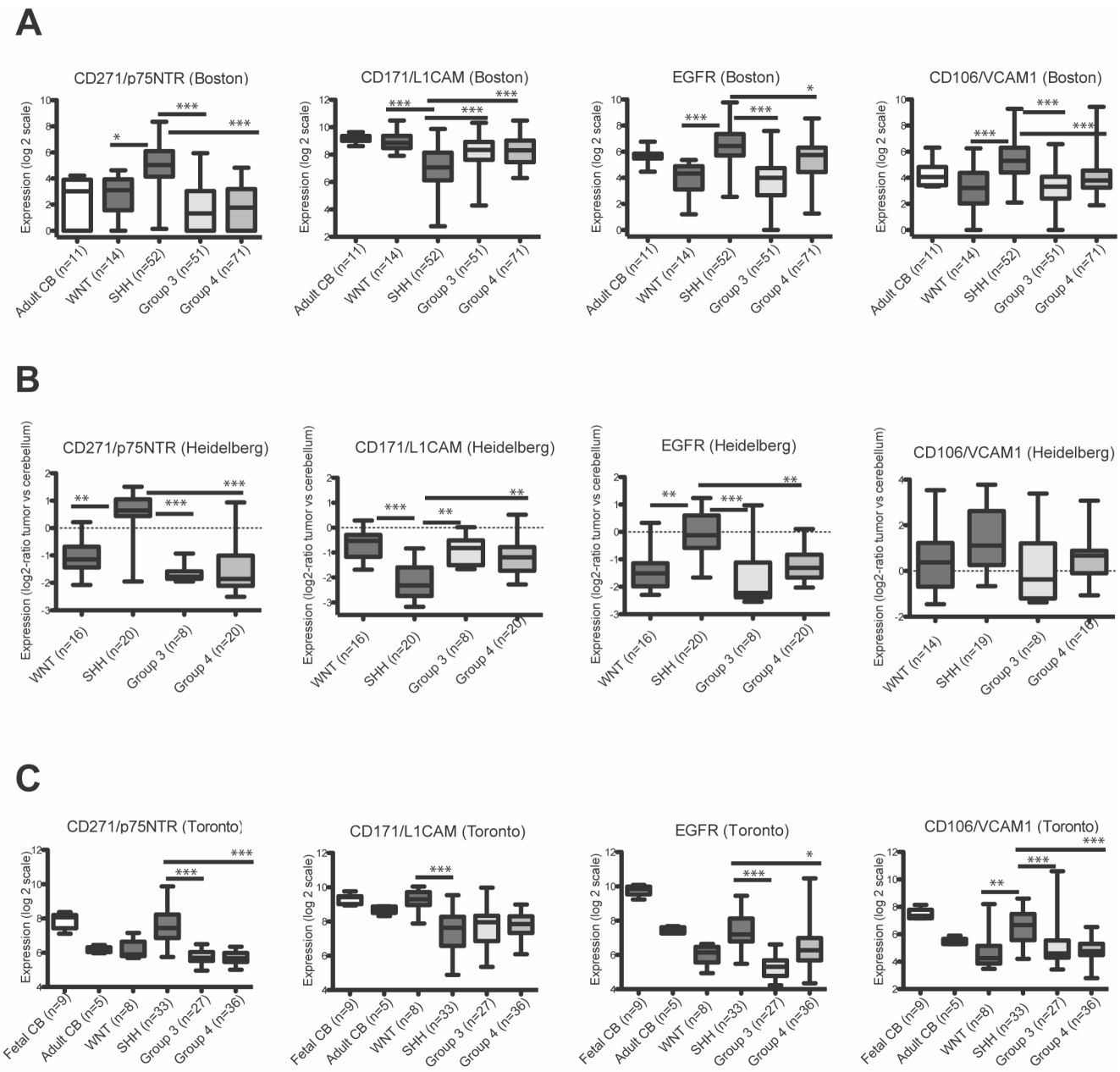

Figure 3.1.2: Heat maps and transcript levels of CD271/p75NTR, CD171L1CAM, EGFR and CD106/VCAM1 across the 4 MB molecular variants. Note that the CD271 Toronto dataset was previously published in Neoplasia, 15, Morrison et al., *Deconstruction of Medulloblastoma cellular heterogeneity reveals differences between the most highly invasion and self-renewing phenotypes, 384-398, Copyright Elsevier (2013).* **A-C.** Gene expression profiling data from 3 independent datasets representing 548 patient samples showing relative enrichment of CD106/VCAM1, CD271/p75NTR and EGFR and downregulation of CD171/NCAM-L1 in SHH tumors compared with the other variants. Bars denote 1.5 interquartile range within each group. All subgroups were compared using a Kruskal-Wallis test for significance. Data are presented as log2 -transformed signal intensity. $P<0.05$*, $P<0.01$**, $P<0.001$***

3.1.3: CD271, CD106 and CD171 are differentially expressed in MB cell lines/primary cultures and patient samples at the protein level

We next evaluated expression levels of these 4 markers in MB tumorspheres from a variety of cell lines by flow cytometry. In addition to Daoy, we utilized the UI226 low passage primary cultures that have been subtyped by nanoString as previously described (231) and designated SHH. Low passage primary cultures, which are more clinically relevant, provide an excellent complementary model to cultured cell lines such as Daoy. D341 (227) is a Group 3 MB, and D283 (228) has recently been classified as Group 4 (229); however, previous studies have demonstrated that D283 also exhibits features of Group 3 such as high c-myc levels (230). To our knowledge, there are no WNT MB cell lines; thus, we used both D341 and D283 as representative non-SHH variant cells. Based on the gene expression profiling results, we predicted that CD271, CD106 and EGFR would be higher and CD171 lower in Daoy and UI226 relative to D341 and D283 tumorspheres. Indeed, CD271, CD106 and EGFR are higher and CD171 is lower in Daoy and UI226 vs. D341 and D283 tumorspheres (Figure 3.1.3). However, EGFR levels were quite low across all cell lines, and we did not pursue this marker further.

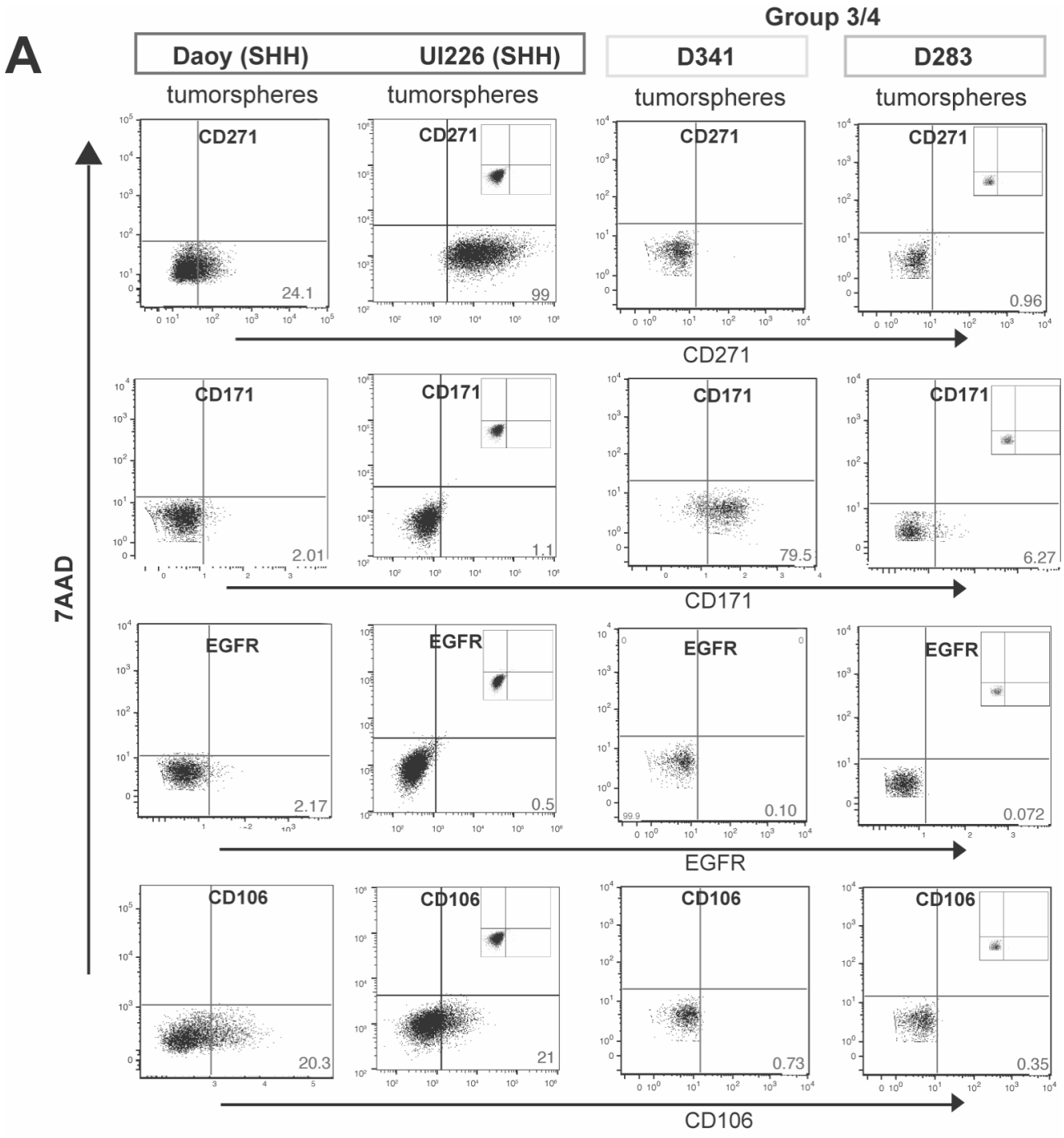

Figure 3.1.3: Candidate cell surface markers are differentially expressed in MB cell lines/primary cultures. Representative dot plots of staining for candidate biomarkers in Daoy and UI226 tumorspheres (SHH variant) vs. tumorspheres from Group 3/Group 4 cell lines by flow cytometry. Insets: respective isotype controls. 7AAD: 7-aminoactinomycin D cell viability dye.

Immunohistochemical staining of paraffin embedded sections from primary MB core tumor patient samples also revealed differential CD271 and CD171 expression patterns between the molecular variants (Figure 3.1.4). Specifically, CD271 levels were higher in SHH MB samples and in the external granular layer (EGL) of 23-week human fetal cerebellum relative to the other MB variants. Interestingly, CD171 exhibited a nodular staining pattern in some areas of SHH tumor samples, while displaying uniformly positive staining throughout the other 3 variants as well as in 23-week human fetal cerebellum. In contrast, CD106 expression was restricted to small foci of neurons in the fetal cerebellum and was not detectable in the MB samples. Note that these are tumor core primary samples and not recurrent/metastatic disease and therefore these findings do not exclude the possibility that some of these markers are in fact related to migration and metastasis

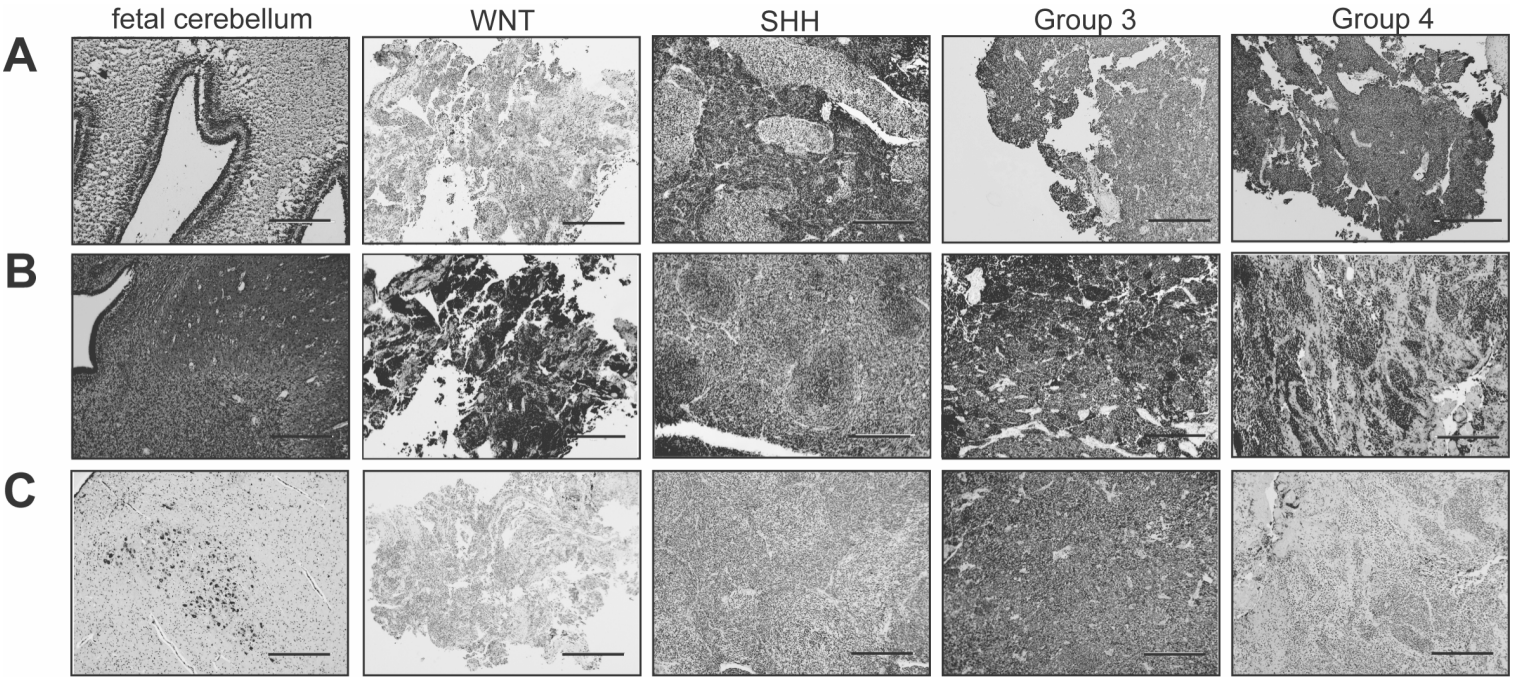

Figure 3.1.4: Candidate cell surface markers are differentially expressed in MB patient samples. A-C. CD271 **(A)**, CD171 **(B)** and CD106 **(C)** expression in paraffin embedded sections of fetal cerebellum and primary medulloblastoma samples. Scale bar: 400 µm.

It should be noted that 3 of the 25 cell surface makers from our Lyoplate ™ screens (GD2, SSEA4, and CD57), are not proteins and therefore, would not be represented in the transcriptome datasets. Therefore, we evaluated expression levels of these markers by flow cytometry in cell lines. Although GD2 levels were much higher in self-renewing vs. non-self-renewing cells (Table 1), GD2 levels varied in tumorspheres from all 4 cell lines tested. CD57 levels were inconsistent, and SSEA4 showed negligible expression in all cell lines examined (data not shown).

Collectively, our results suggest that CD271, CD106 and CD171 are the best candidates for additional functional testing. Importantly, these data validate our previous findings demonstrating higher expression of CD271 in stem/progenitor SHH Daoy MB cells (168).

3.1.4: Migrating MB Cells Exhibit Decreased CD271 and Increased CD106 Expression

We have found that our Daoy SHH MB subclones differentially express CD271, CD106, EGFR and CD171 (Figure 3.1.1). We have also found that these surface markers are consistently and differentially expressed in SHH variant tumors when compared to all other variants (Figure 3.1.2). To test the possibility that these cell surface markers are also differentially expressed in other biologic assays, we generated hanging drop aggregates and subsequently plated them on tissue culture

plates to separate the core stationary cells from the migrating cells (Figure 2.5). Specifically, MB hanging drop aggregates from the parental Daoy cell line were allowed to adhere to a cell culture plate surface and individual cells migrated out from the center over a 48-hour period. The aggregate core was mechanically dissected and both " core" and "migrating" cell populations were dissociated and subjected to a flow cytometry surface marker antibody screen of CD57, CD106, CD108, CD171, CD271, CD273, EGFR, SSEA4, and GD2 (Figure 3.1.5).

CD271 levels were higher in the core cell population, whereas CD106 was higher in the migrating cells (Figure 3.1.5 B,E). CD171 was elevated in migrating cells however, the difference was not significant (Figure 3.1.5 D). Taken together, these results demonstrate that SHH MB consistently expresses higher levels of CD271 and CD106 relative to the other variants; however that expression level is not homogenous within the tumor and may be dependent on cell state or phenotype. This may also explain why CD106 expression was not observed in our patient samples by IHC, as these were primary, well encapsulated tumors that did not contain highly infiltrative cells. Based on our findings we chose to further pursue the functional roles of both CD271 and CD106 for additional experiments.

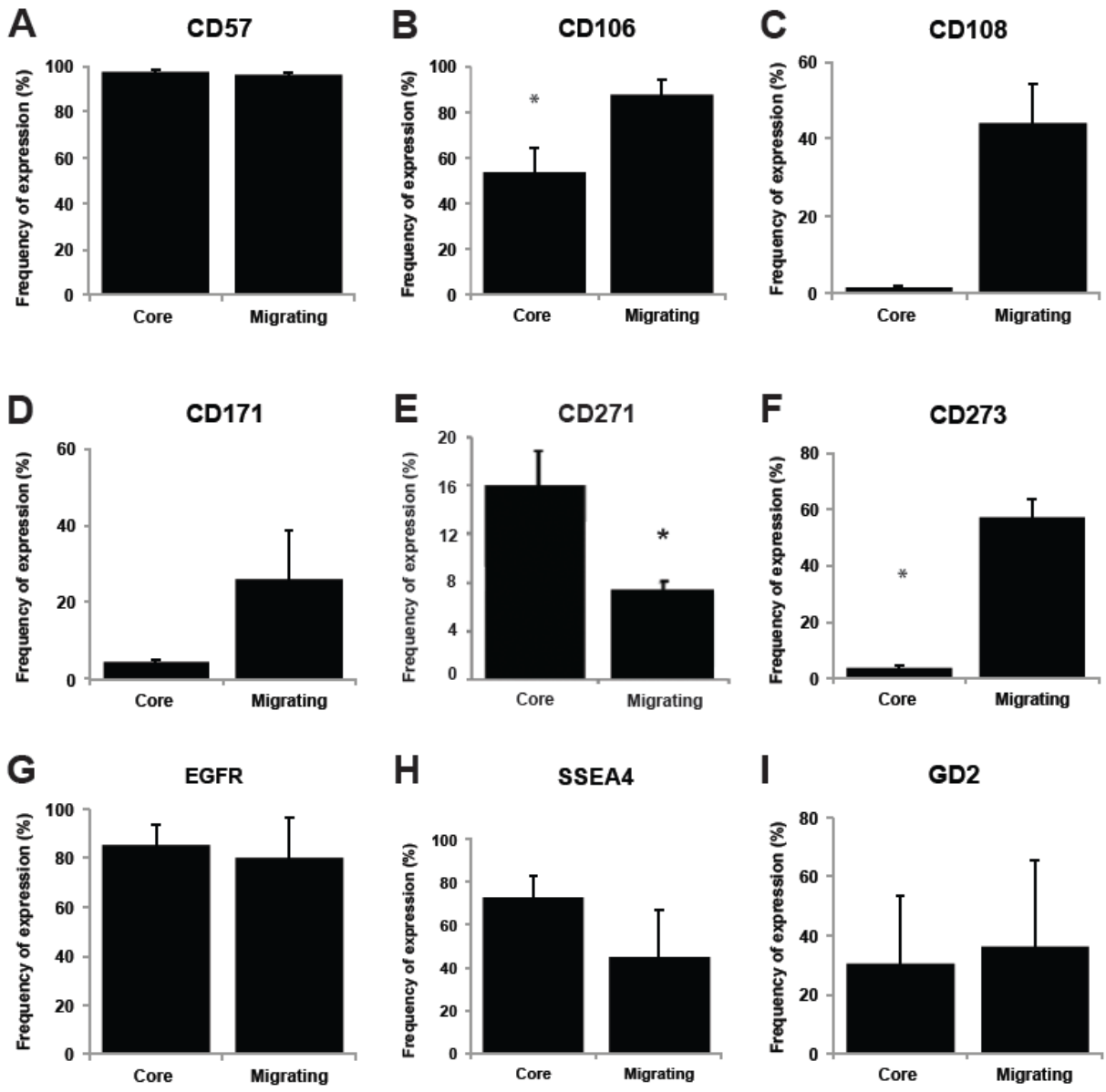

Figure 3.1.5: Migrating MB Cells Exhibit Decreased CD271 and Increased CD106 expression. Comparative cell surface marker expression from "core" versus "migrating" MB cells reveals differential expression of CD271 and CD106. CD171 and EGFR showed no difference between core and migrating cell populations. **A-I**. Cell surface marker antibody screen on the "core" versus "migrating" cells from MB aggregates 48 hours after attachment. Error bars, SEM; *P < .05; N =4 and N = 3 independent experiments. **D.** *Duplicated from Morrison et al. (1) with permission from the publisher.*

3.1.5: CD106 overexpression shows no effect on self-renewal, invasion, cell viability or cellular proliferation in the SHH MB DAOY cell line *in vitro*

CD106 plays an important role in leukocyte-endothelial cell adhesion and signal transduction in healthy cells (250). In cancer, CD106 serum levels have been linked to tumor progression in a variety of non-brain tumors including colorectal, lung, bladder, lymphoma and others (250-257). CD106 has also been shown to be an important pathological and prognostic factor in a variety of other cancers such as ovarian, esophageal, renal and breast cancer (258-262). Functionally, CD106 plays a role in metastasis and angiogenesis in a variety of cancers and this is dependent on the location of CD106 on the tumor cell vs. endothelial cell, as well as the niche (262-264). Very little is known, however, about the role of CD106 in in brain tumors and stem cells.

In order to look at the effect of CD106 on self-renewal, invasion and proliferation, CD106 was overexpressed in Daoy parental cells and confirmed using flow cytometry (Figure 3.1.6 A-B). Self-renewal was measured using a tumorsphere assay over 3 passages. Overexpression of CD106 had no effect on tumorsphere number when compared to controls (Figure 3.1.6 C-G). Cellular invasion was measured using a 3-dimensional *in vitro* type I collagen invasion assay over three days. Cells overexpressing CD106 showed no significant difference in invasion capacity on day 1,2 or 3 through the collagen matrix when compared with the controls (Figure 3.1.6 H-J). Lastly, proliferation and viability where measured by plating 2.5 x 10^4 cells in adherent dishes containing brain tumor media, (serum free

cellular media with 10% fetal bovine serum added). After four days, proliferation and viability, as assessed by trypan blue staining, were measured using an automated cell counter. No significant differences were observed in total cell counts or viability between wells containing cells overexpressing CD106 and control cells (Figure 3.1.6 K-L).

CD106 has no effect on self-renewal, invasion or cellular survival and proliferation *in vitro* based on gain of function studies. Based on these findings, CD106 was no longer pursued as a marker.

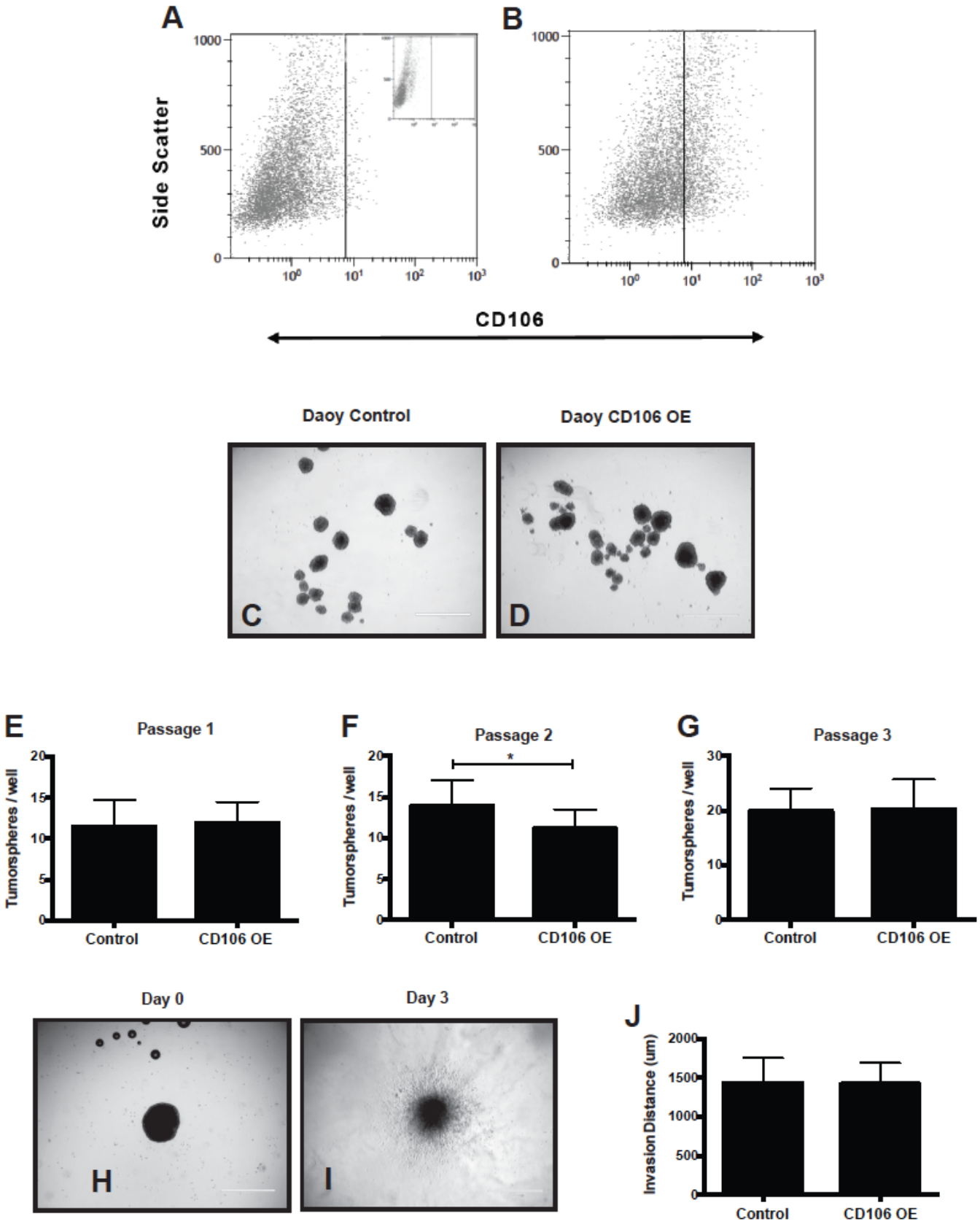
A
B
Side Scatter
1000
500
0
10^0
10^1
10^2
10^3
CD106
Daoy Control
Daoy CD106 OE
C
D
E
Passage 1
Tumorspheres / well
20
15
10
5
0
Control
CD106 OE
F
Passage 2
*
G
Passage 3
30
H
Day 0
I
Day 3
J
Invasion Distance (um)
2000
1500
1000
500

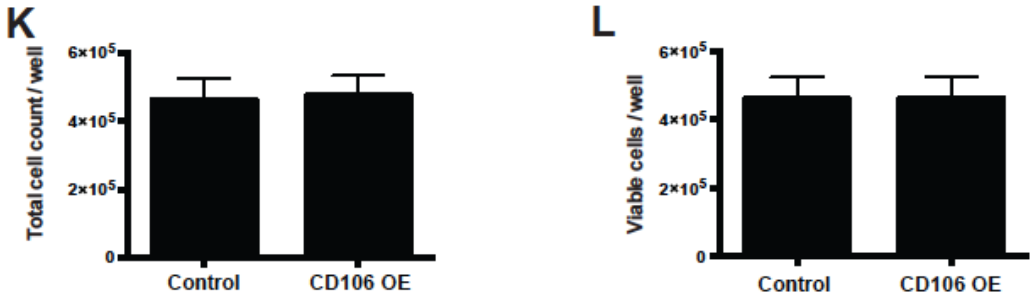

Figure 3.1.6: CD106 has no effect on tumorsphere number, invasion or cellular growth and viability in MB SHH Daoy tumor cells. A-B Flow plots demonstrating endogenous levels in control cell population (unstained control inset) **(A)** and elevated level of CD106 in cells overexpressing the surface marker **(B)**. **C-D.** Passage 3 tumorspheres of control cells **(C)** and cells overexpressing CD106 **(D)**. Scale bar = 1000 μm. **E-G.** Tumorsphere counts/well for passage 1 **(E)** passage 2 **(F)** and passage 3 **(G)** spheres. Control showed no difference in tumorsphere count as compared to CD106 overexpression groups in passage 1, while showing a significant decrease in tumorsphere numbers in the CD106 OE group in the second passage, but losing that difference when passed to third passage. s.e.m. p = 0.013. **H-I.** Cellular invasion assay at day 0 **(H)** and Day 3 **(I)** after implantation of hanging drops composed of cells overexpressing CD106 into Type I collagen. Scale bar = 1000 μm **J.** Invasive distance of control and cells overexpressing CD106 and after 3 days. Control showed no difference in invasion as compared to overexpression groups. **K-L.** Total cell counts (alive + dead) per well **(K)** and viable cells / well **(L)** 4 days after plating 25,000 cells in serum containing media. Control showed no difference in total cell count or viability as compared to CD106 overexpression groups.

3.1.6: CD271 overexpression results in a decrease in tumorsphere number but an increase in tumorsphere size over subsequent passage *in vitro*

This work was performed by Ms. Lisa Liang, PhD candidate, Ogilvie lab

To gain further insight into the functional role of CD271 in SHH MB cells**,** we also generated a stably overexpressing CD271+ line from adherent SHH Daoy MB cells using lentiviral constructs. The Daoy line is traditionally cultured in serum, and under these differentiated conditions, CD271 levels are negligible (168). However, when Daoy cells are adapted to tumorsphere culture in stem cell medium as shown in our flow cytometry screens and analyses, CD271 levels increase (168). As this is a dynamic process, we wanted to test the effects of constitutive CD271 overexpression in SHH MB cells. Following stable selection, CD271 overexpression was validated by flow cytometry and Western Blot (Figure 3.1.7 A-B). To measure self-renewal capacity, tumorsphere assays were performed over 3 passages. CD271 OE resulted in a significant increase in tumorsphere number, and tumorsphere size compared with the negative controls (Figure 3.1.7 C, F-G). Following passage to secondary spheres (P2), we observed a decrease in sphere number (Figure 3.1.7 D-H); however, the larger tumorsphere size was maintained in CD271 OE cells relative to controls (Figure 3.1.7 I). The same patterns were seen following passage to tertiary (P3) tumorspheres (Figure 3.1.7 E, J-K). There was an increase in total cell counts in P1 tumorspheres (Figure 3.1.7 L), however there was no significant difference in P2 and P3 tumorspheres (Figure 3.1.7 M-N) or viability as measured by

Trypan blue staining (Figure 3.1.7 O-Q). In support of our total cell count data, expression of cell cycle genes (*CDK2*, *CDK6*, *CCND1*, *CCND2*) as measured by qPCR showed no significant difference between CD271 OE and control tumorspheres (Figure 3.1.7 R). Staining for the proliferation marker Ki67 showed similar results as there was no difference in the frequency of positive cells (Figure 3.1.7 S).

We next evaluated tumor cell invasion in CD271 OE cells relative to controls using a hanging drop assay followed by implantation of aggregates into collagen gels (234). Following 3 days invasion, there was no significant difference in CD271 OE vs. control cells (Figure 3.1.7 T). Collectively, the loss of tumorsphere number over passage and maintenance of larger tumorsphere size suggest that stable overexpression of CD271 may regulate the self-renewing phenotype in SHH MB.

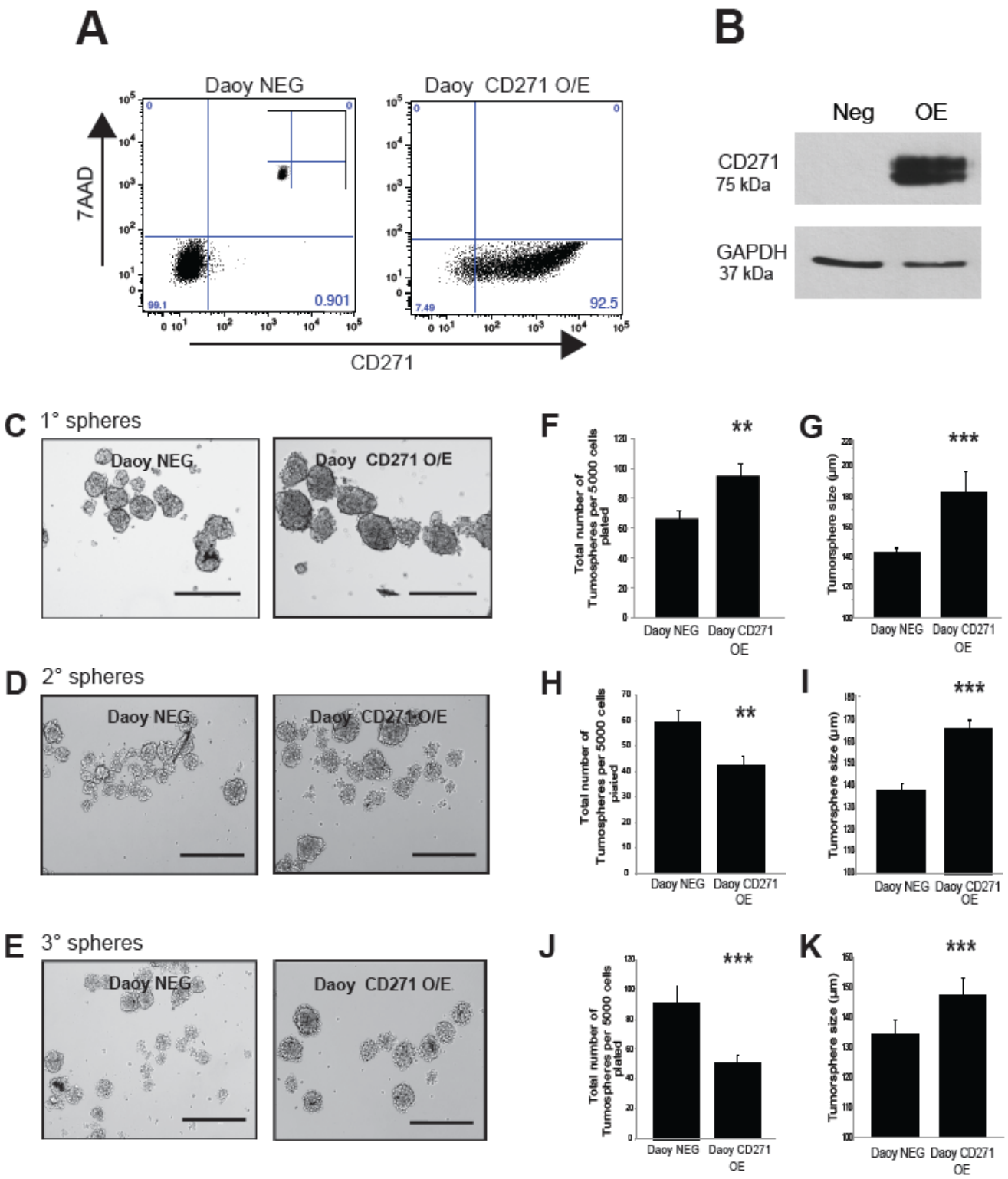
A
Daoy NEG
Daoy CD271 O/E
7AAD
CD271
0.901
92.5
B
Neg
OE
CD271
75 kDa
GAPDH
37 kDa
C
1° spheres
Daoy NEG
Daoy CD271 O/E
D
2° spheres
Daoy NEG
Daoy CD271 O/E
E
3° spheres
Daoy NEG
Daoy CD271 O/E
F
Total number of Tumospheres per 5000 cells plated
**
Daoy NEG
Daoy CD271 OE
G
Tumorsphere size (µm)
***
Daoy NEG
Daoy CD271 OE
H
Total number of Tumospheres per 5000 cells plated
**
Daoy NEG
Daoy CD271 OE
I
Tumorsphere size (µm)
***
Daoy NEG
Daoy CD271 OE
J
Total number of Tumospheres per 5000 cells plated
***
Daoy NEG
Daoy CD271 OE
K
Tumorsphere size (µm)
***
Daoy NEG
Daoy CD271 OE

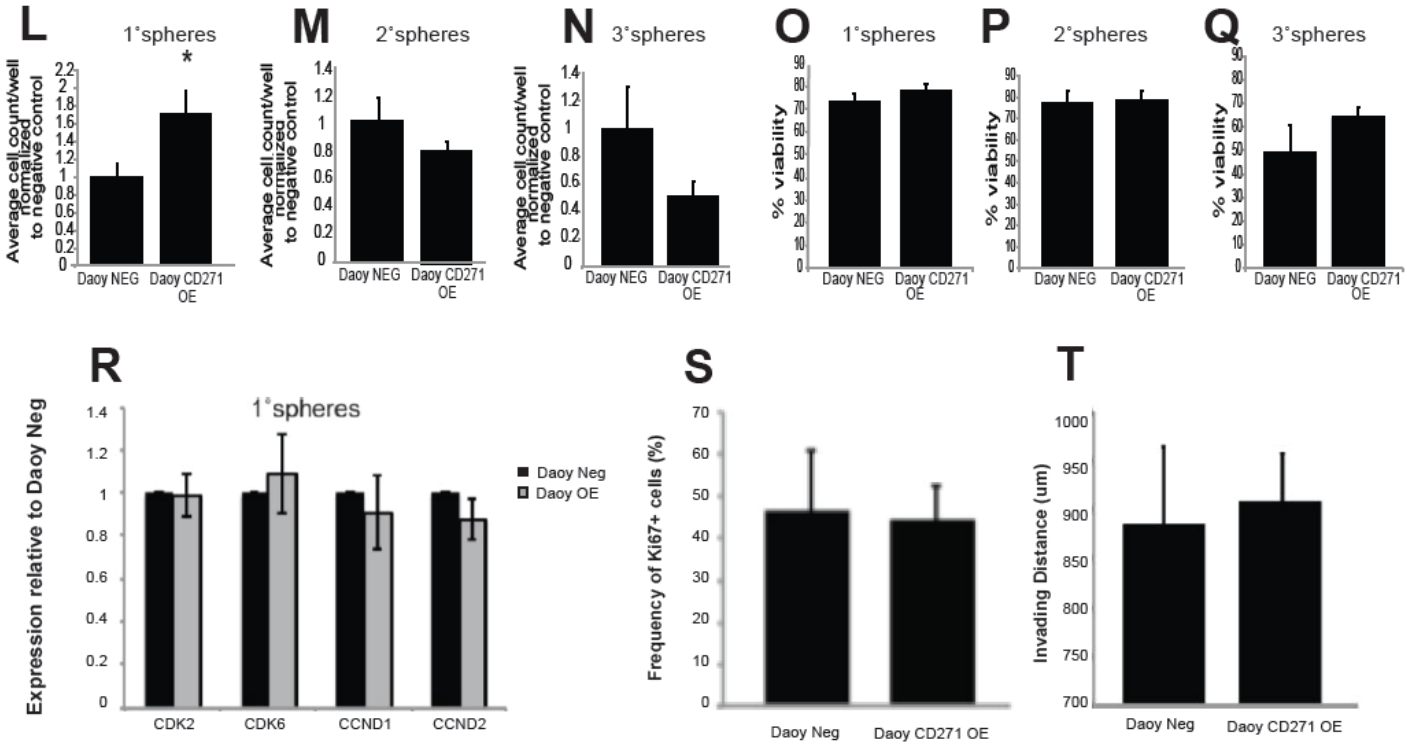

Figure 3.1.7: CD271 overexpression changes the size and number of Daoy tumorspheres. A-B. Validation of CD271 OE in Daoy cells by flow cytometry **(A)** and Western blot **(B).** GAPDH serves as a loading control. Reproduced from Morrison et al. with permission from the publisher. **C-E.** Representative images of primary **(C)**, secondary **(D)**, and tertiary **(E)** tumorspheres from Daoy negative control cells and stable Daoy CD271 OE cells. **F-G.** Primary tumorsphere number **(F)** and tumorsphere size **(G)** are increased in Daoy OEs vs. controls. **H-K.** Tumorsphere number is decreased in secondary **(H)** and tertiary **(J)** Daoy OE cells compared to controls; whereas tumorsphere size is increased in secondary **(I)** and tertiary Daoy CD271 OEs **(K)**. Error bars: s.e.m. P<0.01**, P<0.001***. **L-N.** Average cell count/well normalized to negative control for Daoy CD271 OE tumorspheres. **O-Q.** Quantification of cell viability in primary **(O)**, secondary **(P)**, and tertiary **(Q)** CD271 OE tumorspheres vs. negative control. **R.** qPCR analysis of *CDK2, CKD6, CCND1,* and *CCND2* gene expression in Daoy OE vs. negative control P2 tumorspheres. **S.** Frequency of Ki67+ cells in Daoy NEG and Daoy CD271 OE P2 tumorspheres. **T.** Quantification of invasion for Daoy NEG and Daoy CD271 OE aggregates in a collagen matrix. Error bars: s.e.m. P<0.05*.

3.1.7: CD271 knockdown results in generation of smaller tumorspheres *in vitro*

This work was performed by Ms. Lisa Liang, PhD candidate, Ogilvie lab

To complement our CD271 overexpression studies and to look at specificity of CD271 using a more direct method, we generated CD271 knockdown (KD) cells from our CD271 OE line as well as UI226 SHH cells which, as opposed to Daoy, were originally derived and cultured in stem-cell propagating conditions and therefore express very high endogenous levels of CD271 (Figure 3.1.3). Two different shRNA sequences targeting CD271 were used, along with a scrambled negative control. Both sequences resulted in a KD of CD271 compared to scrambled in all cells tested (Figure 3.1.8 A, F, K). CD271 KD in Daoy OE cells exhibited an increase in tumorsphere number and decrease in tumorsphere size compared to controls in P1 and P2 tumorspheres (Figure 3.1.8 B-E). CD271 KD in MED311 and UI226 cells also results in a decrease in P1 and P2 tumorsphere size compared to controls; however, no significant changes in tumorsphere number were observed (Figure 3.1.8 G-J, L-O)

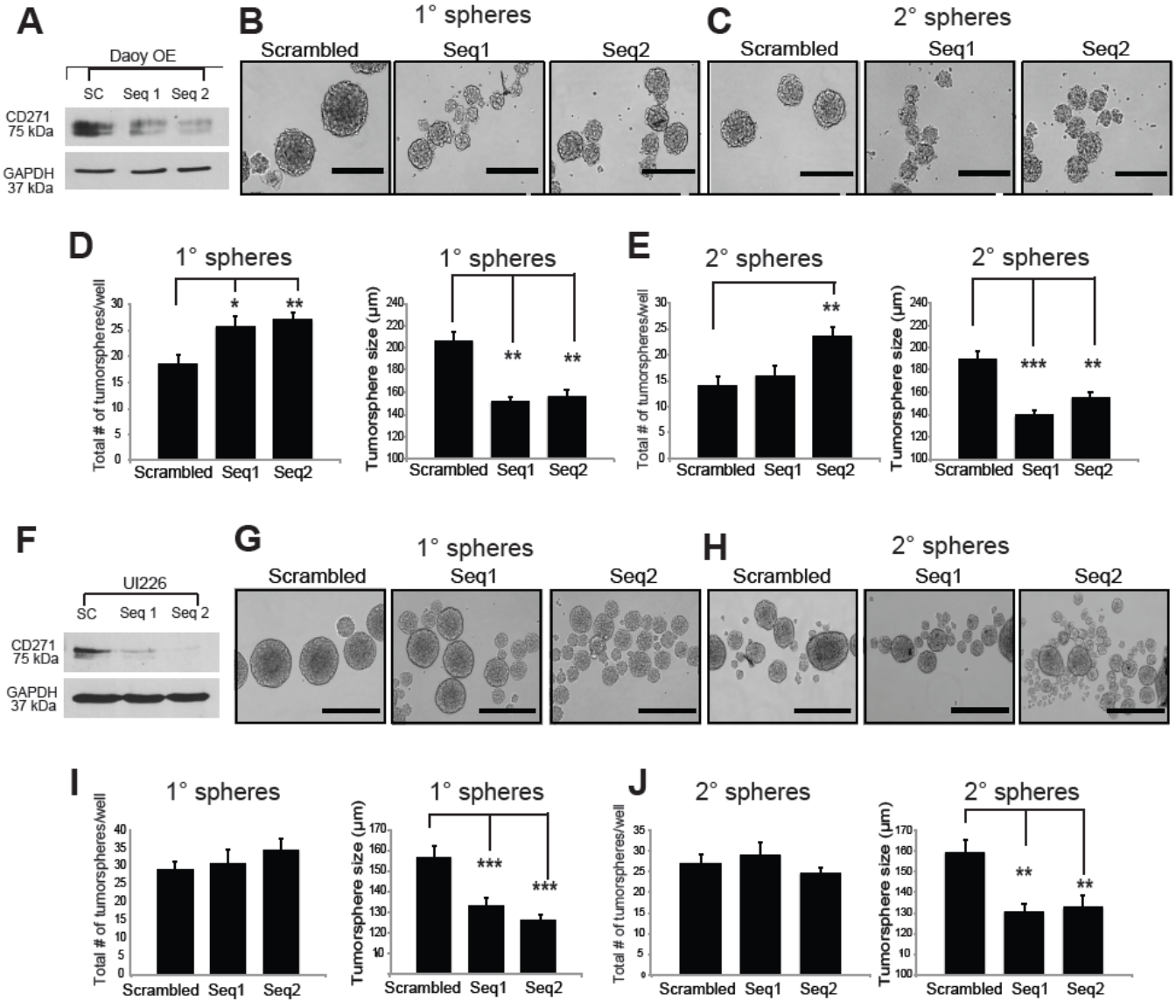
A
Daoy OE
SC
Seq 1
Seq 2
CD271
75 kDa
GAPDH
37 kDa
B
1° spheres
Scrambled
Seq1
Seq2
C
2° spheres
Scrambled
Seq1
Seq2
D
1° spheres
Total # of tumorspheres/well
Scrambled
Seq1
Seq2
1° spheres
Tumorsphere size (µm)
Scrambled
Seq1
Seq2
E
2° spheres
Total # of tumorspheres/well
Scrambled
Seq1
Seq2
2° spheres
Tumorsphere size (µm)
Scrambled
Seq1
Seq2
F
UI226
SC
Seq 1
Seq 2
CD271
75 kDa
GAPDH
37 kDa
G
1° spheres
Scrambled
Seq1
Seq2
H
2° spheres
Scrambled
Seq1
Seq2
I
1° spheres
Total # of tumorspheres/well
Scrambled
Seq1
Seq2
1° spheres
Tumorsphere size (µm)
Scrambled
Seq1
Seq2
J
2° spheres
Total # of tumorspheres/well
Scrambled
Seq1
Seq2
2° spheres
Tumorsphere size (µm)
Scrambled
Seq1
Seq2

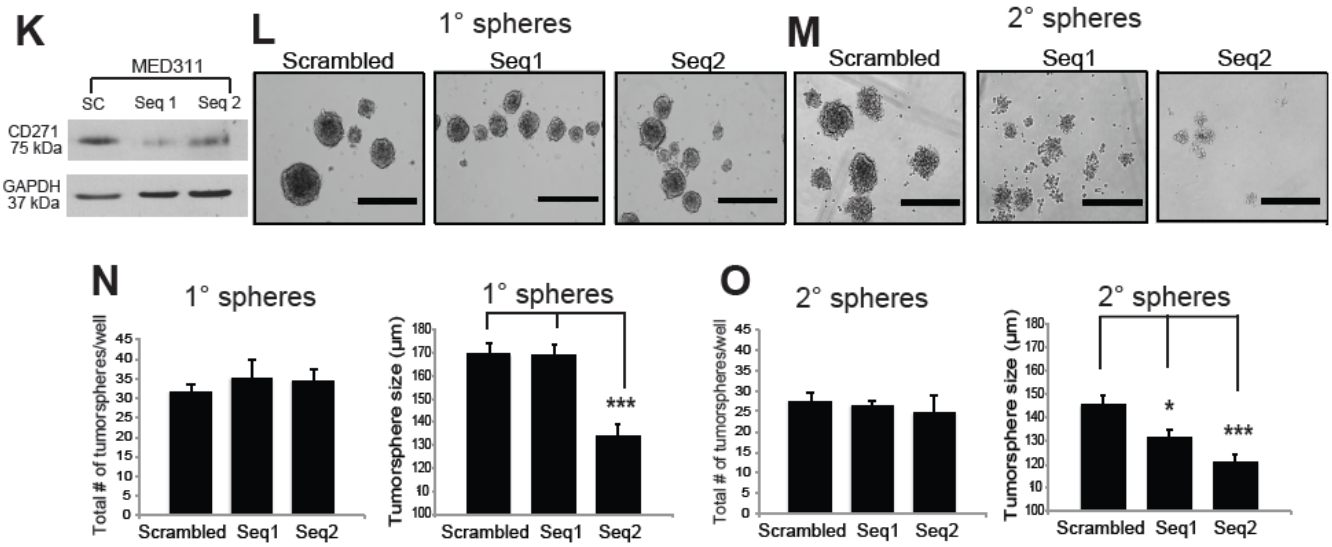

Figure 3.1.8: CD271 knockdown results in significantly smaller tumorspheres. **A.** Validation of shRNA CD271 KD in Daoy OE cells by Western blot. **B-C.** Representative images of primary **(B)** and secondary **(C)** tumorspheres from Daoy OE cells infected with scrambled negative control vs. stable CD271 KD from 2 independent shRNA sequences. **D-E.** Quantification of primary **(D)** and secondary **(E)** tumorsphere number and size following CD271 KD in Daoy CD271 OE cells. **F.** Validation of shRNA CD271 KD in UI226 cells by Western blot. **G-H.** Representative images of primary **(G)** and secondary **(H)** tumorspheres from UI226 cells infected with scrambled negative control vs. stable CD271 KD from 2 independent shRNA sequences. **I-J.** Quantification of primary **(I)** and secondary **(J)** tumorsphere number and size following CD271 KD in UI226 cells. **K.** Validation of shRNA CD271 KD in MED311 cells by Western blot. GAPDH serves as a loading control. **L-M.** Representative images of primary **(L)** and secondary **(M)** tumorspheres from MED311 cells infected with scrambled negative control vs. stable CD271 KD from 2 independent shRNA sequences. **N-O.** Quantification of primary **(N)** and secondary **(O)** tumorsphere number and size following CD271 KD in MED311 cells. Error bars: s.e.m. $P < 0.05$*, $P < 0.01$**, $P < 0.001$ ***. Reproduced from Morrison et al with permission from the publisher.

We did not observe consistent changes in total cell counts and viability as measured by Trypan blue staining in Daoy OE, UI226 or MED311 cells (Figures not shown). Cell cycle gene (CDK2, CDK6, CCND1, CCND2) expression was also measured by qPCR in UI226 and MED311KD cells, and the differences were either not significant or inconsistent between the 2 shRNA sequences. These KD data provide additional support for our overexpression studies and suggests that CD271 plays a role in regulating the SHH MB stem/progenitor cell state.

3.1.8: Sorted CD271+ cells when xenografted into NOD SCID mice show no difference in tumor grade and tumor area when compared to CD271- cells

The work presented from here on was completed by myself

We next wanted to see what effect CD271 had on tumor grade, tumor area, tumor initiating capacity and self-renewal *in vivo*. We injected both sorted CD271+/- cells and CD271 OE cells into NOD SCID mice. Based on our *in vitro* overexpression and knockdown data, we hypothesize that CD271 is selecting for a lower self-renewing stem or progenitor cell in SHH MB. Both cell types are potential cells of origin for this molecular variant (12, 96, 166, 167). A decreased self-renewal capacity in CD271 OE cells, irrespective of whether selection is for a stem or progenitor cell, may result in decreased tumor growth following injection of CD271+ and CD271 OE cells *in vivo*.

To measure tumor grade, area and tumor initiating capacity, cultured FACS

sorted CD271+/– cells were xenografted into the right cerebral cortex of NOD SCID mice at $5x10^4$ and $1x10^3$ cell numbers. All mice injected with $5x10^4$ CD271+/- cells formed tumors (N=3 and N=6 respectively), while 80% (N=5) of mice injected with $1x10^3$ CD271+ and 50% (N=4) of mice injected with $1x10^3$ CD271- cells formed tumors (Figure 3.1.9 A). Tumor grade and area were on average higher for tumors that formed from $5x10^4$ and $1x10^3$ CD271+ injected cells as compared to CD271- cells, however these differences were not significant (Figure 3.1.9 B-E).

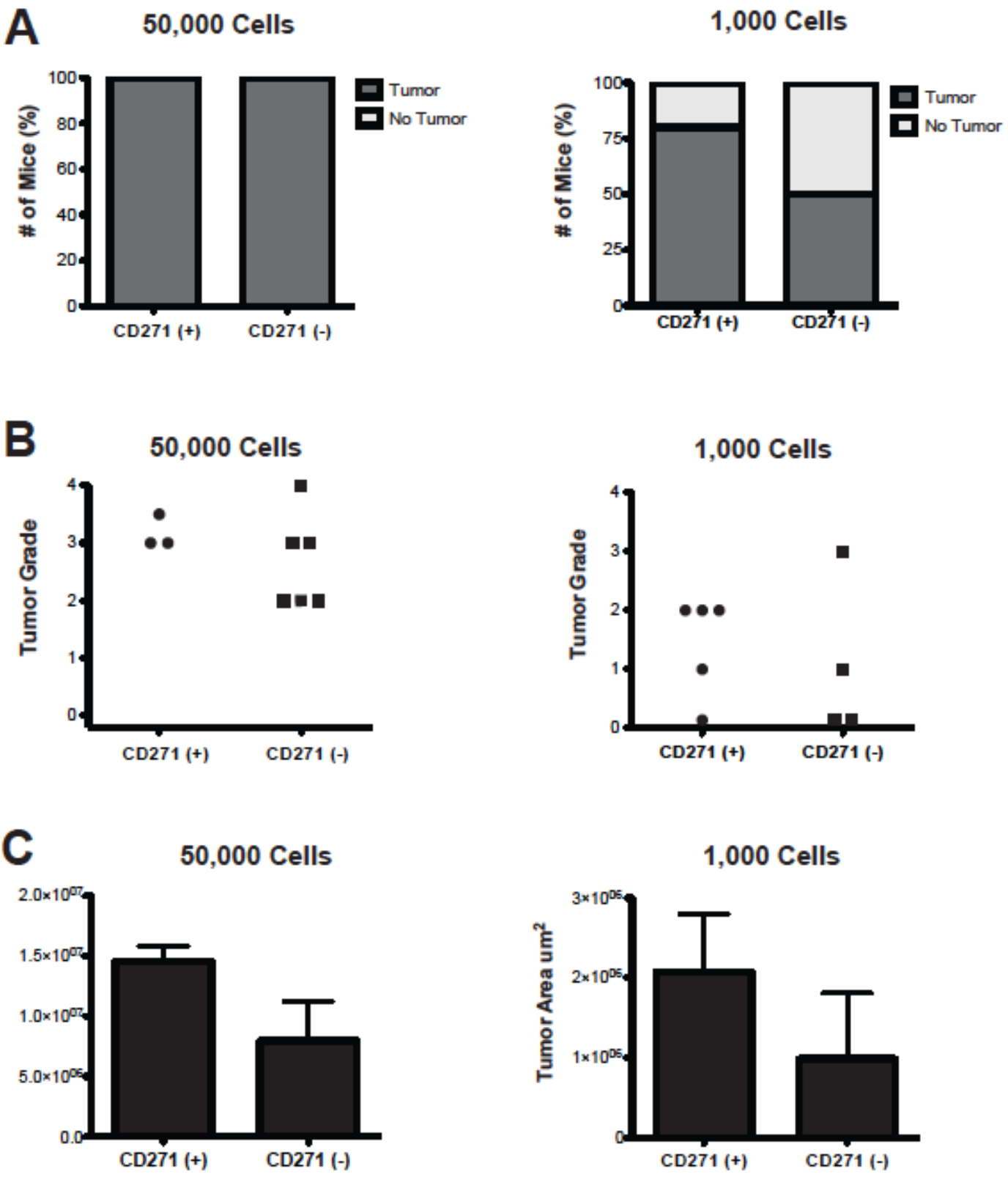
A
50,000 Cells
1,000 Cells
# of Mice (%)
Tumor
No Tumor
CD271 (+)
CD271 (-)
B
Tumor Grade
C
Tumor Area um²

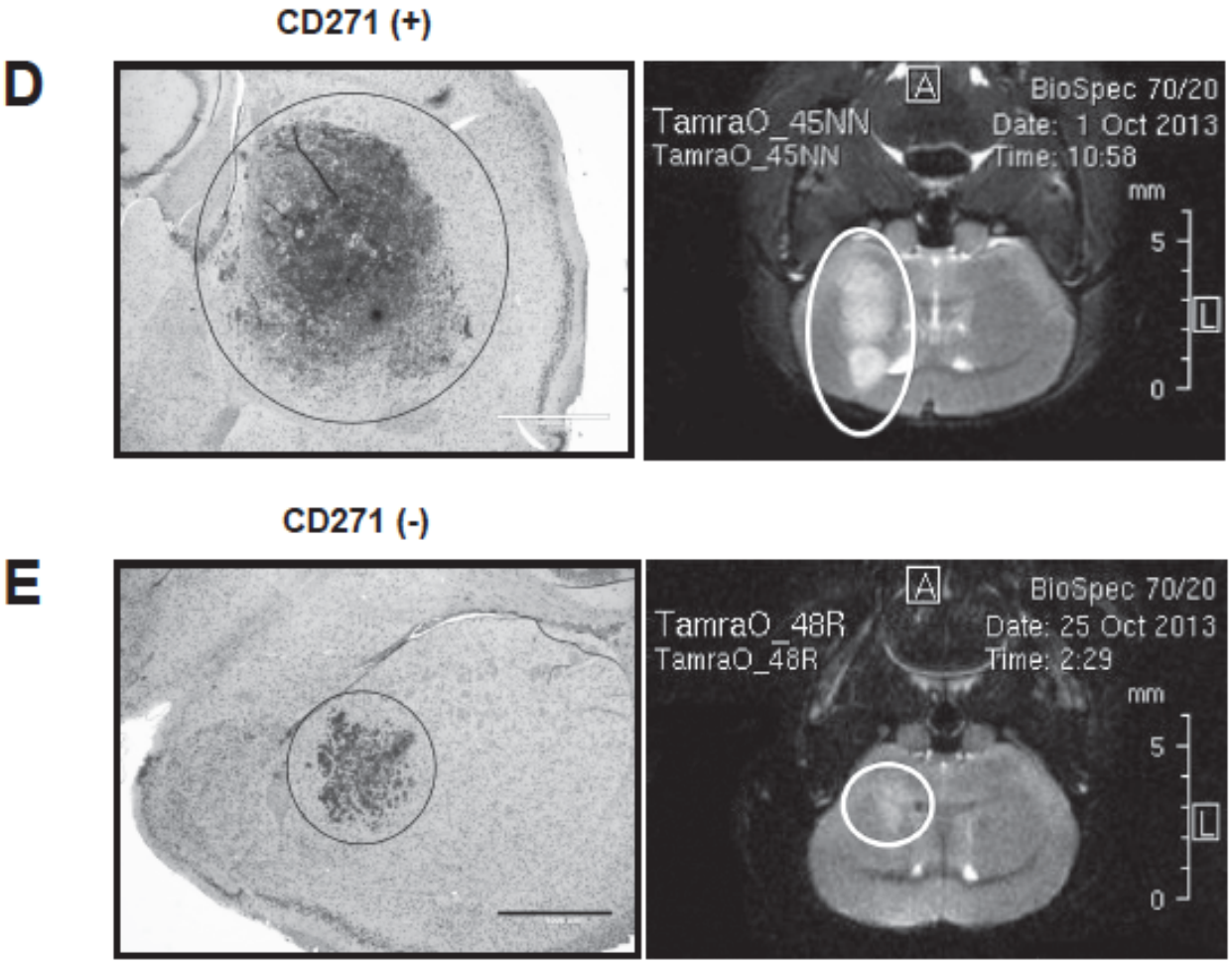

Figure 3.1.9: Sorted CD271+/- cells show no difference in tumor initiating capacity or tumor grade *in vivo*. A. The percentage of mice that developed tumors when 50,000 and 1,000 CD271+ and CD271- cells were injected into the right frontal cortex of NOD SCID mice. N = 3,6,5,4 respectively. **B.** Tumor grade from mice injected with 50,000 and 1,000 CD271+ and CD271- cells. **C.** Tumor area from mice injected with 50,000 and 1,000 CD271+ and CD271- cells. . **D-E.** Representative H&E staining and MRI images of tumors from mice injected with CD271+ cells **(D)** and CD271- **(E).**

3.1.9: Secondary tumors derived from primary CD271+ tumors showed no difference in tumor penetrance, tumor grade and tumor area when compared to secondary tumors derived from primary CD271- tumors

The gold standard in measuring self-renewal *in vivo* is to perform limiting dilutions and secondary tumor transplants in immunodeficient mice. Secondary tumor injections were performed from mice initially injected with CD271+/- cells. The brains of mice that contained primary tumors from the injection of CD271+/- cells were harvested, dissociated and tumor cells recovered using FACS sorting based on HLA+ CD45- (Figure 2.5). Recovered cells were then re-injected into NOD SCID mice to measure the ability of these cells to be serially passaged *in vivo*. It is important to note that CD271 was only used as a sorting parameter for the primary tumor injections, and not in the recovered cells dissociated from primary tumors for secondary injections. An N of 3 was performed for recovered cells originating from CD271+ primary tumors and N of 2 from cells originating from CD271- primary tumors. All 3 mice from the CD271+ group formed tumors while only 1 of the 2 mice from the CD271- group (N=2) formed tumors (Figure 3.1.10 A). On average, tumor grade and tumor area were higher in secondary mice from the CD271+ group as compared to the CD271- group, however, these differences were not statistically different (Figure 3.1.10 B-C). Small sample sizes in this experiment were due to difficulty in recovering adequate cell number for secondary transplants.

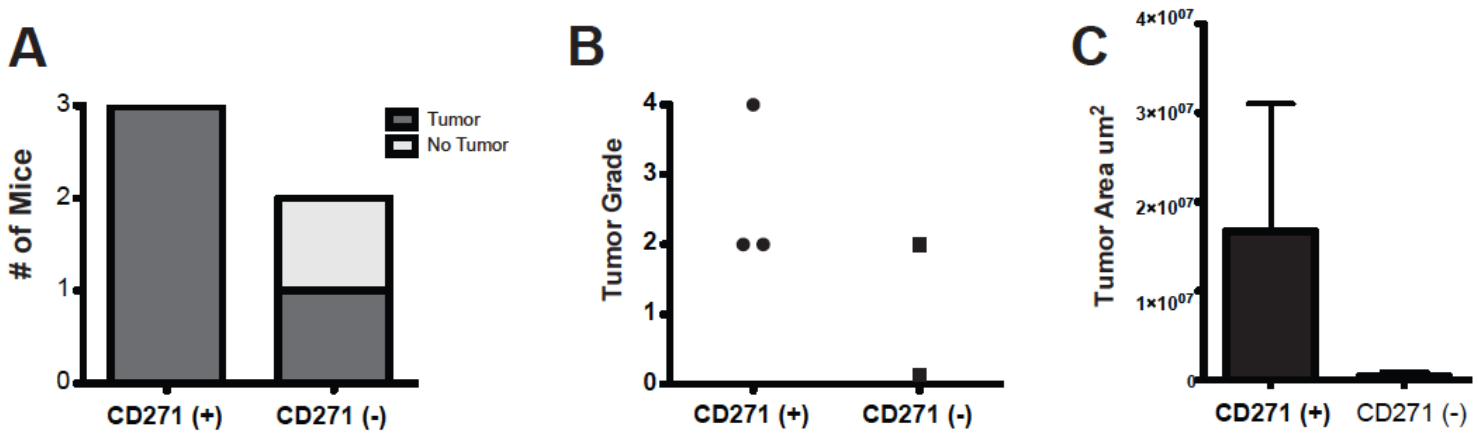

Figure: 3.1.10: Secondary tumors derived from CD271+ and CD271- primary tumors. CD271 was only used as a sorting parameter for the primary tumor injections, and not in the recovered cells dissociated from primary tumors for secondary injections **A.** Number of mice that formed/did not form tumors after xenografting primary tumor cells into secondary mice. **B-C.** Grade **(B)** and tumor area **(C)** of same mice. These differences were not statistically significant. N = 3 and N=2 respectively.

Despite our hypothesis that a lower self-renewing cellular population would result in a decreased tumor size *in vivo*, there were no significant differences between CD271+ and CD271- cells in our animal models. Our previous studies (168), as well as additional unpublished work in the laboratory have shown that sorted subpopulations reset phenotypic equilibrium in culture. For example, we demonstrated that CD271+ cells can give rise to CD271- cells and vice versa within 5 days after sorting (168) (Liang et al., 2018, accepted at Cancer Research). Therefore, sorted populations exhibit phenotypic plasticity, in line with the updated view of CSC theory (170). It was thought that this reestablishment could lead to tumor initiation from both populations after sorting *in vivo*. It can be assumed that after xenografting, cells sorted based on CD271 status will undergo a reestablishment of their CD271 equilibrium, similar to *in vitro*. To test this theory would require additional staining for CD271 by immunohistochemistry *in vivo*. Due to the inherent instability of CD271 status of cells after sorting, we decided that gain of function studies would provide a better measure of what effect CD271 has on tumor formation *in vivo*.

3.1.10: CD271 overexpression results in smaller tumors *in vivo.*

For gain of function studies, 5 x 10^4 Daoy MB cells from passage 1 tumorspheres overexpressing CD271 (N=6) and their controls (N=4) were xenografted into the cerebral cortex of NOD SCID mice and evaluated after 13

weeks. Immunohistochemical staining revealed sustained overexpression of CD271 after 13 weeks *in vivo* (Figure 3.1.11 A-D). Indeed, cells stably overexpressing CD271 formed tumors; however, they were significantly smaller as demonstrated by a decreased tumor area and lower tumor grade, when compared to control cells expressing lower endogenous levels of CD271 (Figure 3.1.11 E-F). Control cells formed very large tumors in the striatum and thalamus, whereas CD271 OE cells formed masses consisting of small tumor deposits in the striatum (Figure 3.1.11 G-J).

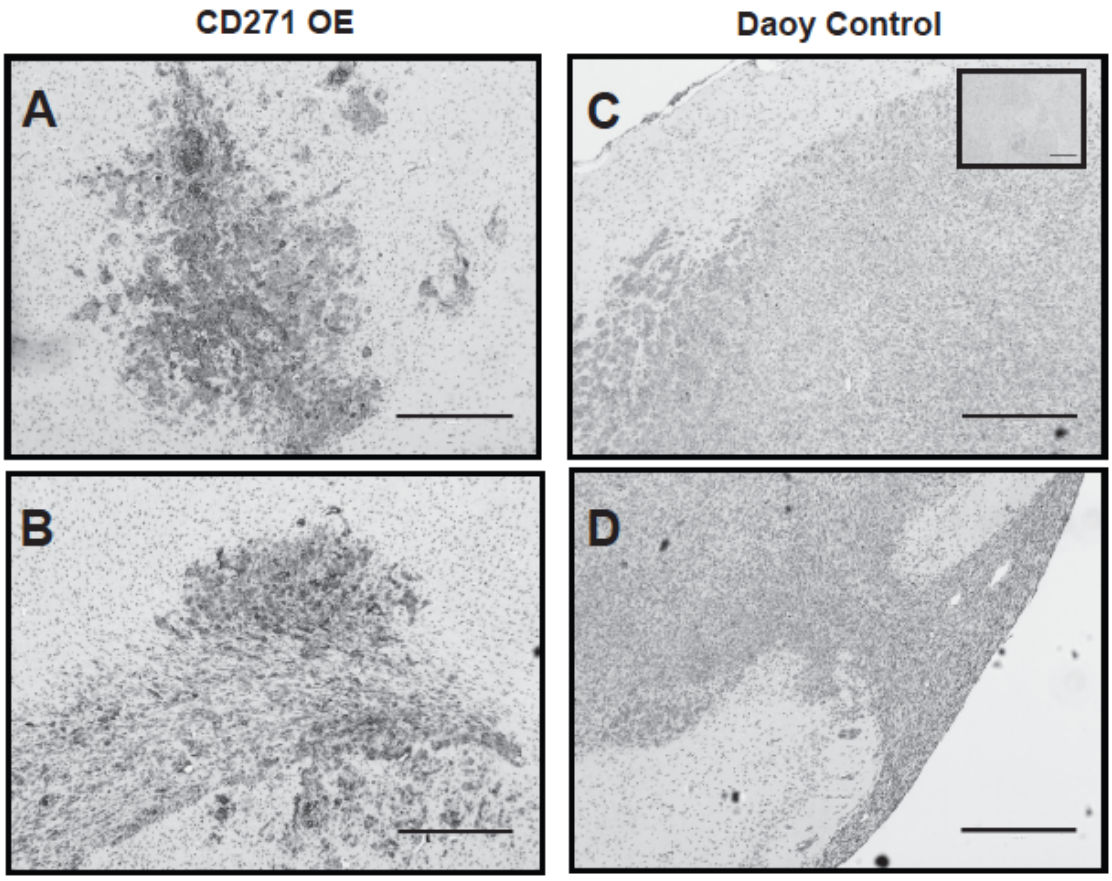
CD271 OE
Daoy Control
A
B
C
D

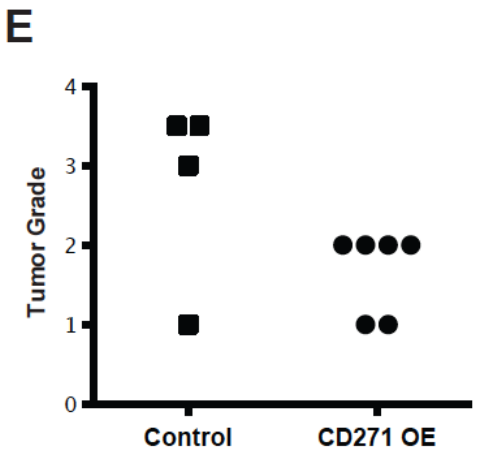
E
Tumor Grade
4
3
2
1
0
Control
CD271 OE

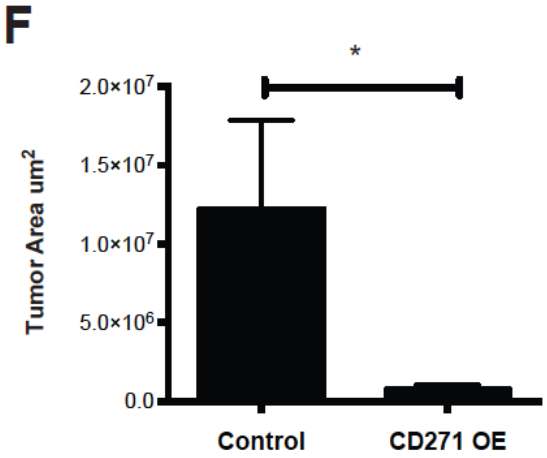
F
*
Tumor Area um2
2.0×10^7
1.5×10^7
1.0×10^7
5.0×10^6
0.0
Control
CD271 OE

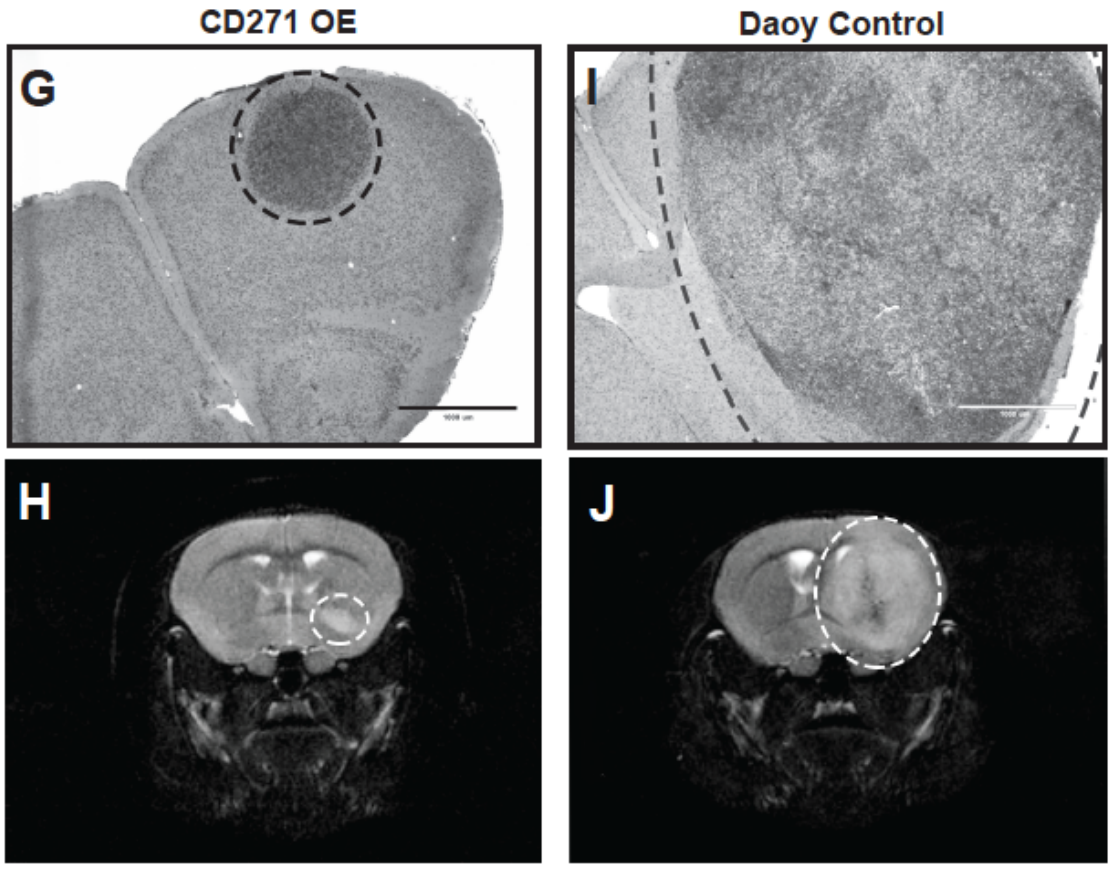

Figure 3.1.11: Overexpression of CD271 results in smaller and lower grade tumors *in vivo*. A-D. Immunohistochemistry staining for CD271 in xenografts derived from Daoy CD271 OE **(A,B)** and Daoy NEG **(C,D)** tumorsphere cells injected intracranially into NOD SCID mice. Inset: secondary only negative control. Scale bar: 400 µm. **E-F.** Injection of CD271 OE cells into NOD SCID mice results in tumors with a lower grade **(E)** p = 0.1461 and significantly smaller tumor area **(F)**, p = 0.0334, than cells expressing lower, endogenous levels of CD271. **G-J.** Representative H&E staining and MRI of tumors from mice injected with CD271 OE cells **(G-H)** and Daoy control cells **(I,J)**. Scale bar = 1000 µm

Chapter 3.2: Uncoupling *in vivo* properties from *in vitro* tumor propagating cell properties

3.2.1: Rationale

Xenotransplantation into immunodeficient mice has become the gold standard for evaluation of TPC properties from human tumor cells *in vivo* (188). This assay is used to determine the tumor initiating capacity (TIC) of human cells (188). Dissociation of primary tumors and transplantation into secondary mouse recipients enables one to evaluate self-renewal *in vivo.* Previously, the general consensus within the literature was that cells exhibiting a high self-renewal capacity *in vitro* demonstrate larger and faster tumor growth, increased tumor penetrance and decreased survival *in vivo* (70, 154, 207, 248). However, a handful of papers have revealed an inverse correlation between these characteristics in genetic mouse models of the adult glioblastoma (GB) (265-267). For example Barrett *et al*. using a PDGF- and KRAS-driven murine model of glioma showed that cells expressing high levels of Id1 ($Id1^{high}$) (Inhibitor of DNA-binding), displayed a higher SR capacity *in vitro* than $Id1^{low}$ cells (266). However, when injected into the cortex of nude mice, $Id1^{low}$ cells generated tumors more rapidly and with higher penetrance than $Id1^{high}$ cells. Similarly, Li et al. discovered a population of nestin expressing progenitor cells located in the developing mouse cerebellum (265). This cellular population, despite not forming tumorspheres *in vitro*, showed similar tumorigenic potential *in vivo* as granule neuron precursors when SHH was aberrantly expressed. This has also been shown in a human model of AML (268), however to our knowledge has not been shown in a solid human tumor model of cancer.

To test this principle in our medulloblastoma xenograft model, we looked at the tumor forming characteristics of our higher and non-SR subclones, cellular populations that are derived from the same cell line that display very unique and contrasting characteristics *in vitro*. We evaluated tumor initiating capacity, self-renewal, survival and tumor aggressiveness *in vivo* to determine if cellular characteristics seen *in vitro* translate *in vivo*.

3.2.2: A non self-renewing sub-clone when compared to a higher-self renewing sub-clone derived from the Daoy MB cell line demonstrates a higher primary tumor grade, shorter survival and comparable tumor penetrance when xenografted into NOD SCID mice.

We previously derived sub-clones from a parental Daoy MB cell line using single cell FACS (Figure 3.2.1 A-B) (168). Tumor cells were xenografted into the right frontal cortex of NOD SCID mice. The non-SR sub-clone formed much larger tumors in a significantly shorter time period with well-defined borders, focal necrosis and minimal perivascular infiltration and cell deposition in the subarachnoid space (SAS) (Figure 3.2.1 C-E). Higher SR sub-clones formed smaller tumors with a small cellular collection at site of injection and significant perivascular infiltration and cell deposition in the SAS (Figure 3.2.1 F-H). MRI imaging and histological analysis revealed these two cellular populations form very distinct tumor phenotypes with distinguishing clinical presentations.

To evaluate the tumor-initiating capacity of these cellular populations, we used limiting dilution analyses. Limiting dilutions evaluate the minimum number of cells required to form a tumor. This can be seen as a surrogate measure of cancer stem cell density as cellular populations with higher CSC populations will theoretically develop tumors at lower cell numbers as compared to cell populations with a lower percentage of CSCs. Cell numbers of $5x10^4$, $1x10^3$ and $1x10^2$ were injected into the frontal cortex of NOD SCID mice. Tumor penetrance showed no significant difference between higher and non-SR sub-clones (Figure 3.2.1 I-K). Only mice injected with $1x10^3$ cell number and greater formed tumors indicating that at minimum, more than $1x10^2$ and less than $1x10^3$ cells are needed for tumor initiation in our cellular populations. These results demonstrate that less than 1% of our cellular population exhibits tumor initiating capacity (TIC),. Tumor grade was significantly higher in mice injected with non-SR cells in the $5x10^4$ group ($p=0.0024$) (Figure 3.2.1 L). While the highest tumor grades were observed in the $1x10^3$ cell group, the difference was not significant ($p=0.2453$) (Figure 3.2.1 M). No tumors were formed when $1x10^2$ cells were injected using either subclone (Figure 3.2.1 N).

Survival was measured using matched cell number injections ($5x10^4$) for each population. End point was set at 25% weight loss from the maximum weight the mouse achieved. Mice injected with the non-SR sub-clone (N=7) showed a significantly reduced survival when compared to mice injected with higher SR sub-clone (N=6) using a Mantel-Cox test ($p=0.0275$) (Figure 3.2.1 O). Mice injected with non-SR tumors developed large tumors very quickly causing a large mass effect and herniation. Mice injected with the higher SR subclone on the other hand slowly

developed significant hydrocephalus due to the significant SAS spread causing a blockage in the CFS.

Overall, the non-SR sub-clones were found to exhibit a shorter survival, higher tumor grade and similar tumor penetrance *in vivo* when compared to a higher SR sub-clone. Together, these results demonstrate that a cellular population that contains a higher self-renewing cellular population *in vitro* does not necessarily lead to a more aggressive tumor and lower survival when xenografted into an immunodeficient mouse model system.

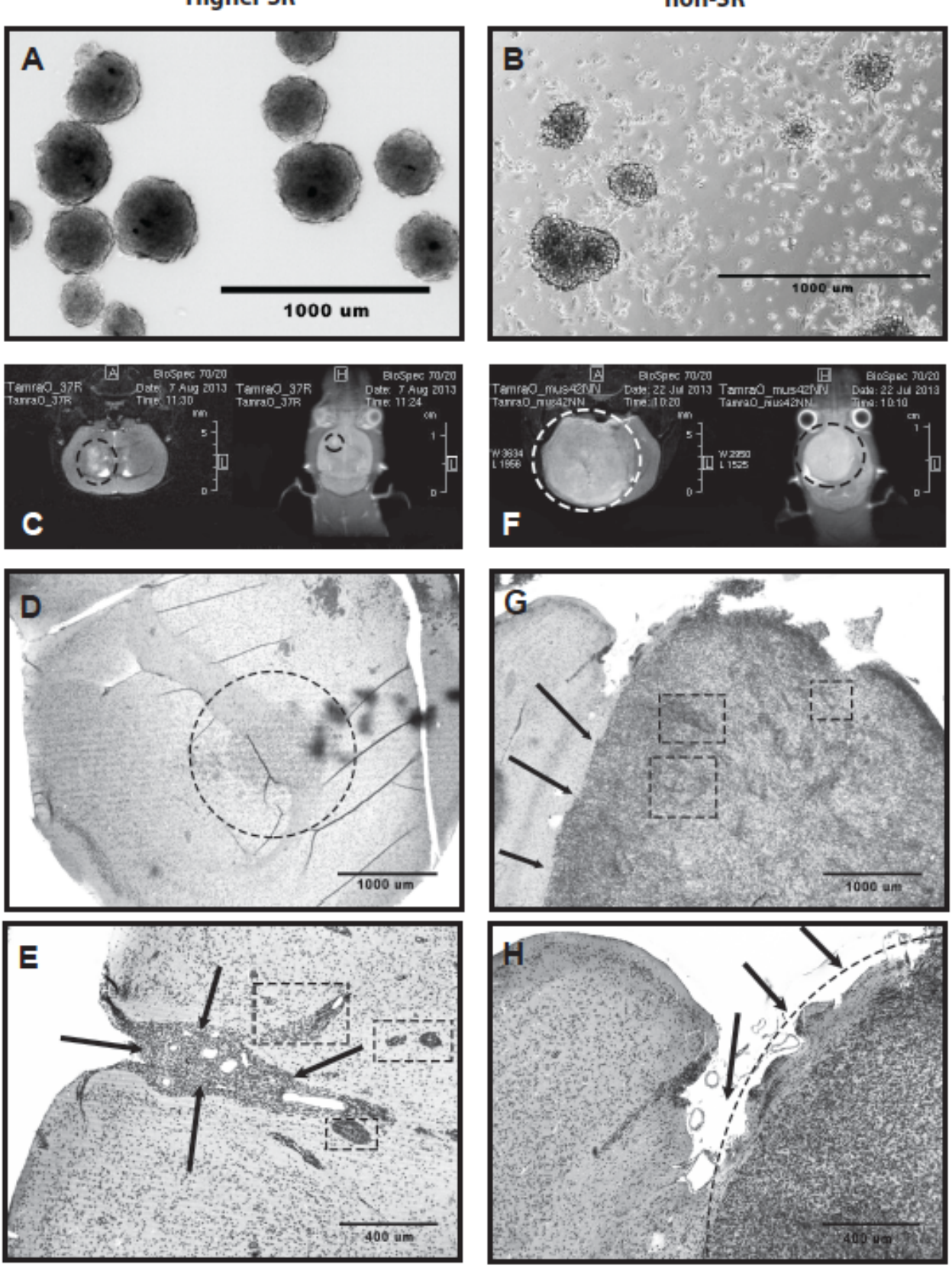
Higher SR
non-SR
A
1000 um
B
1000 um
C
F
D
1000 um
G
1000 um
E
400 um
H
400 um

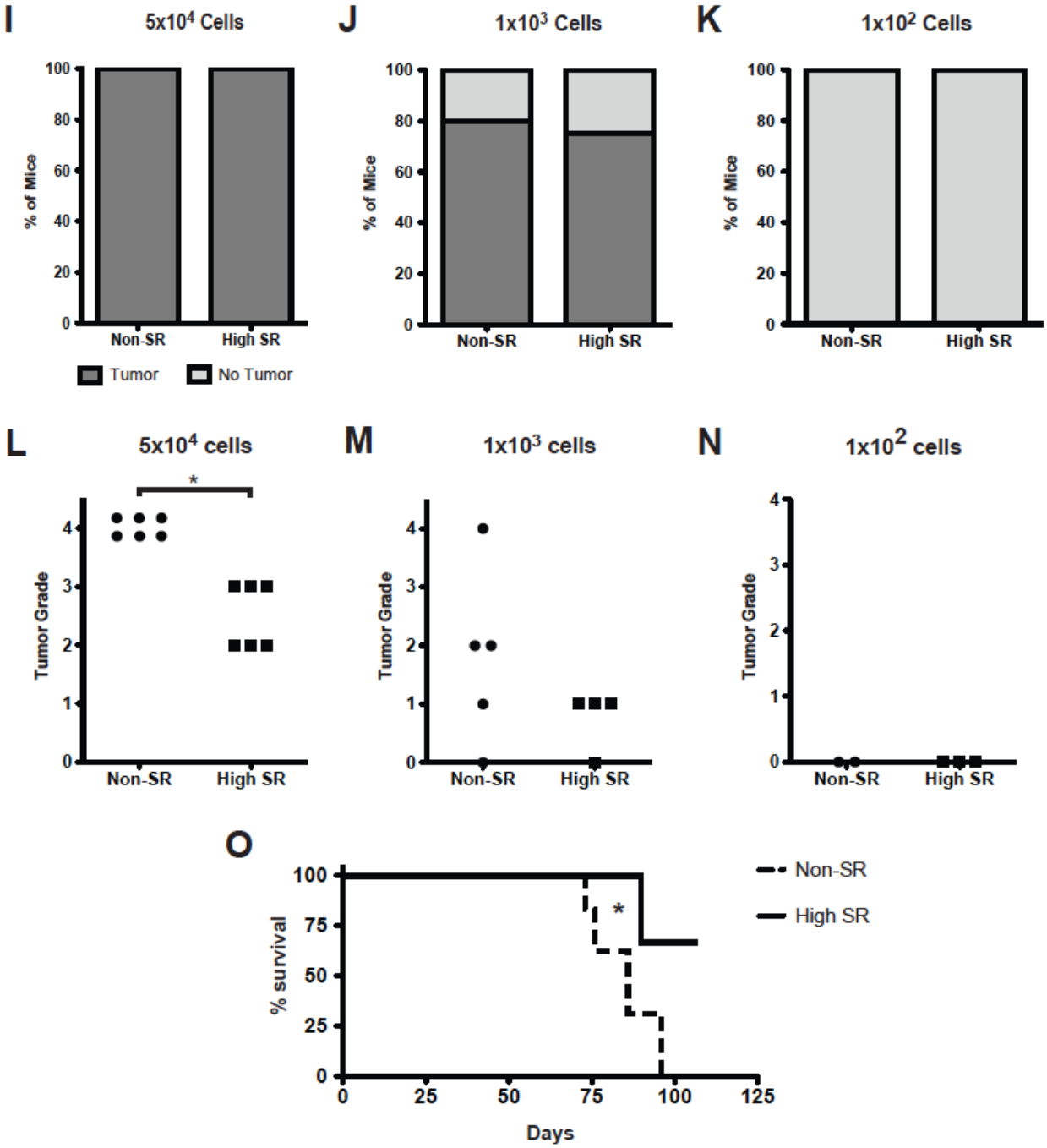

Figure 3.2.1: A non self-renewing sub-clone when compared to a higher-self renewing sub-clone derived from the Daoy MB cell line forms larger tumors with well defined borders and minimal infiltration A-B. P(2) Tumorspheres prior to injection into NOD SCID mice. **A)** shows a higher SR subclone vs **B)** showing a non-SR subclone with tumor cells losing self renewal potential and adhering to plate. **C-D.** Representative MRI images of mice injected with higher SR

(**C)** and non-SR **(D)** subclones. Note Tumor size is significantly reduced in higher SR clone as compared to non-SR clone. **E-H.** Representative histology of mice injected with higher SR **(E,F)** and non-SR **(G,H)** subclones. Higher SR subclone developed tumors with a small cellular collection at site of injection **(E)** and significant perivascular infiltration (box) **(F)** and cell deposition in the subarachnoid space (black arrows). Non-SR subclone formed much larger tumors **(G)** with well defined borders (black arrows), focal necrosis (box) and minimal perivascular infiltration and cell deposition in the subarachnoid space (black arrows) **(H)**. Images taken at 4X **(E,G)** and 10X **(F,H)** magnification. **I-K.** No difference was seen in tumor penetrance between higher and non-SR subclones at any cell number. **L-M.** Non-SR subclone formed higher grade tumors at $5x10^4$ **(L)** and $1x10^3$ **(M)** cell numbers, while no tumors were formed at $1x10^2$ **(N)** cell number. **O.** Non-SR subclone resulted in a decreased survival. * = $p < 0.05$

3.2.3: The same non self-renewing sub-clone when compared to a higher-self renewing sub-clone derived from the Daoy MB cell line demonstrates a higher secondary tumor grade and similar self-renewal and tumor penetrance when isolated from primary tumors and xenografted into secondary NOD SCID mice.

Secondary tumor transplantation is the gold standard measure of self-renewal *in vivo*. This is analogous to the tumorsphere assay used to measure SR *in vitro*. The ability to propagate tumors from one mouse to another is used as a measure of SR, the same way subsequent tumorsphere passage is utilized in culture. Theoretically, a cellular population with a higher self-renewal capacity will form tumors at a higher penetrance in secondary mice when compared to cellular populations with a lower SR.

The same non-SR and higher SR sub-clones derived from the Daoy SHH cell line used above were infected with turbo RFP construct and xenografted into primary mice. RFP+ tumors cells from primary xenograft tumors were dissected, dissociated and isolated using FACS sorting (Figure 2.6). This was a far superior method when compared to sorting based on HLA as no antibody was needed. In addition. I was able to dissect the tumor from the brain using a dissecting microscope, thereby increasing the proportion of tumors cells in our sorting sample. Five thousand isolated primary tumor cells were then re-injected into the right cortex of NOD SCID (secondary) mice. A total of 7 mice were injected per cellular population with secondary tumor cells.

Both tumor populations formed secondary tumors with similar phenotypes seen in the primary tumors above (Figure 3.2.2 A-B). The Non-SR subclone formed tumors with a significantly higher tumor grade as compared to tumors derived from the higher SR Daoy subclone ($p=0.0153$) (Figure 3.2.2 C). Although a smaller number of mice injected with higher SR sub-clone formed tumors, there was no significant difference seen in tumor penetrance between sub-clones ($p=0.4615$) (Figure 3.2.1 D).

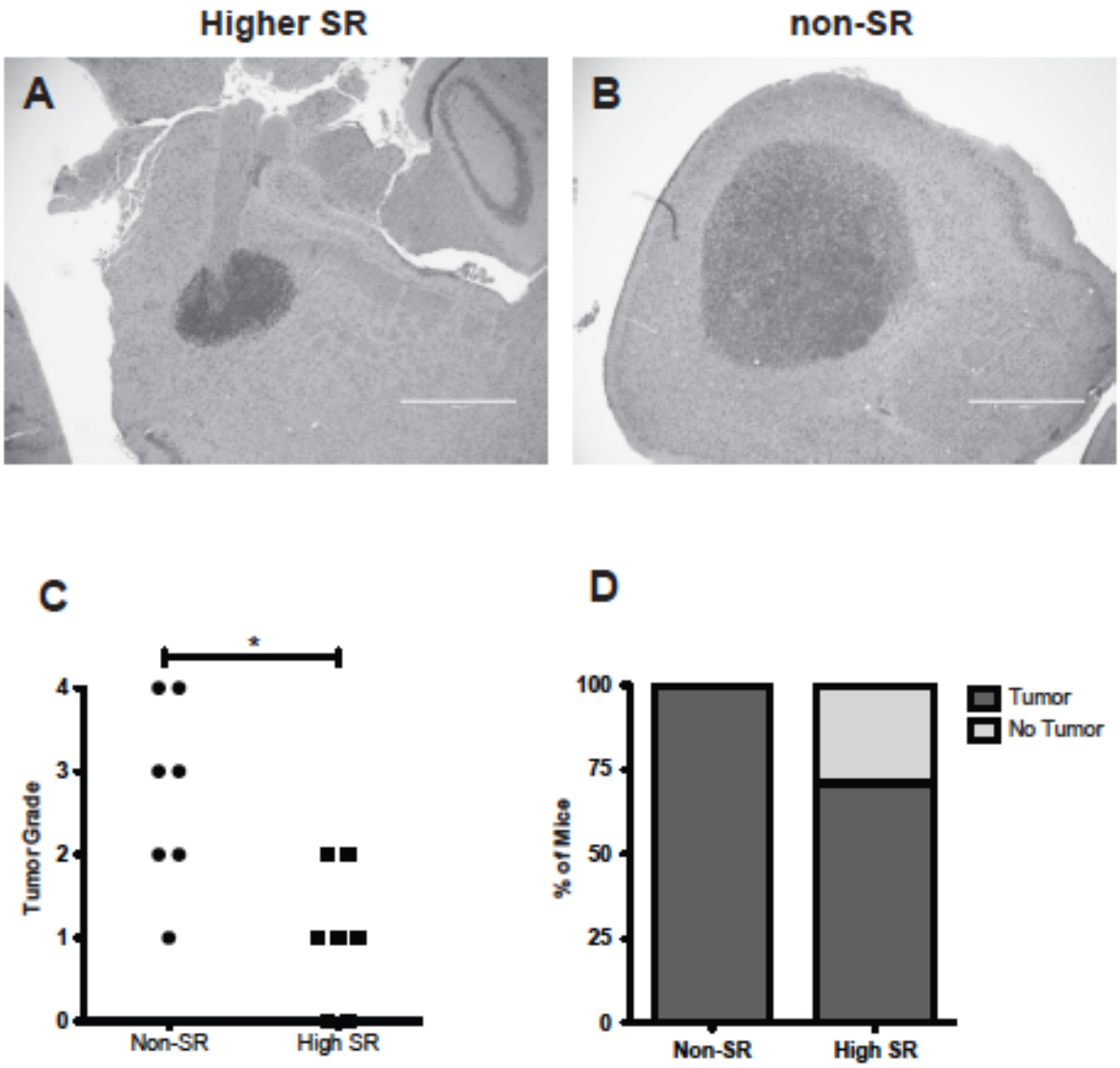

Figure 3.2.2: Secondary tumors derived from non-SR subclones form tumors with a higher grade and similar tumor penetrance when compared to secondary tumors derived from higher SR subclones. A-B. Representative histology of secondary tumors from higher SR **(A)** and non-SR subclones **(B)**. **C-D**. Secondary tumors derived from non-SR subclone form tumors with a larger tumor grade **(C)** and equivalent tumor penetrance **(D)** as compared to the higher SR subclone.

Our primary limiting dilutions combined with our secondary tumor data showed no difference in tumor initiating capacity or self-renewal *in vivo* between the two subclones tested. A difference was seen in tumor characteristics, with the sub-clone displaying lower self renewal *in vitro* resulting in a higher primary and secondary tumor grade, and decreased survival when xenografted into immunodeficient mice. Together, these results confirm cellular populations with a higher SR *in vitro* do not always translate to lower survival and higher tumor penetrance *in vivo*. These results have important implications in translational research and drug discovery, as testing of compounds in pre-clinical animal models typically follows higher throughput drug screening *in vitro*. One must therefore proceed with caution when interpreting the utility of this measure of self-renewal and the translation of its findings when going from the controlled environment of a dish to the complex milieu of the mouse.

Chapter 4: Discussion

4.1: Functional validation of CD271 and CD106 in SHH Medulloblastoma

We utilized an integrated approach of high throughput flow cytometry screening combined with gene expression profiling to identify 4 cell surface markers, CD271, CD106, CD171 and EGFR, that are differentially expressed in higher vs. non self-renewing SHH MB cells as well as in SHH MB vs. other 3 MB variants. Although the Lyoplate platform has been utilized for delineating specific cell phenotypes in multiple cancers (240, 242), this technique had not been used in pediatric cancers such as MB. While gene expression profiling and genomic sequencing are powerful techniques for delineating the dysregulated pathways driving tumorigenesis; these methods do not preserve cellular integrity or function. Characterization of the cell surface proteome enables researchers to employ strategies for isolation of specific cellular phenotypes that can then be utilized for additional molecular, functional and pre-clinical testing *in vitro* and *in vivo.* Moreover, MB subtype specific biomarkers can be useful as a diagnostic tool.

Of the four surface markers that were differentially expressed, further validation was performed on MB cell lines and IHC staining of formalin fixed paraffin-embedded tumor samples. Interestingly EGFR levels were low across all cell lines tested; thus, we did not pursue this marker further. CD171 showed uniformly increased expression in non-SHH cell lines and stained tumor samples as expected. Although CD171 was an interesting candidate for further functional investigation, we decided to prioritize CD106 and CD271 for further functional testing based on our existing data.

Our laboratory has heavily focused on elucidating the functional role of CD271 since we first published on its role in SHH MB in 2013 and again in 2015 (168, 171). Since these publications, ongoing research in our laboratory conducted by Lisa Liang (Liang et al., 2018, accepted at Cancer Research) has given us a much better understanding of what role CD271 plays in SHH MB, including targetable pathways for novel drug discovery. The specificity of CD271 expression in SHH tumors also makes it an interesting candidate for simple and fast diagnostic screening for this subtype using flow cytometry or immunohistochemistry immediately after tumor resection. Indeed, our results are consistent with previous findings demonstrating high expression levels in tumors specifically with desmoplastic histology that typically belong to the SHH subgroup (269, 270). Despite being unable to define a functional role for CD106 in our assays, based on the current literature and the link CD106 has to tumorgenesis, future elucidation of the functional relevance of CD106 in SHH MB tumorigenesis continues to be a viable option.

We have successfully used cell surface marker screening as a component of a systematic discovery platform to demonstrate that MB stem/progenitor marker profiles are not universal but can be subtype specific across all 4 molecular variants. Furthermore, these findings recently allowed our laboratory to begin drug testing looking at inhibitor combinations that are capable of disrupting the signaling pathways associated with these surface marker profiles.

4.1a: CD106

Functional assays were performed to determine the effect of CD106 on self-renewal and invasion in SHH MB. CD106, also known as vascular cell adhesion protein 1 (VCAM-1), is a cell surface sialoglycoprotein expressed in cytokine-activated endothelial cells. Its primary role in healthy cells is to mediate leukocyte-endothelial cell adhesion/extravasation and signal transduction (250). CD106 is found on a variety of human cells including activated endothelial cells, bone marrow stromal cells, spleen stromal cells, thymic epithelial cells, peripheral lymph node and mesenteric lymph node endothelial venules, and some dendritic cells in the spleen (271). CD106 plays an integral role in the immune surveillance of numerous diseases, plays an important role in immunomodulation and is necessary for fetal viability in mice (271).

In tumors, elevated CD106 serum levels have been linked to tumor progression in a variety of non-brain tumors including colorectal, lung, bladder, lymphoma and others (250-257). CD106 has also been shown to be an important pathological and prognostic factor in a variety of other cancers such as ovarian, esophageal, renal and breast cancer (258-262). While our data showed that CD106 is highest in SHH MB as compared to all other MB subgroups, there was no prognostic disadvantage of high CD106 levels in MB.

We found no difference in SR, invasion, survival or proliferation between the cells overexpressing CD106 and control. Although CD106 does not appear to play a functional role in SR in our cellular population, previous studies suggest that it plays

an integral role in normal stem cell biology. Cell to cell adhesion mediated by CD106 is necessary for T cell activation and leukocyte recruitment to the site of inflammation, making it a key player in immune modulation (272). Alternatively, CD106 is critical for mesenchymal stem cell (MSC) mediated immunosuppression (273). CD106 was shown to identify a unique population of human chorionic villi derived mesenchymal stem cells (CV-MSCs) with powerful immunosuppressive activity when compared to CD106- CV-MSCs (274). In this study, CV-MSCs were found to have the highest level of CD106 when compared to MSCs derived from human umbilical cord, adult bone marrow and adipose tissue. When immunomodulation was measured *in vitro*, CD106+ CV-MSCs were more potent modulators of T helper subsets but possessed decreased colony forming capacity (274). CD106 however was not a reliable marker of higher SR cells, as it was not expressed on the surface of human multipotent MSCs derived from various regions. These studies support our findings that CD106 levels in non-SR subclones.

Functionally, CD106 plays a role in metastasis, angiogenesis and immunomodulation in a variety of cancer types. The role it plays differs depending on the location of CD106 on the tumor cell vs endothelial cell, as well as the niche (262-264). Tumor cell expression was shown to promote T-cell migration away from the tumor cells, resulting in decreased accumulation of T cells in the tumor microenvironment (271). Reduced accumulation of T cells could potentially increase the ability of CD106 expressing tumor cells to escape immune attack. CD106 has been shown to play a role in metastasis of breast cancer to the lung and bone (263, 275). This proposed mechanism contributing to metastasis is not related

to endothelial adhesion, invasion or transendothelial migration of TCs. Instead, this study showed binding of CD106 to VLA-4 on monocytes and tumor associated macrophages causes recruitment of these immune cells to the lungs as well as clustering of CD106 on the tumor cell wall. Clustered CD106 on the tumor cell wall results in the activation of a prosurvival Akt mediated downstream intracellular pathway (263, 275). In bone metastasis, it was shown that CD106 on the surface of the cancer cell attracts and binds α4 integrin–expressing osteoclast progenitors to assist their maturation into multinucleated osteoclasts that mediate osteolytic metastasis (275).

Despite seeing a difference in CD106 expression in migrating vs core stationary cells in our dissection assays, we observed no difference between CD106 overexpressing cells vs control when invasion was measured in a Type I collagen invasion assay. These assays are similar in their setup, however the dissection assay is a measure of migration, whereas cells in our invasion assay must also degrade the collagen matrix. In addition, our core and migrating assay is based on endogenous levels of CD106 whereas the invasion assay is based on forced sustained expression of CD106. We also saw conflicting results from these assays in our paper published in 2013 (168). The higher SR subclone with an elevated level of CD271 showed a higher invasive capacity in Type I collagen, however CD271 levels were reduced in our migratory cells using the dissection assay. These experiments demonstrated the importance of the biologic context or cellular conditions on the outcome of functional assays used in the laboratory.

Despite showing that CD106 is upregulated in SHH MB, we observed only small foci of CD106 via IHC in tumor samples. One explanation for this could be that CD106 is associated with a migratory phenotype as shown in our dissection assay. Our patient samples are small sections from the primary core tumor; thus, higher CD106 expression may be seen if IHC was performed on SHH MB samples at the leading edge of the tumor where migratory cells reside, or in metastatic tumor samples due to its known role it plays in microenvironment modulation at the site of metastasis.

The literature suggests that the role CD106 plays in metastasis is not related cell adhesion, but rather cellular signaling and alteration of the cellular microenvironment/immunomodulation. Monocytes and tumor-associated macrophages promote tumor initiation by creating an inflammatory environment that is mutagenic and promotes growth (276-278). As tumors progress, macrophages stimulate angiogenesis, enhance tumor cell migration and invasion, and cause immunosuppression in the tumor microenvironment (276-278). It is possible that CD106 has no direct effect on cellular migration or invasion but instead cells that are in the migratory phase upregulate CD106 in anticipation of encountering a greater immune response outside the immediate tumor environment. The potential implications of these findings will be further discussed in “Future Directions” section of this thesis.

4.1 b: CD271

As a proof of principle, we performed functional cellular assays on the cell surface marker, CD271, that we previously demonstrated to be associated with SHH MB (168). CD271 appears to be linked to a stem/progenitor like cell in SHH MB, however there is no way of distinguishing between the two cell states with current markers. More specifically, CD271 is linked to proliferation and survival of these cell populations in SHH MB. CD271 is a transmembrane glycoprotein that plays a variety of roles in normal neurodevelopment including growth cone elongation, axon guidance, cell survival and cell death, depending on the cellular context (279). The four CD271 ligands, NGF, BDNF, NT-3 and NT-4 exist in both pro-neurotrophin form and mature form, and this results in different effects depending on the presence/absence of ligand as well as which ligand is bound (279). For example, CD271 has been shown to induce apoptosis in the absence of ligand or binding of an unprocessed neurotrophin (pro-neurotrophin) (280). Activation of the JNK pathway appears to play a role in CD271 mediated cell death, whereas signaling through the NFκB pathway promotes survival (280). In addition to its role in neurodevelopment, CD271 has been shown to regulate adult glioblastoma brain tumor invasion and has been shown to be a selective tumor propagating cell marker in melanoma, esophageal squamous cell carcinoma, and hypopharyngeal cancer (281, 282). Importantly, CD271 has also been shown to mark a neurogenic precursor population in the subventricular zone (SVZ) from both rats and mice (283). Using FACS to isolate CD271+ postnatal rat SVZ, the authors showed that sorted cells with

the highest levels of CD271 generated the most neurospheres. They also demonstrated that CD271 regulates neurogenesis and the ongoing generation of olfactory bulb neurons in the SVZ (283). However, in this study, they did not determine whether CD271 selects for a stem or progenitor cell population.

Studies conducted in mouse models have shown that the SHH variant of MB arises from granule precursor cells in the external granular layer (EGL) of the cerebellum (12, 96). In addition, Li et al. showed that a population of nestin-expressing progenitor cells, distinct from granular neuroprogenitor cells in the EGL, are responsible for tumorigenesis (265). CD271 staining in paraffin embedded sections of 23-week human fetal cerebellum (Figure 3.1.4 A) revealed high expression of CD271 in the EGL, an area with a high density of progenitor cells, and is consistent with staining profiles previously observed (269, 284). Combined with the functional studies both *in vitro* and *in vivo*, our working model suggests that CD271 is associated with a SHH MB progenitor cell population that exhibits a limited capacity for self-renewal relative to the stem cell fraction. While previous work has demonstrated conflicting roles for CD271 in MB apoptosis (270, 285), in both cases, experiments were conducted with D283, or non-SHH MB cells, further underscoring the need to evaluate the function of a cell surface marker in both a subtype-specific and cell context-dependent manner.

More recent unpublished RNA sequencing data from Liang et al., 2018, accepted at Cancer Research) in our laboratory have revealed upregulation in proliferation, survival and motility gene pathways in the CD271+ relative to the CD271- cells (personal communication). These findings were confirmed *in vitro*

using the established Daoy cell line and low passage primary UI226 SHH tumorspheres. These data support our findings that CD271 overexpression results in larger tumorspheres *in vitro*. Additional *in vivo* experiments using cells overexpressing CD271 revealed an increase in migration of the CD271 OE population generating tumors with increased infiltration into the perivascular space and SAS (personal communication) following intracerebellar transplantation. These new findings however do not explain why we continue to see smaller tumors *in vivo* despite there being an increase in proliferation and survival *in vitro*. A possible explanation is that these results reinforce our hypothesis that CD271 overexpression results in a smaller tumor *in vivo* due to a smaller TIC/TPC population in this cellular population. Alternatively, these cell populations undergoing a phenotypic switch as a result of the microenvironment they are placed in may explain these findings. Sommer et al. have shown in melanoma that CD271 plays a dual role in phenotypic switching by decreasing proliferation while at the same time promoting invasiveness (286).

These results can be explained by CD271 cell plasticity and the ability of CD271 cell populations to transition from one cell state to another (287). We previously showed that CD271 + and CD271- cell populations equilibrate shortly after sorting (168). This demonstrates that these cell populations can transition between the CD271- and CD271+ and explains why we see very little, if no difference in tumor size and penetrance in our CD271+/- sorted xenografts. Thus, when CD271 is overexpressed, these cell populations can no longer transition to

CD271- cell state, resulting in reduced tumor propagation and expansion and increased tumor cell migration and invasion.

Activation of the SHH signalling pathway is characteristic of SHH MB. Current clinical trials utilizing SHH inhibitors have shown that patients display an initial response, however this is followed by eventual relapse attributed to drug resistance (288-291). Zhukova et al. recently shed light on this issue by demonstrating that *TP53* mutations are associated with poor outcome for SHH patients, and this may account for treatment failure within this subgroup (95). Intratumoral heterogeneity likely contributes to SHH pathway inhibitor resistance. Wang *et al.* (243) recently showed elevated expression of SHH pathway genes and increased sensitivity to pathway inhibition in the CD133+ stem cell fraction in Daoy cells. In contrast, we demonstrated CD271+ cells, a cell population previously shown to be mutually exclusive to CD133+ cells (168), exhibit a down regulation of SHH pathway genes. As such, CD271+ cells may be less responsive to SHH pathway inhibition emphasizing the importance of understanding tumor heterogeneity when attempting to dissect the complex factors leading to targeted therapy resistance. Indeed, follow-up studies have demonstrated that the molecular signatures of CD271+ and CD271- cells are distinct (Liang et al., 2018, accepted at Cancer Research).

Current treatment for MB involves surgery, chemotherapy and radiation which mainly target the proliferating cell population and tumor mass [68]. Identification of tumor propagating cell populations for specific MB molecular variants will enable isolation of a novel cell resource for design of next generation

targeted therapies that target both tumor stem cell and progenitor populations. This can only be achieved through combinatorial therapy targeting multiple cell populations. While SHH pathway antagonists may be ideal for targeting a portion of the stem cell population, additional treatment would be required to selectively target the CD271+ progenitor or stem cell fractions that are in a lower self-renewing state. Treatment aimed at both CD271+ and CD271- cells could ultimately lessen the broad impact of toxic treatments such as radiation and chemotherapy on the child's developing nervous system and improve the quality of life for those who survive long-term.

4.1 c: Conclusion:

We have used high throughput screening with functional characterization to show CD271 selects for a subtype specific progenitor-like cell in SHH MB. This technique was taken from surface marker screening, to subgroup specific validation, through functional validation to drug discovery. Although we have focused on selective isolation of more primitive stem/progenitor cells, this screening technique combined with functional validation can be used for delineating signatures associated with a variety of oncogenic properties including invasion, metastasis, adhesion, and drug resistance. We characterized CD271 and performed initial functional validation of CD106 as a proof of principle, however the additional 2 cell surface markers identified from our screen have been shown to play a role in a variety of cancers and are candidates for additional functional studies and

combinatorial testing. These markers may provide further insight not only into MB stem/progenitor populations, but also cells exhibiting other tumor related phenotypes. While our study focused on SHH MB, the utility of this integrated approach can be seen in normal stem cell biology and across all forms of cancer that exhibit vast heterogeneity.

4.2: Uncoupling *in vivo* properties from *in vitro* properties of higher and non self-renewing cellular populations in SHH MB

Using a high SR and non-SR subclones derived from the Daoy SHH MB cell line, we showed that cells exhibiting increased self-renewal *in vitro* do not always display increased tumorigenic potential, increased self renewal and decreased survival *in vivo*. Histological analysis revealed that the lower SR cells form much larger tumors with well-defined borders, focal necrosis and minimal perivascular infiltration and cell deposition in the subarachnoid space. Higher SR cells show a very different tumor type with a small cellular collection at site of injection and significant perivascular infiltration and cell deposition in the subarachnoid space.

We have shown that a non-SR subclone that is incapable of forming tumorspheres over subsequent passage *in vitro* exhibits the same tumor initiating capacity and self-renewal capabilities *in vivo* as highly self renewing subclone. In the literature, it is generally assumed that SR *in vitro* is a surrogate for tumor initiation *in vivo* (70, 150, 154, 207, 248). For example, when screening the effect of a particular drug or small molecule inhibitor, a reduction in tumorsphere formation often provides the rationale for pursuing *in vivo* studies. Our results suggest that *in vitro* findings may be poor indicators of drug efficiency *in vivo*. The necessity of multimodal therapy when designing cancer stem cell targeted therapies was first shown in Chapter 4.1 with the CD271- and CD271+ cellular populations. We have now further shown this *in vivo* in an additional model displaying differential self-renewal *in vitro*. To understand these discrepancies between *in vitro* and *in vivo*

findings, one must look at the cell of origin of SHH MB, and plasticity of the cellular population initiating and driving these tumors.

The cell of origin of SHH Medulloblastoma remains unclear. Yang et al. showed that SHH Medulloblastoma can be initiated by the activation of SHH signaling in both neural progenitors as well as stem cells (96). However tumor formation in stem cells only proceeds once there is commitment to and expansion of the neural lineage (96). Read et al. were able to show that CD15 in combination with the progenitor marker Math1 selected for a progenitor-like cell in the Patched mutant mouse model of Shh Medulloblastoma (166). Conversely, Ward et al. showed that CD15 selects for a stem-cell like cell in the same mouse model. In the case of SHH MB, it is therefore necessary to eradicate both the stem cells and the more differentiated progenitor cell population. Cancer stem cell populations are propagated *in vitro* using serum free stem cell conditions. If SHH MB is initiated and/or driven by a further differentiated progenitor as some research suggests, our *in vitro* tumorsphere assay would not be predictive of *in vivo* results when screening for novel drugs capable of eradicating the TPC population. Despite being incapable of forming tumorspheres when passaged in stem cell conditions *in vitro*, our non-SR subclone not only forms tumors at the same rate as the higher SR subclone, but forms larger tumors with a decreased survival time suggesting that the stem cells may not be the only population contributing to tumor initiation and progression, or alternatively that these differences are seen due to culture conditions *in vitro* as compared to the microenvironment *in vivo*.

Alternatively, phenotypic plasticity of TPC populations would allow TPC populations to transition between varying states of differentiation and SR. This mechanism of cellular equilibrium has been demonstrated by our research in SHH MB as described in chapter 4.1, in addition to several other forms of cancer (292-297). Phenotypic plasticity has been shown to be a major factor in cancer stem cell targeted therapy resistance (298-300). A major driver of this resistance is the ability of CSCs to undergo epithelial to mesenchymal transition (EMT). Liu et al. recently evaluated phenotypic plasticity in breast cancer stem cells (BCSCs) by showing that BCSCs can exist as both a mesenchymal-like (epithelial-mesenchymal transition [EMT]) and epithelial-like (mesenchymal-epithelial transition [MET]) cell state (292). Epithelial-like BCSCs were highly proliferative and concentrated in the center of the tumor while the mesenchymal-like BCSCs were found predominantly found at the invasive front and were relatively quiescent. These cellular populations were shown to have phenotypic plasticity, demonstrating the ability to transition from one cellular state to another. Both stem cell populations were capable of self-renewal and multi lineage differentiation (292). We see a similar pattern in our higher and non-SR subclones when xenografted into NOD SCID mice. The non-SR subclone forms large circumscribed tumors with little negligible migration or invasion; whereas, the high SR cell clone forms small tumors at the sight of injection with highly diffuse tumor formation into the perivascular space and SAS.

Recent research has shown that CSCs can maintain themselves in a hybrid epithelial/mesenchymal phenotype that shows increased phenotypic plasticity and stem cell-like properties. The presence of these cells in a hybrid state was shown to

be an indicator of poor prognosis in oral squamous cell carcinoma (301) and lung cancer (302). These multipotent bi-directional CSCs demonstrate both therapeutic resistance and the ability to leave the primary tumor site and re-establish a metastatic tumor in distant organs (293, 298, 303). Therefore, the eradication of the highly SR stem cell population could simply result in more differentiated progenitors to transition to a more primitive stem cell population, or vice versa, allowing tumor formation and propagation to continue. As we have demonstrated, the existence of transient cell states makes it difficult to study these highly TPCs. A method using TGFβ and retinoic acid has been used to keep TPCs in an EMT state making it easier to study these cellular populations *in vitro* (298).

It is important to note however that at this time, we have not elucidated the mechanism responsible for the transition between CD271+ and CD271 – cellular populations, nor have we investigated the difference in drivers responsible for tumor phenotype seen in our higher and non-SR subclones. Investigating EMT-associated genes including vimentin, zinc finger E-box-binding homeobox 1 (ZEB1), ZEB2, b-catenin (CTNNB1), and matrix metalloproteinase-1 (MMP9), and MET associated genes including cadherin, occludin, claudins and desmoplakin (292) using real time polymerase chain reaction (RT-PCR) would indicate if a transition from one cell state to another is responsible for the changes we see between cell populations. This could be done in tumorsphere populations of both high and non-SR sub clones, cells that have been isolated from tumors grown from both sub clones, as well as in sorted CD271+/- and cellular populations and cells overexpressing CD271.

It is highly likely that both the cell of origin and plasticity of these TICs play a large role in explaining why we see little difference in xenograft tumor phenotype in sorted populations based on CD271 status as well as such significant tumor formation from the SHH MB subclone that is incapable of SR *in vitro*. Both *in vitro* and *in vivo*, TPCs are inheritably unstable and capable of bi-directional plasticity based on their microenvironment. One must therefore take this into consideration when choosing targeted therapy approaches toward TPC populations to reduce the likelihood of therapy resistance.

The reliability of the tumorsphere assay to truly measure the cancer stem cell population *in vitro*, as well as the reliability of xenografts in NOD SCID mice to measure the true SR potential and CSC fraction has been repeatedly questioned in the past (176, 177, 189). However, despite these limitations, we have shown that novel screening approaches, in combination with comprehensive genomic data, functional validation and *in vivo* studies can overcome these shortfalls and lead research towards innovative targets in cancer stem cell therapy.

Future Directions

In our overexpression studies, we were not able to find any association of CD106 with a change in invasion, self-renewal or cellular proliferation/survival. As previously discussed, it is possible that CD106 has no direct effect on cellular migration or invasion in SHH MB, but instead indirectly affects cellular metastasis and invasion through upregulation in cells with upregulated invasion and migration pathways in anticipation of encountering a greater immune response outside the immediate tumor environment.

To test this theory, global gene expression analysis could be performed to evaluate changes in migration and invasion genes as well as gene pathways used in immune evasion in our CD106+ vs CD106- cell population from *in vitro* tumorspheres as well as cells in tumorsphere conditions overexpressing CD106 compared to control. It is also possible that we did not see any difference in invasion *in vitro* as the effect of CD106 on invasion is not directly linked to the upregulation of invasion pathways and is instead a secondary effect of immune modulation and invasion, something the invasion assay we currently utilize cannot evaluate. Thus, characterizing the effect of CD106 on invasion and metastasis *in vivo* may be more relevant. In order to do this, we would have to utilize a SHH MB cell line that is known to metastasize. Gain and loss of function studies in this model would help us understand the effect CD106 has on metastasis *in vivo*.

Our laboratory has continued to focus on CD271 beyond my studies. Significant progress has been determining the role it plays in SHH MB. I will therefore not further comment on the future direction of this marker.

Another avenue of investigation to pursue as a future direction is to better understand what is driving the difference in tumor characteristics between the non-SR and higher SR MB SHH Daoy subclones. We focused entirely on the characteristics of tumor formation, survival and tumor grade between these two subclones. Our laboratory has studied these two subclones extensively as they are the model we rely on for higher and lower SR populations from the same cell line. We have not evaluated the molecular differences between these 2 phenotypes. The histology from these tumors is similar to what is seen *in vivo* when cells are transitioned between a mesenchymal-like state with increased migration and a more epithelial-like state with more proliferation. The higher SR subclone shows significant migration and collection along the SAS, similar to what is seen in humans when MB metastasizes to the spinal cord. In contrast, the non-SR subclone exhibits negligible migration but instead significant proliferation forming very large well encapsulated tumors., It will be important to conduct gene expression analyses comparing the tumors derived from both SR and non-SR clones to determine what state these cells are in, either epithelial or mesenchymal as well as the migration and proliferation profiles in the two subclones.

References

1. Roussel MF, Hatten ME. Cerebellum development and medulloblastoma. Curr Top Dev Biol. 2011;94:235-82.
2. Wingate RJ, Hatten ME. The role of the rhombic lip in avian cerebellum development. Development. 1999;126(20):4395-404.
3. Joyner AL, Liu A, Millet S. Otx2, Gbx2 and Fgf8 interact to position and maintain a mid–hindbrain organizer. Current Opinion in Cell Biology. 2000;12(6):736-41.
4. Joyner AL. Engrailed, Wnt and Pax genes regulate midbrain-hindbrain development. Trends in Genetics. 1996;12(1):15-20.
5. Cajal SR. Estructura de los centros nerviosos de las aves. Rev Trim Histol Normal Patol. 1888;1:1–10.
6. Cajal SR. Sobre las fibras nerviosas de la capa molecular del cerebelo. Rev Trim Histol Normal Patol. 1888;1:33-49.
7. Ramón y Cajal S. Histologie du système nerveux de l'homme & des vertébrés. Paris :: Maloine; 1909.
8. Mugnaini E, Floris A. The unipolar brush cell: a neglected neuron of the mammalian cerebellar cortex. J Comp Neurol. 1994;339(2):174-80.
9. Laine J, Axelrad H. The candelabrum cell: a new interneuron in the cerebellar cortex. J Comp Neurol. 1994;339(2):159-73.
10. Wang VY, Rose MF, Zoghbi HY. Math1 Expression Redefines the Rhombic Lip Derivatives and Reveals Novel Lineages within the Brainstem and Cerebellum. Neuron. 2005;48(1):31-43.
11. Sotelo C. Cellular and genetic regulation of the development of the cerebellar system. Progress in Neurobiology. 2004;72(5):295-339.
12. Schuller U, Heine VM, Mao J, Kho AT, Dillon AK, Han YG, et al. Acquisition of granule neuron precursor identity is a critical determinant of progenitor cell competence to form Shh-induced medulloblastoma. Cancer Cell. 2008;14(2):123-34.
13. Palay S, Chan-Palay V. Cerebellar cortex: cytology and organization. Berlin, Germany: Springer; 1974.
14. Rodriguez CI, Dymecki SM. Origin of the Precerebellar System. Neuron. 2000;27(3):475-86.
15. Millen KJ, Millonig JH, Wingate RJT, Alder J, Hatten ME. Neurogenetics of the Cerebellar System. Journal of Child Neurology. 1999;14(9):574-81.
16. Ben-Arie N, Bellen HJ, Armstrong DL, McCall AE, Gordadze PR, Guo Q, et al. Math1 is essential for genesis of cerebellar granule neurons. Nature. 1997;390(6656):169-72.
17. Nagai T, Aruga J, Takada S, Günther T, Spörle R, Schughart K, et al. The Expression of the MouseZic1, Zic2,andZic3Gene Suggests an Essential Role forZicGenes in Body Pattern Formation. Developmental Biology. 1997;182(2):299-313.
18. Engelkamp D, Rashbass P, Seawright A, van Heyningen V. Role of Pax6 in development of the cerebellar system. Development. 1999;126(16):3585-96.

19. Morales D, Hatten ME. Molecular Markers of Neuronal Progenitors in the Embryonic Cerebellar Anlage. The Journal of Neuroscience. 2006;26(47):12226-36.
20. Ábrahám H, Tornóczky T, Kosztolányi G, Seress L. Cell formation in the cortical layers of the developing human cerebellum. International Journal of Developmental Neuroscience. 2001;19(1):53-62.
21. Yu J, Virshup David M. Updating the Wnt pathways. Bioscience Reports. 2014;34(5):e00142.
22. Niehrs C. The complex world of WNT receptor signalling. Nat Rev Mol Cell Biol. 2012;13(12):767-79.
23. Cavallo RA, Cox RT, Moline MM, Roose J, Polevoy GA, Clevers H, et al. Drosophila Tcf and Groucho interact to repress Wingless signalling activity. Nature. 1998;395(6702):604-8.
24. Roose J, Molenaar M, Peterson J, Hurenkamp J, Brantjes H, Moerer P, et al. The Xenopus Wnt effector XTcf-3 interacts with Groucho-related transcriptional repressors. Nature. 1998;395(6702):608-12.
25. Bilić J, Huang Y-L, Davidson G, Zimmermann T, Cruciat C-M, Bienz M, et al. Wnt Induces LRP6 Signalosomes and Promotes Dishevelled-Dependent LRP6 Phosphorylation. Science. 2007;316(5831):1619-22.
26. Zeng X, Huang H, Tamai K, Zhang X, Harada Y, Yokota C, et al. Initiation of Wnt signaling: control of Wnt coreceptor Lrp6 phosphorylation/activation via frizzled, dishevelled and axin functions. Development. 2008;135(2):367-75.
27. Cadigan KM, Waterman ML. TCF/LEFs and Wnt Signaling in the Nucleus. Cold Spring Harbor Perspectives in Biology. 2012;4(11).
28. Mosimann C, Hausmann G, Basler K. [beta]-Catenin hits chromatin: regulation of Wnt target gene activation. Nat Rev Mol Cell Biol. 2009;10(4):276-86.
29. Lee SM, Tole S, Grove E, McMahon AP. A local Wnt-3a signal is required for development of the mammalian hippocampus. Development. 2000;127(3):457-67.
30. Ikeya M, Lee SMK, Johnson JE, McMahon AP, Takada S. Wnt signalling required for expansion of neural crest and CNS progenitors. Nature. 1997;389(6654):966-70.
31. Dickinson ME, Krumlauf R, McMahon AP. Evidence for a mitogenic effect of Wnt-1 in the developing mammalian central nervous system. Development. 1994;120(6):1453-71.
32. Parr BA, Shea MJ, Vassileva G, McMahon AP. Mouse Wnt genes exhibit discrete domains of expression in the early embryonic CNS and limb buds. Development. 1993;119(1):247-61.
33. Thomas KR, Capecchi MR. Targeted disruption of the murine int-1 proto-oncogene resulting in severe abnormalities in midbrain and cerebellar development. Nature. 1990;346(6287):847-50.
34. McMahon AP, Bradley A. The Wnt-1 (int-1) proto-oncogene is required for development of a large region of the mouse brain. Cell. 1990;62(6):1073-85.
35. McMahon AP, Joyner AL, Bradley A, McMahon JA. The midbrain-hindbrain phenotype of Wnt-1−Wnt-1− mice results from stepwise deletion of engrailed-expressing cells by 9.5 days postcoitum. Cell. 1992;69(4):581-95.

36. Pei Y, Brun SN, Markant SL, Lento W, Gibson P, Taketo MM, et al. WNT signaling increases proliferation and impairs differentiation of stem cells in the developing cerebellum. Development. 2012;139(10):1724-33.
37. Dahmane N, Ruiz-i-Altaba A. Sonic hedgehog regulates the growth and patterning of the cerebellum. Development. 1999;126(14):3089-100.
38. Wallace VA. Purkinje-cell-derived Sonic hedgehog regulates granule neuron precursor cell proliferation in the developing mouse cerebellum. Current Biology. 1999;9(8):445-8.
39. Wechsler-Reya RJ, Scott MP. Control of Neuronal Precursor Proliferation in the Cerebellum by Sonic Hedgehog. Neuron. 1999;22(1):103-14.
40. Briscoe J, Therond PP. The mechanisms of Hedgehog signalling and its roles in development and disease. Nat Rev Mol Cell Biol. 2013;14(7):416-29.
41. Taipale J, Cooper MK, Maiti T, Beachy PA. Patched acts catalytically to suppress the activity of Smoothened. Nature. 2002;418(6900):892-6.
42. Svärd J, Henricson KH, Persson-Lek M, Rozell B, Lauth M, Bergström Å, et al. Genetic Elimination of Suppressor of Fused Reveals an Essential Repressor Function in the Mammalian Hedgehog Signaling Pathway. Developmental Cell. 2006;10(2):187-97.
43. Park HL, Bai C, Platt KA, Matise MP, Beeghly A, Hui CC, et al. Mouse Gli1 mutants are viable but have defects in SHH signaling in combination with a Gli2 mutation. Development. 2000;127(8):1593-605.
44. Kenney AM, Cole MD, Rowitch DH. Nmyc upregulation by sonic hedgehog signaling promotes proliferation in developing cerebellar granule neuron precursors. Development. 2003;130(1):15-28.
45. Pons S, Trejo JL, Martinez-Morales JR, Marti E. Vitronectin regulates Sonic hedgehog activity during cerebellum development through CREB phosphorylation. Development. 2001;128(9):1481-92.
46. Kleihues P, Sobin LH. World Health Organization classification of tumors. Cancer. 2000;88(12):2887.
47. delCharco JO, Bolek TW, McCollough WM, Maria BL, Kedar A, Braylan RC, et al. Medulloblastoma: time–dose relationship based on a 30-year review. International Journal of Radiation Oncology*Biology*Physics. 1998;42(1):147-54.
48. Pomeroy SL. Treatment and prognosis of medulloblastoma. In: UpToDate Waltham, MA. : UpToDate; [updated June 25 2014.
49. Taylor MD, Northcott PA, Korshunov A, Remke M, Cho YJ, Clifford SC, et al. Molecular subgroups of medulloblastoma: the current consensus. Acta Neuropathol. 2012;123(4):465-72.
50. Crawford JR, MacDonald TJ, Packer RJ. Medulloblastoma in childhood: new biological advances. The Lancet Neurology. 2007;6(12):1073-85.
51. Kool M, Korshunov A, Remke M, Jones DT, Schlanstein M, Northcott PA, et al. Molecular subgroups of medulloblastoma: an international meta-analysis of transcriptome, genetic aberrations, and clinical data of WNT, SHH, Group 3, and Group 4 medulloblastomas. Acta Neuropathol. 2012;123(4):473-84.
52. Ray A, Ho M, Ma J, Parkes RK, Mainprize TG, Ueda S, et al. A Clinicobiological Model Predicting Survival in Medulloblastoma. Clinical Cancer Research. 2004;10(22):7613-20.

53. Ellison DW, Onilude OE, Lindsey JC, Lusher ME, Weston CL, Taylor RE, et al. beta-Catenin status predicts a favorable outcome in childhood medulloblastoma: the United Kingdom Children's Cancer Study Group Brain Tumour Committee. J Clin Oncol. 2005;23(31):7951-7.
54. Gajjar A, Hernan R, Kocak M, Fuller C, Lee Y, McKinnon PJ, et al. Clinical, Histopathologic, and Molecular Markers of Prognosis: Toward a New Disease Risk Stratification System for Medulloblastoma. Journal of Clinical Oncology. 2004;22(6):984-93.
55. Gilbertson R, Wickramasinghe C, Hernan R, Balaji V, Hunt D, Jones-Wallace D, et al. Clinical and molecular stratification of disease risk in medulloblastoma. Br J Cancer. 2001;85(5):705-12.
56. Clifford SC, Lusher ME, Lindsey JC, Langdon JA, Gilbertson RJ, Straughton D, et al. Wnt/Wingless pathway activation and chromosome 6 loss characterize a distinct molecular sub-group of medulloblastomas associated with a favorable prognosis. Cell Cycle. 2006;5(22):2666-70.
57. Pfister S, Remke M, Benner A, Mendrzyk F, Toedt G, Felsberg J, et al. Outcome Prediction in Pediatric Medulloblastoma Based on DNA Copy-Number Aberrations of Chromosomes 6q and 17q and the MYC and MYCN Loci. Journal of Clinical Oncology. 2009;27(10):1627-36.
58. Pan E, Pellarin M, Holmes E, Smirnov I, Misra A, Eberhart CG, et al. Isochromosome 17q Is a Negative Prognostic Factor in Poor-Risk Childhood Medulloblastoma Patients. Clinical Cancer Research. 2005;11(13):4733-40.
59. Northcott PA, Korshunov A, Witt H, Hielscher T, Eberhart CG, Mack S, et al. Medulloblastoma comprises four distinct molecular variants. J Clin Oncol. 2011;29(11):1408-14.
60. Cavalli FMG, Remke M, Rampasek L, Peacock J, Shih DJH, Luu B, et al. Intertumoral Heterogeneity within Medulloblastoma Subgroups. Cancer Cell. 2017;31(6):737-54.e6.
61. Schwalbe EC, Lindsey JC, Nakjang S, Crosier S, Smith AJ, Hicks D, et al. Novel molecular subgroups for clinical classification and outcome prediction in childhood medulloblastoma: a cohort study. The Lancet Oncology. 2017;18(7):958-71.
62. Louis DN, Perry A, Reifenberger G, von Deimling A, Figarella-Branger D, Cavenee WK, et al. The 2016 World Health Organization Classification of Tumors of the Central Nervous System: a summary. Acta Neuropathol. 2016;131(6):803-20.
63. Eberhart CG. In Search of the Medulloblast: Neural Stem Cells and Embryonal Brain Tumors. Neurosurgery Clinics of North America. 2007;18(1):59-69.
64. Goumnerova L. Growth factor receptors and medulloblastoma. J Neuro-Oncol. 1996;29(1):85-9.
65. Pomeroy S, Sutton M, Goumnerova L, Segal R. Neurotrophins in cerebellar granule cell development and medulloblastoma. J Neuro-Oncol. 1997;35(3):347-52.
66. Yokota N, Aruga J, Takai S, Yamada K, Hamazaki M, Iwase T, et al. Predominant Expression of Human Zic in Cerebellar Granule Cell Lineage and Medulloblastoma. Cancer Res. 1996;56(2):377-83.
67. Salsano E, Pollo B, Eoli M, Giordana MT, Finocchiaro G. Expression of MATH1, a marker of cerebellar granule cell progenitors, identifies different medulloblastoma sub-types. Neuroscience Letters. 2004;370(2–3):180-5.

68. BÜHREN J, CHRISTOPH AHA, BUSLEI R, ALBRECHT S, WIESTLER OD, PIETSCH T. Expression of the Neurotrophin Receptor p75NTR in Medulloblastomas Is Correlated with Distinct Histological and Clinical Features: Evidence for a Medulloblastoma Subtype Derived from the External Granule Cell Layer. Journal of Neuropathology & Experimental Neurology. 2000;59(3):229-40.
69. Hemmati HD, Nakano I, Lazareff JA, Masterman-Smith M, Geschwind DH, Bronner-Fraser M, et al. Cancerous stem cells can arise from pediatric brain tumors. Proceedings of the National Academy of Sciences. 2003;100(25):15178-83.
70. Singh SK, Hawkins C, Clarke ID, Squire JA, Bayani J, Hide T, et al. Identification of human brain tumour initiating cells. Nature. 2004;432(7015):396-401.
71. Gorovoy IR, de Alba Campomanes A. A potential life-saving diagnosis—recognizing Turcot syndrome. Journal of American Association for Pediatric Ophthalmology and Strabismus. 2014;18(2):186-8.
72. Hamilton SR, Liu B, Parsons RE, Papadopoulos N, Jen J, Powell SM, et al. The Molecular Basis of Turcot's Syndrome. New England Journal of Medicine. 1995;332(13):839-47.
73. Baeza N, Masuoka J, Kleihues P, Ohgaki H. AXIN1 mutations but not deletions in cerebellar medulloblastomas. Oncogene. 2003;22(4):632.
74. EBERHART CG, TIHAN T, BURGER PC. Nuclear Localization and Mutation of β - Catenin in Medulloblastomas. Journal of Neuropathology & Experimental Neurology. 2000;59(4):333-7.
75. Huang H, Mahler-Araujo BM, Sankila A, Chimelli L, Yonekawa Y, Kleihues P, et al. APC mutations in sporadic medulloblastomas. Am J Pathol. 2000;156(2):433-7.
76. Koch A, Waha A, Tonn JC, Sörensen N, Berthold F, Wolter M, et al. Somatic mutations of WNT/wingless signaling pathway components in primitive neuroectodermal tumors. International Journal of Cancer. 2001;93(3):445-9.
77. Zurawel RH, Chiappa SA, Allen C, Raffel C. Sporadic Medulloblastomas Contain Oncogenic β-Catenin Mutations. Cancer Res. 1998;58(5):896-9.
78. Robinson G, Parker M, Kranenburg TA, Lu C, Chen X, Ding L, et al. Novel mutations target distinct subgroups of medulloblastoma. Nature. 2012;488(7409):43-8.
79. Remke M, Hielscher T, Northcott PA, Witt H, Ryzhova M, Wittmann A, et al. Adult Medulloblastoma Comprises Three Major Molecular Variants. Journal of Clinical Oncology. 2011;29(19):2717-23.
80. Jones DT, Jager N, Kool M, Zichner T, Hutter B, Sultan M, et al. Dissecting the genomic complexity underlying medulloblastoma. Nature. 2012;488(7409):100-5.
81. Northcott PA, Shih DJH, Peacock J, Garzia L, Sorana Morrissy A, Zichner T, et al. Subgroup-specific structural variation across 1,000 medulloblastoma genomes. Nature. 2012;488(7409):49-56.
82. Orsulic S, Huber O, Aberle H, Arnold S, Kemler R. E-cadherin binding prevents beta-catenin nuclear localization and beta-catenin/LEF-1-mediated transactivation. Journal of Cell Science. 1999;112(8):1237-45.
83. Choi Y-J, Lee S-G. The DEAD-box RNA helicase DDX3 interacts with DDX5, co-localizes with it in the cytoplasm during the G2/M phase of the cycle, and affects its

shuttling during mRNP export. Journal of Cellular Biochemistry. 2012;113(3):985-96.
84. Lai M-C, Lee Y-HW, Tarn W-Y. The DEAD-Box RNA Helicase DDX3 Associates with Export Messenger Ribonucleoproteins as well asTip-associated Protein and Participates in Translational Control. Molecular Biology of the Cell. 2008;19(9):3847-58.
85. Hecht A, Vleminckx K, Stemmler MP, van Roy F, Kemler R. The p300/CBP acetyltransferases function as transcriptional coactivators of β‐catenin in vertebrates. The EMBO Journal. 2000;19(8):1839-50.
86. Barker N, Hurlstone A, Musisi H, Miles A, Bienz M, Clevers H. The chromatin remodelling factor Brg‐1 interacts with β‐catenin to promote target gene activation. The EMBO Journal. 2001;20(17):4935-43.
87. Carrera I, Janody F, Leeds N, Duveau F, Treisman JE. Pygopus activates Wingless target gene transcription through the mediator complex subunits Med12 and Med13. Proceedings of the National Academy of Sciences. 2008;105(18):6644-9.
88. Gibson P, Tong Y, Robinson G, Thompson MC, Currle DS, Eden C, et al. Subtypes of medulloblastoma have distinct developmental origins. Nature. 2010;468(7327):1095-9.
89. Storm R, Cholewa-Waclaw J, Reuter K, Bröhl D, Sieber M, Treier M, et al. The bHLH transcription factor Olig3 marks the dorsal neuroepithelium of the hindbrain and is essential for the development of brainstem nuclei. Development. 2009;136(2):295-305.
90. Rogers HA, Sousa S, Salto C, Arenas E, Coyle B, Grundy RG. WNT/[beta]-catenin pathway activation in Myc immortalised cerebellar progenitor cells inhibits neuronal differentiation and generates tumours resembling medulloblastoma. Br J Cancer. 2012;107(7):1144-52.
91. Rutkowski S, Bode U, Deinlein F, Ottensmeier H, Warmuth-Metz M, Soerensen N, et al. Treatment of Early Childhood Medulloblastoma by Postoperative Chemotherapy Alone. New England Journal of Medicine. 2005;352(10):978-86.
92. John AM, Schwartz RA. Basal Cell Nevus Syndrome: An Update on Genetics and Treatment. British Journal of Dermatology. 2015:n/a-n/a.
93. Pugh TJ, Weeraratne SD, Archer TC, Pomeranz Krummel DA, Auclair D, Bochicchio J, et al. Medulloblastoma exome sequencing uncovers subtype-specific somatic mutations. Nature.488(7409):106-10.
94. Northcott PA, Hielscher T, Dubuc A, Mack S, Shih D, Remke M, et al. Pediatric and adult sonic hedgehog medulloblastomas are clinically and molecularly distinct. Acta Neuropathol. 2011;122(2):231-40.
95. Zhukova N, Ramaswamy V, Remke M, Pfaff E, Shih DJ, Martin DC, et al. Subgroup-Specific Prognostic Implications of TP53 Mutation in Medulloblastoma. J Clin Oncol. 2013.
96. Yang ZJ, Ellis T, Markant SL, Read TA, Kessler JD, Bourboulas M, et al. Medulloblastoma can be initiated by deletion of Patched in lineage-restricted progenitors or stem cells. Cancer Cell. 2008;14(2):135-45.

97. Cho YJ, Tsherniak A, Tamayo P, Santagata S, Ligon A, Greulich H, et al. Integrative genomic analysis of medulloblastoma identifies a molecular subgroup that drives poor clinical outcome. J Clin Oncol. 2011;29(11):1424-30.
98. Cho YJ, Tsherniak A, Tamayo P, Santagata S, Ligon A, Greulich H, et al. Integrative genomic analysis of medulloblastoma identifies a molecular subgroup that drives poor clinical outcome. J Clin Oncol.29(11):1424-30.
99. Pasini D, Hansen KH, Christensen J, Agger K, Cloos PAC, Helin K. Coordinated regulation of transcriptional repression by the RBP2 H3K4 demethylase and Polycomb-Repressive Complex 2. Genes & Development. 2008;22(10):1345-55.
100. Khan A, Shover W, Goodliffe JM. Su(z)2 Antagonizes Auto-Repression of Myc in Drosophila, Increasing Myc Levels and Subsequent Trans-Activation. PLoS ONE. 2009;4(3):e5076.
101. Spatz A, Borg C, Feunteun J. X-Chromosome Genetics and Human Cancer. Nat Rev Cancer. 2004;4(8):617-29.
102. Yang F, Babak T, Shendure J, Disteche CM. Global survey of escape from X inactivation by RNA-sequencing in mouse. Genome Research. 2010;20(5):614-22.
103. Kawauchi D, Robinson G, Uziel T, Gibson P, Rehg J, Gao C, et al. A Mouse Model of the Most Aggressive Subgroup of Human Medulloblastoma. Cancer Cell. 2012;21(2):168-80.
104. Pei Y, Moore CE, Wang J, Tewari AK, Eroshkin A, Cho YJ, et al. An animal model of MYC-driven medulloblastoma. Cancer Cell. 2012;21(2):155-67.
105. Eberhart Charles G. Three Down and One To Go: Modeling Medulloblastoma Subgroups. Cancer Cell. 2012;21(2):137-8.
106. Swartling FJ, Grimmer MR, Hackett CS, Northcott PA, Fan Q-W, Goldenberg DD, et al. Pleiotropic role for MYCN in medulloblastoma. Genes & Development. 2010;24(10):1059-72.
107. Swartling Fredrik J, Savov V, Persson Anders I, Chen J, Hackett Christopher S, Northcott Paul A, et al. Distinct Neural Stem Cell Populations Give Rise to Disparate Brain Tumors in Response to N-MYC. Cancer Cell. 2012;21(5):601-13.
108. Fidler IJ, Hart IR. Biological Diversity in Metastatic Neoplasms: Origins and Implications. Science. 1982;217(4564):998-1003.
109. Heppner GH. Tumor Heterogeneity. Cancer Res. 1984;44(6):2259-65.
110. Fidler IJ, Kripke ML. Metastasis Results from Preexisting Variant Cells Within a Malignant Tumor. Science. 1977;197(4306):893-5.
111. Barranco SC, Ho DHW, Drewinko B, Romsdahl MM, Humphrey RM. Differential Sensitivities of Human Melanoma Cells Grown in Vitro to Arabinosylcytosine. Cancer Res. 1972;32(12):2733-6.
112. Nowell PC. The Clonal Evolution of Tumor Cell Populations. Science. 1976;194(4260):23-8.
113. Baylin SB, Jones PA. A decade of exploring the cancer epigenome — biological and translational implications. Nat Rev Cancer. 2011;11(10):726-34.
114. Burrell RA, McGranahan N, Bartek J, Swanton C. The causes and consequences of genetic heterogeneity in cancer evolution. Nature. 2013;501(7467):338-45.
115. Greaves M, Maley CC. Clonal evolution in cancer. Nature. 2012;481(7381):306-13.

116. Gerlinger M, Rowan AJ, Horswell S, Larkin J, Endesfelder D, Gronroos E, et al. Intratumor Heterogeneity and Branched Evolution Revealed by Multiregion Sequencing. New England Journal of Medicine. 2012;366(10):883-92.
117. Sottoriva A, Spiteri I, Piccirillo SGM, Touloumis A, Collins VP, Marioni JC, et al. Intratumor heterogeneity in human glioblastoma reflects cancer evolutionary dynamics. Proceedings of the National Academy of Sciences. 2013;110(10):4009-14.
118. Vanner RJ, Remke M, Gallo M, Selvadurai HJ, Coutinho F, Lee L, et al. Quiescent sox2(+) cells drive hierarchical growth and relapse in sonic hedgehog subgroup medulloblastoma. Cancer Cell. 2014;26(1):33-47.
119. Ishikawa F, Yoshida S, Saito Y, Hijikata A, Kitamura H, Tanaka S, et al. Chemotherapy-resistant human AML stem cells home to and engraft within the bone-marrow endosteal region. Nat Biotechnol. 2007;25(11):1315-21.
120. Saito Y, Uchida N, Tanaka S, Suzuki N, Tomizawa-Murasawa M, Sone A, et al. Induction of cell cycle entry eliminates human leukemia stem cells in a mouse model of AML. Nat Biotech. 2010;28(3):275-80.
121. Inaba H, Greaves M, Mullighan CG. Acute lymphoblastic leukaemia. The Lancet.381(9881):1943-55.
122. Mullighan CG, Phillips LA, Su X, Ma J, Miller CB, Shurtleff SA, et al. Genomic Analysis of the Clonal Origins of Relapsed Acute Lymphoblastic Leukemia. Science. 2008;322(5906):1377-80.
123. Yachida S, Jones S, Bozic I, Antal T, Leary R, Fu B, et al. Distant metastasis occurs late during the genetic evolution of pancreatic cancer. Nature. 2010;467(7319):1114-7.
124. Campbell PJ, Yachida S, Mudie LJ, Stephens PJ, Pleasance ED, Stebbings LA, et al. The patterns and dynamics of genomic instability in metastatic pancreatic cancer. Nature. 2010;467(7319):1109-13.
125. Shah SP, Morin RD, Khattra J, Prentice L, Pugh T, Burleigh A, et al. Mutational evolution in a lobular breast tumour profiled at single nucleotide resolution. Nature. 2009;461(7265):809-13.
126. Wu X, Northcott PA, Dubuc A, Dupuy AJ, Shih DJ, Witt H, et al. Clonal selection drives genetic divergence of metastatic medulloblastoma. Nature. 2012;482(7386):529-33.
127. Morrissy AS, Garzia L, Shih DJH, Zuyderduyn S, Huang X, Skowron P, et al. Divergent clonal selection dominates medulloblastoma at recurrence. Nature. 2016;21(529).
128. Iorio MV, Croce CM. MicroRNA dysregulation in cancer: diagnostics, monitoring and therapeutics. A comprehensive review. EMBO Molecular Medicine. 2012;4(3):143-59.
129. Ning B, Li W, Zhao W, Wang R. Targeting epigenetic regulations in cancer. Acta Biochimica et Biophysica Sinica. 2015.
130. Roesch A, Fukunaga-Kalabis M, Schmidt EC, Zabierowski SE, Brafford PA, Vultur A, et al. A Temporarily Distinct Subpopulation of Slow-Cycling Melanoma Cells Is Required for Continuous Tumor Growth. Cell. 2010;141(4):583-94.
131. Sparmann A, van Lohuizen M. Polycomb silencers control cell fate, development and cancer. Nat Rev Cancer. 2006;6(11):846-56.

132. Ley TJ, Ding L, Walter MJ, McLellan MD, Lamprecht T, Larson DE, et al. DNMT3A Mutations in Acute Myeloid Leukemia. New England Journal of Medicine. 2010;363(25):2424-33.
133. Glasspool RM, Teodoridis JM, Brown R. Epigenetics as a mechanism driving polygenic clinical drug resistance. British Journal of Cancer. 2006;94(8):1087-92.
134. Sharma SV, Lee DY, Li B, Quinlan MP, Takahashi F, Maheswaran S, et al. A chromatin-mediated reversible drug tolerant state in cancer cell subpopulations. Cell. 2010;141(1):69-80.
135. Polyak K, Haviv I, Campbell IG. Co-evolution of tumor cells and their microenvironment. Trends in Genetics. 2009;25(1):30-8.
136. Anderson ARA, Weaver AM, Cummings PT, Quaranta V. Tumor Morphology and Phenotypic Evolution Driven by Selective Pressure from the Microenvironment. Cell. 2006;127(5):905-15.
137. Bhowmick NA, Neilson EG, Moses HL. Stromal fibroblasts in cancer initiation and progression. Nature. 2004;432(7015):332-7.
138. Nelson CM, Bissell MJ. Of Extracellular Matrix, Scaffolds, and Signaling: Tissue Architecture Regulates Development, Homeostasis, and Cancer. Annual Review of Cell and Developmental Biology. 2006;22(1):287-309.
139. Magee JA, Piskounova E, Morrison SJ. Cancer stem cells: impact, heterogeneity, and uncertainty. Cancer Cell. 2012;21(3):283-96.
140. Kleinsmith LJ, Pierce GB, Jr. Multipotentiality of Single Embryonal Carcinoma Cells. Cancer Res. 1964;24:1544-51.
141. Pierce GB, Jr., Dixon FJ, Jr., Verney EL. Teratocarcinogenic and tissue-forming potentials of the cell types comprising neoplastic embryoid bodies. Lab Invest. 1960;9:583-602.
142. Baylin SB, Weisburger WR, Eggleston JC, Mendelsohn G, Beaven MA, Abeloff MD, et al. Variable Content of Histaminase, L-Dopa Decarboxylase and Calcitonin in Small-Cell Carcinoma of the Lung. New England Journal of Medicine. 1978;299(3):105-10.
143. Bennett DC, Peachey LA, Durbin H, Rudland PS. A possible mammary stem cell line. Cell. 1978;15(1):283-98.
144. Hager JC, Fligiel S, Stanley W, Richardson AM, Heppner GH. Characterization of a Variant-producing Tumor Cell Line from a Heterogeneous Strain BALB/cfC3H Mouse Mammary Tumor. Cancer Res. 1981;41(4):1293-300.
145. Clarkson B, Ohkita T, Ota K, Fried J. Studies of Cellular Proliferation in Human Leukemia. I. Estimation of Growth Rates of Leukemic and Normal Hematopoietic Cells in Two Adults with Acute Leukemia Given Single Injections of Tritiated Thymidine *. The Journal of Clinical Investigation. 1967;46(4):506-29.
146. Clarkson B, Ohkita T, Ota K, Oconnor A. Studies of Cellular Proliferation in Acute Leukemia. J Clin Invest. 1965;44:1035.
147. Clarkson B, Fried J, Strife A, Sakai Y, Ota K, Ohkita T. Studies of cellular proliferation in human leukemia. III. Behavior of leukemic cells in three adults with acute leukemia given continuous infusions of 3H-thymidine for 8 or 10 days. Cancer. 1970;25(6):1237-60.
148. Hamburger AW, Salmon SE. Primary Bioassay of Human Tumor Stem Cells. Science. 1977;197(4302):461-3.

149. Bonner WA, Hulett HR, Sweet RG, Herzenberg LA. Fluorescence Activated Cell Sorting. Review of Scientific Instruments. 1972;43(3):404-9.
150. Bonnet D, Dick JE. Human acute myeloid leukemia is organized as a hierarchy that originates from a primitive hematopoietic cell. Nat Med. 1997;3(7):730-7.
151. Lapidot T, Sirard C, Vormoor J, Murdoch B, Hoang T, Caceres-Cortes J, et al. A cell initiating human acute myeloid leukaemia after transplantation into SCID mice. Nature. 1994;367(6464):645-8.
152. Shultz LD, Schweitzer PA, Christianson SW, Gott B, Schweitzer IB, Tennent B, et al. Multiple defects in innate and adaptive immunologic function in NOD/LtSz-scid mice. J Immunol. 1995;154(1):180-91.
153. Al-Hajj M, Wicha MS, Benito-Hernandez A, Morrison SJ, Clarke MF. Prospective identification of tumorigenic breast cancer cells. Proc Natl Acad Sci U S A. 2003;100(7):3983-8.
154. Singh SK, Clarke ID, Terasaki M, Bonn VE, Hawkins C, Squire J, et al. Identification of a Cancer Stem Cell in Human Brain Tumors. Cancer Res. 2003;63(18):5821-8.
155. O'Brien CA, Pollett A, Gallinger S, Dick JE. A human colon cancer cell capable of initiating tumour growth in immunodeficient mice. Nature. 2007;445(7123):106-10.
156. Ricci-Vitiani L, Lombardi DG, Pilozzi E, Biffoni M, Todaro M, Peschle C, et al. Identification and expansion of human colon-cancer-initiating cells. Nature. 2006.
157. Li C, Heidt DG, Dalerba P, Burant CF, Zhang L, Adsay V, et al. Identification of pancreatic cancer stem cells. Cancer Res. 2007;67(3):1030-7.
158. Alvero AB, Chen R, Fu H-H, Montagna M, Schwartz PE, Rutherford T, et al. Molecular phenotyping of human ovarian cancer stem cells unravel the mechanisms for repair and chemo-resistance. Cell cycle (Georgetown, Tex). 2009;8(1):158-66.
159. Curley MD, Therrien VA, Cummings CL, Sergent PA, Koulouris CR, Friel AM, et al. CD133 expression defines a tumor initiating cell population in primary human ovarian cancer. Stem Cells. 2009;27(12):2875-83.
160. Stewart JM, Shaw PA, Gedye C, Bernardini MQ, Neel BG, Ailles LE. Phenotypic heterogeneity and instability of human ovarian tumor-initiating cells. Proc Natl Acad Sci U S A. 2011;108(16):6468-73.
161. Zhang S, Balch C, Chan MW, Lai HC, Matei D, Schilder JM, et al. Identification and characterization of ovarian cancer-initiating cells from primary human tumors. Cancer Res. 2008;68(11):4311-20.
162. Singh SK, Clarke ID, Terasaki M, Bonn VE, Hawkins C, Squire J, et al. Identification of a cancer stem cell in human brain tumors. Cancer Res. 2003;63(18):5821-8.
163. Yin AH, Miraglia S, Zanjani ED, Almeida-Porada G, Ogawa M, Leary AG, et al. AC133, a Novel Marker for Human Hematopoietic Stem and Progenitor Cells1997 1997-12-15 00:00:00. 5002-12 p.
164. Uchida N, Buck DW, He D, Reitsma MJ, Masek M, Phan TV, et al. Direct isolation of human central nervous system stem cells. Proceedings of the National Academy of Sciences. 2000;97(26):14720-5.
165. Wu Y, Wu PY. CD133 as a marker for cancer stem cells: progresses and concerns. Stem Cells Dev. 2009;18(8):1127-34.

166. Read TA, Fogarty MP, Markant SL, McLendon RE, Wei Z, Ellison DW, et al. Identification of CD15 as a marker for tumor-propagating cells in a mouse model of medulloblastoma. Cancer Cell. 2009;15(2):135-47.
167. Ward RJ, Lee L, Graham K, Satkunendran T, Yoshikawa K, Ling E, et al. Multipotent CD15+ cancer stem cells in patched-1-deficient mouse medulloblastoma. Cancer Res. 2009;69(11):4682-90.
168. Morrison LC, McClelland R, Aiken C, Bridges M, Liang L, Wang X, et al. Deconstruction of medulloblastoma cellular heterogeneity reveals differences between the most highly invasive and self-renewing phenotypes. Neoplasia. 2013;15(4):384-98.
169. Ahlfeld J, Favaro R, Pagella P, Kretzschmar HA, Nicolis S, Schuller U. Sox2 requirement in sonic hedgehog-associated medulloblastoma. Cancer Res. 2013;73(12):3796-807.
170. Batlle E, Clevers H. Cancer stem cells revisited. Nature Medicine. 2017;23:1124.
171. Liang L, Aiken C, McClelland R, Morrison LC, Tatari N, Remke M, et al. Characterization of novel biomarkers in selecting for subtype specific medulloblastoma phenotypes. Oncotarget. 2015;6(16):38881-900.
172. Gupta PB, Fillmore CM, Jiang G, Shapira SD, Tao K, Kuperwasser C, et al. Stochastic state transitions give rise to phenotypic equilibrium in populations of cancer cells. Cell. 2011;146(4):633-44.
173. Chaffer Christine L, Marjanovic Nemanja D, Lee T, Bell G, Kleer Celina G, Reinhardt F, et al. Poised Chromatin at the ZEB1 Promoter Enables Breast Cancer Cell Plasticity and Enhances Tumorigenicity. Cell. 2013;154(1):61-74.
174. Chow K-H, Shin D-M, Jenkins MH, Miller EE, Shih DJ, Choi S, et al. Epigenetic States of Cells of Origin and Tumor Evolution Drive Tumor-Initiating Cell Phenotype and Tumor Heterogeneity. Cancer Res. 2014;74(17):4864-74.
175. Williams RT, den Besten W, Sherr CJ. Cytokine-dependent imatinib resistance in mouse BCR-ABL+, Arf-null lymphoblastic leukemia. Genes Dev. 2007;21(18):2283-7.
176. Kelly PN, Dakic A, Adams JM, Nutt SL, Strasser A. Tumor growth need not be driven by rare cancer stem cells. Science. 2007;317(5836):337.
177. Quintana E, Shackleton M, Sabel MS, Fullen DR, Johnson TM, Morrison SJ. Efficient tumour formation by single human melanoma cells. Nature. 2008;456(7222):593-8.
178. Barker N, Ridgway RA, van Es JH, van de Wetering M, Begthel H, van den Born M, et al. Crypt stem cells as the cells-of-origin of intestinal cancer. Nature. 2009;457(7229):608-11.
179. Cozzio A, Passegué E, Ayton PM, Karsunky H, Cleary ML, Weissman IL. Similar MLL-associated leukemias arising from self-renewing stem cells and short-lived myeloid progenitors. Genes & Development. 2003;17(24):3029-35.
180. Huntly BJP, Shigematsu H, Deguchi K, Lee BH, Mizuno S, Duclos N, et al. MOZ-TIF2, but not BCR-ABL, confers properties of leukemic stem cells to committed murine hematopoietic progenitors. Cancer Cell. 2004;6(6):587-96.

181. Zhao Z, Zuber J, Diaz-Flores E, Lintault L, Kogan SC, Shannon K, et al. p53 loss promotes acute myeloid leukemia by enabling aberrant self-renewal. Genes & Development. 2010;24(13):1389-402.
182. Bao S, Wu Q, McLendon RE, Hao Y, Shi Q, Hjelmeland AB, et al. Glioma stem cells promote radioresistance by preferential activation of the DNA damage response. Nature. 2006;444(7120):756-60.
183. Diehn M, Cho RW, Lobo NA, Kalisky T, Dorie MJ, Kulp AN, et al. Association of reactive oxygen species levels and radioresistance in cancer stem cells. Nature. 2009;458(7239):780-3.
184. Zhang M, Atkinson RL, Rosen JM. Selective targeting of radiation-resistant tumor-initiating cells. Proceedings of the National Academy of Sciences. 2010;107(8):3522-7.
185. Anderson K, Lutz C, van Delft FW, Bateman CM, Guo Y, Colman SM, et al. Genetic variegation of clonal architecture and propagating cells in leukaemia. Nature. 2011;469(7330):356-61.
186. Clappier E, Gerby B, Sigaux F, Delord M, Touzri F, Hernandez L, et al. Clonal selection in xenografted human T cell acute lymphoblastic leukemia recapitulates gain of malignancy at relapse. The Journal of Experimental Medicine. 2011;208(4):653-61.
187. Notta F, Mullighan CG, Wang JCY, Poeppl A, Doulatov S, Phillips LA, et al. Evolution of human BCR-ABL1 lymphoblastic leukaemia-initiating cells. Nature. 2011;469(7330):362-7.
188. Aiken C, Werbowetski-Ogilvie T. Animal models of cancer stem cells: What are they really telling us? . Current Pathobiology Reports 2013;1(2):91-9.
189. Pastrana E, Silva-Vargas V, Doetsch F. Eyes wide open: a critical review of sphere-formation as an assay for stem cells. Cell Stem Cell.8(5):486-98.
190. Reynolds BA, Weiss S. Generation of neurons and astrocytes from isolated cells of the adult mammalian central nervous system. Science. 1992;255(5052):1707-10.
191. Weiss S, Dunne C, Hewson J, Wohl C, Wheatley M, Peterson AC, et al. Multipotent CNS Stem Cells Are Present in the Adult Mammalian Spinal Cord and Ventricular Neuroaxis. The Journal of Neuroscience. 1996;16(23):7599-609.
192. Vescovi AL, Reynolds BA, Fraser DD, Weiss S. bFGF regulates the proliferative fate of unipotent (neuronal) and bipotent (neuronal/astroglial) EGF-generated CNS progenitor cells. Neuron. 1993;11(5):951-66.
193. Coles-Takabe BLK, Brain I, Purpura KA, Karpowicz P, Zandstra PW, Morshead CM, et al. Don't Look: Growing Clonal Versus Nonclonal Neural Stem Cell Colonies. STEM CELLS. 2008;26(11):2938-44.
194. Wang JC, Doedens M, Dick JE. Primitive human hematopoietic cells are enriched in cord blood compared with adult bone marrow or mobilized peripheral blood as measured by the quantitative in vivo SCID-repopulating cell assay. Blood. 1997;89(11):3919-24.
195. Porter EH, Berry RJ. The Efficient Design of Transplantable Tumour Assays. Br J Cancer. 1963;17:583-95.

196. Kuperwasser C, Chavarria T, Wu M, Magrane G, Gray JW, Carey L, et al. Reconstruction of functionally normal and malignant human breast tissues in mice. Proc Natl Acad Sci U S A. 2004;101(14):4966-71.
197. Joyce JA. Therapeutic targeting of the tumor microenvironment. Cancer Cell. 2005;7(6):513-20.
198. Schatton T, Murphy GF, Frank NY, Yamaura K, Waaga-Gasser AM, Gasser M, et al. Identification of cells initiating human melanomas. Nature. 2008;451(7176):345-9.
199. Kennedy JA, Barabe F, Poeppl AG, Wang JC, Dick JE. Comment on "Tumor growth need not be driven by rare cancer stem cells". Science. 2007;318(5857):1722; author reply
200. Eppert K, Takenaka K, Lechman ER, Waldron L, Nilsson B, van Galen P, et al. Stem cell gene expression programs influence clinical outcome in human leukemia. Nat Med. 2011;17(9):1086-93.
201. Ishizawa K, Rasheed ZA, Karisch R, Wang Q, Kowalski J, Susky E, et al. Tumor-initiating cells are rare in many human tumors. Cell Stem Cell. 2010;7(3):279-82.
202. Buchstaller J, McKeever PE, Morrison SJ. Tumorigenic cells are common in mouse MPNSTs but their frequency depends upon tumor genotype and assay conditions. Cancer Cell.21(2):240-52.
203. Hochedlinger K, Blelloch R, Brennan C, Yamada Y, Kim M, Chin L, et al. Reprogramming of a melanoma genome by nuclear transplantation. Genes Dev. 2004;18(15):1875-85.
204. Utikal J, Maherali N, Kulalert W, Hochedlinger K. Sox2 is dispensable for the reprogramming of melanocytes and melanoma cells into induced pluripotent stem cells. J Cell Sci. 2009;122(Pt 19):3502-10.
205. Held MA, Curley DP, Dankort D, McMahon M, Muthusamy V, Bosenberg MW. Characterization of melanoma cells capable of propagating tumors from a single cell. Cancer Res.70(1):388-97.
206. Vaillant F, Asselin-Labat ML, Shackleton M, Forrest NC, Lindeman GJ, Visvader JE. The mammary progenitor marker CD61/beta3 integrin identifies cancer stem cells in mouse models of mammary tumorigenesis. Cancer Res. 2008;68(19):7711-7.
207. Tamase A, Muraguchi T, Naka K, Tanaka S, Kinoshita M, Hoshii T, et al. Identification of tumor-initiating cells in a highly aggressive brain tumor using promoter activity of nucleostemin. Proc Natl Acad Sci U S A. 2009;106(40):17163-8.
208. Marumoto T, Tashiro A, Friedmann-Morvinski D, Scadeng M, Soda Y, Gage FH, et al. Development of a novel mouse glioma model using lentiviral vectors. Nat Med. 2009;15(1):110-6.
209. Fridman R, Benton G, Aranoutova I, Kleinman HK, Bonfil RD. Increased initiation and growth of tumor cell lines, cancer stem cells and biopsy material in mice using basement membrane matrix protein (Cultrex or Matrigel) co-injection. Nat Protoc. 2012;7(6):1138-44.
210. Barbieri F, Wurth R, Ratto A, Campanella C, Vito G, Thellung S, et al. Isolation of stem-like cells from spontaneous feline mammary carcinomas: phenotypic characterization and tumorigenic potential. Exp Cell Res. 2012;318(7):847-60.

211. Cocola C, Anastasi P, Astigiano S, Piscitelli E, Pelucchi P, Vilardo L, et al. Isolation of canine mammary cells with stem cell properties and tumour-initiating potential. Reprod Domest Anim. 2009;44 Suppl 2:214-7.
212. Eguiara A, Holgado O, Beloqui I, Abalde L, Sanchez Y, Callol C, et al. Xenografts in zebrafish embryos as a rapid functional assay for breast cancer stem-like cell identification. Cell Cycle. 2011;10(21):3751-7.
213. Zon LI, Peterson RT. In vivo drug discovery in the zebrafish. Nat Rev Drug Discov. 2005;4(1):35-44.
214. Lee LM, Seftor EA, Bonde G, Cornell RA, Hendrix MJ. The fate of human malignant melanoma cells transplanted into zebrafish embryos: assessment of migration and cell division in the absence of tumor formation. Dev Dyn. 2005;233(4):1560-70.
215. Haldi M, Ton C, Seng WL, McGrath P. Human melanoma cells transplanted into zebrafish proliferate, migrate, produce melanin, form masses and stimulate angiogenesis in zebrafish. Angiogenesis. 2006;9(3):139-51.
216. Bonnet D, Dick JE. Human acute myeloid leukemia is organized as a hierarchy that originates from a primitive hematopoietic cell. Nature Medicine. 1997;3(7):730-7.
217. Singh SK, Hawkins C, Clarke ID, Squire JA, Bayani J, Takulchiro H, et al. Identification of human brain tumour initiating cells. Nature 2004;432:396-401.
218. Ricci-Vitiani L, Lombardi DG, Pilozzi E, Biffoni M, Todaro M, Peschle C, et al. Identification and expansion of human colon-cancer-initiating cells. Nature. 2007;445(7123):111-5.
219. Alvero AB, Chen R, Fu HH, Montagna M, Schwartz PE, Rutherford T, et al. Molecular phenotyping of human ovarian cancer stem cells unravels the mechanisms for repair and chemoresistance. Cell Cycle. 2009;8(1):158-66.
220. Chen R, Nishimura MC, Bumbaca SM, Kharbanda S, Forrest WF, Kasman IM, et al. A hierarchy of self-renewing tumor-initiating cell types in glioblastoma. Cancer Cell. 2010;17(4):362-75.
221. Mani SA, Guo W, Liao MJ, Eaton EN, Ayyanan A, Zhou AY, et al. The epithelial-mesenchymal transition generates cells with properties of stem cells. Cell. 2008;133(4):704-15.
222. Pang R, Law WL, Chu AC, Poon JT, Lam CS, Chow AK, et al. A subpopulation of CD26+ cancer stem cells with metastatic capacity in human colorectal cancer. Cell Stem Cell. 2010;6(6):603-15.
223. Charafe-Jauffret E, Ginestier C, Iovino F, Wicinski J, Cervera N, Finetti P, et al. Breast cancer cell lines contain functional cancer stem cells with metastatic capacity and a distinct molecular signature. Cancer Res. 2009;69(4):1302-13.
224. Molina JR, Hayashi Y, Stephens C, Georgescu MM. Invasive glioblastoma cells acquire stemness and increased Akt activation. Neoplasia. 2010;12(6):453-63.
225. Shmelkov SV, Butler JM, Hooper AT, Hormigo A, Kushner J, Milde T, et al. CD133 expression is not restricted to stem cells, and both CD133+ and CD133- metastatic colon cancer cells initiate tumors. J Clin Invest. 2008;118(6):2111-20.
226. Jacobsen PF, Jenkyn DJ, Papadimitriou JM. Establishment of a human medulloblastoma cell line and its heterotransplantation into nude mice. J Neuropathol Exp Neurol. 1985;44(5):472-85.

227. Friedman HS, Burger PC, Bigner SH, Trojanowski JQ, Brodeur GM, He XM, et al. Phenotypic and genotypic analysis of a human medulloblastoma cell line and transplantable xenograft (D341 Med) demonstrating amplification of c-myc. Am J Pathol. 1988;130(3):472-84.
228. Friedman HS, Burger PC, Bigner SH, Trojanowski JQ, Wikstrand CJ, Halperin EC, et al. Establishment and characterization of the human medulloblastoma cell line and transplantable xenograft D283 Med. J Neuropathol Exp Neurol. 1985;44(6):592-605.
229. Snuderl M, Batista A, Kirkpatrick ND, Ruiz de Almodovar C, Riedemann L, Walsh EC, et al. Targeting placental growth factor/neuropilin 1 pathway inhibits growth and spread of medulloblastoma. Cell.152(5):1065-76.
230. Siu IM, Lal A, Blankenship JR, Aldosari N, Riggins GJ. c-Myc promoter activation in medulloblastoma. Cancer Res. 2003;63(16):4773-6.
231. Northcott PA, Shih DJ, Remke M, Cho YJ, Kool M, Hawkins C, et al. Rapid, reliable, and reproducible molecular sub-grouping of clinical medulloblastoma samples. Acta Neuropathol. 2012;123(4):615-26.
232. Remke M, Hielscher T, Korshunov A, Northcott PA, Bender S, Kool M, et al. FSTL5 is a marker of poor prognosis in non-WNT/non-SHH medulloblastoma. J Clin Oncol.29(29):3852-61.
233. Northcott PA, Shih DJ, Peacock J, Garzia L, Morrissy AS, Zichner T, et al. Subgroup-specific structural variation across 1,000 medulloblastoma genomes. Nature. 2012;488(7409):49-56.
234. Del Duca D, Werbowetski T, Del Maestro RF. Spheroid preparation from hanging drops: characterization of a model of brain tumor invasion. J Neurooncol. 2004;67(3):295-303.
235. Werbowetski-Ogilvie TE, Seyed Sadr M, Jabado N, Angers-Loustau A, Agar NY, Wu J, et al. Inhibition of medulloblastoma cell invasion by Slit. Oncogene. 2006;25(37):5103-12.
236. Werbowetski-Ogilvie TE, Morrison LC, Fiebig-Comyn A, Bhatia M. In vivo generation of neural tumors from neoplastic pluripotent stem cells models early human pediatric brain tumor formation. Stem Cells. 2012;30(3):392-404.
237. Bien-Willner GA, Mitra RD. Mutation and expression analysis in medulloblastoma yields prognostic variants and a putative mechanism of disease for i17q tumors. Acta neuropathologica communications. 2014;2(1):74.
238. Northcott PA, Nakahara Y, Wu X, Feuk L, Ellison DW, Croul S, et al. Multiple recurrent genetic events converge on control of histone lysine methylation in medulloblastoma. Nat Genet. 2009;41(4):465-72.
239. Parsons DW, Li M, Zhang X, Jones S, Leary RJ, Lin JC, et al. The genetic landscape of the childhood cancer medulloblastoma. Science. 2011;331(6016):435-9.
240. Sukhdeo K, Paramban RI, Vidal JG, Elia J, Martin J, Rivera M, et al. Multiplex flow cytometry barcoding and antibody arrays identify surface antigen profiles of primary and metastatic colon cancer cell lines. PLoS One. 2013;8(1):e53015.
241. Yuan SH, Martin J, Elia J, Flippin J, Paramban RI, Hefferan MP, et al. Cell-surface marker signatures for the isolation of neural stem cells, glia and neurons derived from human pluripotent stem cells. PLoS One.6(3):e17540.

242. Lathia JD, Li M, Sinyuk M, Alvarado AG, Flavahan WA, Stoltz K, et al. High-throughput flow cytometry screening reveals a role for junctional adhesion molecule a as a cancer stem cell maintenance factor. Cell reports. 2014;6(1):117-29.
243. Wang X, Venugopal C, Manoranjan B, McFarlane N, O'Farrell E, Nolte S, et al. Sonic hedgehog regulates Bmi1 in human medulloblastoma brain tumor-initiating cells. Oncogene. 2012;31(2):187-99.
244. Leung C, Lingbeek M, Shakhova O, Liu J, Tanger E, Saremaslani P, et al. Bmi1 is essential for cerebellar development and is overexpressed in human medulloblastomas. Nature. 2004;428(6980):337-41.
245. Dahmane N, Sanchez P, Gitton Y, Palma V, Sun T, Beyna M, et al. The Sonic Hedgehog-Gli pathway regulates dorsal brain growth and tumorigenesis. Development. 2001;128(24):5201-12.
246. Triscott J, Lee C, Foster C, Manoranjan B, Pambid MR, Berns R, et al. Personalizing the treatment of pediatric medulloblastoma: Polo-like kinase 1 as a molecular target in high-risk children. Cancer Res. 2013;73(22):6734-44.
247. Vo DT, Subramaniam D, Remke M, Burton TL, Uren PJ, Gelfond JA, et al. The RNA-binding protein Musashi1 affects medulloblastoma growth via a network of cancer-related genes and is an indicator of poor prognosis. Am J Pathol.181(5):1762-72.
248. Manoranjan B, Wang X, Hallett RM, Venugopal C, Mack SC, McFarlane N, et al. FoxG1 Interacts with Bmi1 to Regulate Self-Renewal and Tumorigenicity of Medulloblastoma Stem Cells. Stem Cells. 2013;31(7):1266-77.
249. Northcott PA, Shih DJ, Peacock J, Garzia L, Morrissy AS, Zichner T, et al. Subgroup-specific structural variation across 1,000 medulloblastoma genomes. Nature.488(7409):49-56.
250. Yamada Y, Arao T, Matsumoto K, Gupta V, Tan W, Fedynyshyn J, et al. Plasma concentrations of VCAM-1 and PAI-1: a predictive biomarker for post-operative recurrence in colorectal cancer. Cancer Sci. 2010;101(8):1886-90.
251. Holubec L, Jr., Topolcan O, Finek J, Holdenrieder S, Stieber P, Pesta M, et al. Markers of cellular adhesion in diagnosis and therapy control of colorectal carcinoma. Anticancer research. 2005;25(3A):1597-601.
252. Dymicka-Piekarska V, Guzinska-Ustymowicz K, Kuklinski A, Kemona H. Prognostic significance of adhesion molecules (sICAM-1, sVCAM-1) and VEGF in colorectal cancer patients. Thrombosis research. 2012;129(4):e47-50.
253. Horn L, Dahlberg SE, Sandler AB, Dowlati A, Moore DF, Murren JR, et al. Phase II study of cisplatin plus etoposide and bevacizumab for previously untreated, extensive-stage small-cell lung cancer: Eastern Cooperative Oncology Group Study E3501. J Clin Oncol. 2009;27(35):6006-11.
254. Coskun U, Sancak B, Sen I, Bukan N, Tufan MA, Gulbahar O, et al. Serum P-selectin, soluble vascular cell adhesion molecule-I (s-VCAM-I) and soluble intercellular adhesion molecule-I (s-ICAM-I) levels in bladder carcinoma patients with different stages. International immunopharmacology. 2006;6(4):672-7.
255. Syrigos KN, Salgami E, Karayiannakis AJ, Katirtzoglou N, Sekara E, Roussou P. Prognostic significance of soluble adhesion molecules in Hodgkin's disease. Anticancer research. 2004;24(2C):1243-7.

256. Shah N, Cabanillas F, McIntyre B, Feng L, McLaughlin P, Rodriguez MA, et al. Prognostic value of serum CD44, intercellular adhesion molecule-1 and vascular cell adhesion molecule-1 levels in patients with indolent non-Hodgkin lymphomas. Leukemia & lymphoma. 2012;53(1):50-6.
257. Kamezaki S, Kurozawa Y, Iwai N, Hosoda T, Okamoto M, Nose T. Serum levels of soluble ICAM-1 and VCAM-1 predict pre-clinical cancer. Eur J Cancer. 2005;41(15):2355-9.
258. Slack-Davis JK, Atkins KA, Harrer C, Hershey ED, Conaway M. Vascular cell adhesion molecule-1 is a regulator of ovarian cancer peritoneal metastasis. Cancer Res. 2009;69(4):1469-76.
259. Huang J, Zhang J, Li H, Lu Z, Shan W, Mercado-Uribe I, et al. VCAM1 expression correlated with tumorigenesis and poor prognosis in high grade serous ovarian cancer. American journal of translational research. 2013;5(3):336-46.
260. Heidemann J, Maaser C, Lugering A, Spahn TW, Zimmer KP, Herbst H, et al. Expression of vascular cell adhesion molecule-1 (CD 106) in normal and neoplastic human esophageal squamous epithelium. International journal of oncology. 2006;28(1):77-85.
261. Hemmerlein B, Scherbening J, Kugler A, Radzun HJ. Expression of VCAM-1, ICAM-1, E- and P-selectin and tumour-associated macrophages in renal cell carcinoma. Histopathology. 2000;37(1):78-83.
262. Lu X, Mu E, Wei Y, Riethdorf S, Yang Q, Yuan M, et al. VCAM-1 promotes osteolytic expansion of indolent bone micrometastasis of breast cancer by engaging alpha4beta1-positive osteoclast progenitors. Cancer Cell. 2011;20(6):701-14.
263. Chen Q, Zhang XHF, Massagué J. Macrophage binding to receptor VCAM-1 transmits survival signals in breast cancer cells that invade the lungs. Cancer Cell. 2011;20(4):538-49.
264. Zheng Y, Yang W, Aldape K, He J, Lu Z. Epidermal Growth Factor (EGF)-enhanced Vascular Cell Adhesion Molecule-1 (VCAM-1) Expression Promotes Macrophage and Glioblastoma Cell Interaction and Tumor Cell Invasion. Journal of Biological Chemistry. 2013;288(44):31488-95.
265. Li P, Du F, Yuelling LW, Lin T, Muradimova RE, Tricarico R, et al. A population of Nestin-expressing progenitors in the cerebellum exhibits increased tumorigenicity. Nat Neurosci. 2013;16(12):1737-44.
266. Barrett LE, Granot Z, Coker C, Iavarone A, Hambardzumyan D, Holland EC, et al. Self-renewal does not predict tumor growth potential in mouse models of high-grade glioma. Cancer Cell. 2012;21(1):11-24.
267. Ghazi SO, Stark M, Zhao Z, Mobley BC, Munden A, Hover L, et al. Cell of Origin Determines Tumor Phenotype in an Oncogenic Ras/p53 Knockout Transgenic Model of High-Grade Glioma. J Neuropath Exp Neur. 2012;71(8):729-40.
268. Klco JM, Spencer DH, Miller CA, Griffith M, Lamprecht TL, O'Laughlin M, et al. Functional heterogeneity of genetically defined subclones in acute myeloid leukemia. Cancer Cell. 2014;25(3):379-92.
269. Buhren J, Christoph AH, Buslei R, Albrecht S, Wiestler OD, Pietsch T. Expression of the neurotrophin receptor p75NTR in medulloblastomas is correlated with distinct histological and clinical features: evidence for a medulloblastoma

subtype derived from the external granule cell layer. J Neuropathol Exp Neurol. 2000;59(3):229-40.
270. Kuchler J, Hartmann W, Waha A, Koch A, Endl E, Wurst P, et al. p75(NTR) induces apoptosis in medulloblastoma cells. Int J Cancer. 2011;128(8):1804-12.
271. Wu T-C. The Role of Vascular Cell Adhesion Molecule-1 in Tumor Immune Evasion. Cancer Res. 2007;67(13):6003-6.
272. Pribila JT, Quale AC, Mueller KL, Shimizu Y. Integrins and T Cell–Mediated Immunity. Annual Review of Immunology. 2004;22(1):157-80.
273. Ren G, Zhao X, Zhang L, Zhang J, Huillier A, Ling W, et al. Inflammatory Cytokine-Induced Intercellular Adhesion Molecule-1 and Vascular Cell Adhesion Molecule-1 in Mesenchymal Stem Cells Are Critical for Immunosuppression. The Journal of Immunology. 2010;184(5):2321.
274. Yang ZX, Han ZB, Ji YR, Wang YW, Liang L, Chi Y, et al. CD106 identifies a subpopulation of mesenchymal stem cells with unique immunomodulatory properties. PLoS One.8(3):e59354.
275. Chen Q, Massagué J. Molecular Pathways: VCAM-1 as a Potential Therapeutic Target in Metastasis. Clinical Cancer Research. 2012;18(20):5520-5.
276. Qian B-Z, Pollard JW. Macrophage Diversity Enhances Tumor Progression and Metastasis. Cell. 2010;141(1):39-51.
277. Qian B, Deng Y, Im JH, Muschel RJ, Zou Y, Li J, et al. A Distinct Macrophage Population Mediates Metastatic Breast Cancer Cell Extravasation, Establishment and Growth. PLOS ONE. 2009;4(8):e6562.
278. Gil-Bernabé AM, Ferjančič Š, Tlalka M, Zhao L, Allen PD, Im JH, et al. Recruitment of monocytes/macrophages by tissue factor-mediated coagulation is essential for metastatic cell survival and premetastatic niche establishment in mice. Blood. 2012;119(13):3164.
279. Chen Y, Zeng J, Cen L, Wang X, Yao G, Wang W, et al. Multiple roles of the p75 neurotrophin receptor in the nervous system. J Int Med Res. 2009;37(2):281-8.
280. Schor NF. The p75 neurotrophin receptor in human development and disease. Progress in neurobiology. 2005;77(3):201-14.
281. Wang L, Rahn JJ, Lun X, Sun B, Kelly JJ, Weiss S, et al. Gamma-secretase represents a therapeutic target for the treatment of invasive glioma mediated by the p75 neurotrophin receptor. PLoS Biol. 2008;6(11):e289.
282. Tomellini E, Lagadec C, Polakowska R, Le Bourhis X. Role of p75 neurotrophin receptor in stem cell biology: more than just a marker. Cellular and molecular life sciences : CMLS. 2014;71(13):2467-81.
283. Young KM, Merson TD, Sotthibundhu A, Coulson EJ, Bartlett PF. p75 neurotrophin receptor expression defines a population of BDNF-responsive neurogenic precursor cells. J Neurosci. 2007;27(19):5146-55.
284. Barnes M, Eberhart CG, Collins R, Tihan T. Expression of p75NTR in fetal brain and medulloblastomas: evidence of a precursor cell marker and its persistence in neoplasia. J Neurooncol. 2009;92(2):193-201.
285. Muragaki Y, Chou TT, Kaplan DR, Trojanowski JQ, Lee VM. Nerve growth factor induces apoptosis in human medulloblastoma cell lines that express TrkA receptors. J Neurosci. 1997;17(2):530-42.

286. Restivo G, Diener J, Cheng PF, Kiowski G, Bonalli M, Biedermann T, et al. The low affinity neurotrophin receptor CD271 regulates phenotype switching in melanoma. Nature communications. 2017;8(1):1988.
287. O'Brien-Ball C, Biddle A. Reprogramming to developmental plasticity in cancer stem cells. Developmental Biology. 2017.
288. Lin TL, Matsui W. Hedgehog pathway as a drug target: Smoothened inhibitors in development. OncoTargets and therapy. 2012;5:47-58.
289. Kool M, Jones DT, Jager N, Northcott PA, Pugh TJ, Hovestadt V, et al. Genome sequencing of SHH medulloblastoma predicts genotype-related response to smoothened inhibition. Cancer Cell. 2014;25(3):393-405.
290. Amakye D, Jagani Z, Dorsch M. Unraveling the therapeutic potential of the Hedgehog pathway in cancer. Nat Med. 2013;19(11):1410-22.
291. Kim J, Aftab BT, Tang JY, Kim D, Lee AH, Rezaee M, et al. Itraconazole and arsenic trioxide inhibit Hedgehog pathway activation and tumor growth associated with acquired resistance to smoothened antagonists. Cancer Cell. 2013;23(1):23-34.
292. Liu S, Cong Y, Wang D, Sun Y, Deng L, Liu Y, et al. Breast cancer stem cells transition between epithelial and mesenchymal states reflective of their normal counterparts. Stem cell reports. 2014;2(1):78-91.
293. Biddle A, Liang X, Gammon L, Fazil B, Harper LJ, Emich H, et al. Cancer Stem Cells in Squamous Cell Carcinoma Switch between Two Distinct Phenotypes That Are Preferentially Migratory or Proliferative. Cancer Res. 2011;71(15):5317.
294. Gupta PB, Onder TT, Jiang G, Tao K, Kuperwasser C, Weinberg RA, et al. Identification of Selective Inhibitors of Cancer Stem Cells by High-Throughput Screening. Cell. 2009;138(4):645-59.
295. Chaffer CL, Brueckmann I, Scheel C, Kaestli AJ, Wiggins PA, Rodrigues LO, et al. Normal and neoplastic nonstem cells can spontaneously convert to a stem-like state. Proceedings of the National Academy of Sciences. 2011;108(19):7950-5.
296. Auffinger B, Tobias AL, Han Y, Lee G, Guo D, Dey M, et al. Conversion of differentiated cancer cells into cancer stem-like cells in a glioblastoma model after primary chemotherapy. Cell Death Differ. 2014;21(7):1119-31.
297. Iliopoulos D, Hirsch HA, Wang G, Struhl K. Inducible formation of breast cancer stem cells and their dynamic equilibrium with non-stem cancer cells via IL6 secretion. Proceedings of the National Academy of Sciences. 2011;108(4):1397-402.
298. Biddle A, Gammon L, Liang X, Costea DE, Mackenzie IC. Phenotypic Plasticity Determines Cancer Stem Cell Therapeutic Resistance in Oral Squamous Cell Carcinoma. EBioMedicine. 2016;4:138-45.
299. Gammon L, Biddle A, Heywood HK, Johannessen AC, Mackenzie IC. Sub-Sets of Cancer Stem Cells Differ Intrinsically in Their Patterns of Oxygen Metabolism. PLOS ONE. 2013;8(4):e62493.
300. Kreso A, Brien CA, van Galen P, Gan OI, Notta F, Brown AMK, et al. Variable Clonal Repopulation Dynamics Influence Chemotherapy Response in Colorectal Cancer. Science. 2013;339(6119):543.
301. Jensen DH, Dabelsteen E, Specht L, Fiehn AMK, Therkildsen MH, Jønson L, et al. Molecular profiling of tumour budding implicates TGFβ-mediated epithelial–mesenchymal transition as a therapeutic target in oral squamous cell carcinoma. The Journal of Pathology. 2015;236(4):505-16.

302. Andriani F, Bertolini G, Facchinetti F, Baldoli E, Moro M, Casalini P, et al. Conversion to stem-cell state in response to microenvironmental cues is regulated by balance between epithelial and mesenchymal features in lung cancer cells. Molecular oncology. 2016;10(2):253-71.
303. Ocaña Oscar H, Córcoles R, Fabra Á, Moreno-Bueno G, Acloque H, Vega S, et al. Metastatic Colonization Requires the Repression of the Epithelial-Mesenchymal Transition Inducer Prrx1. Cancer Cell.22(6):709-24.